

THESIS

ENHANCING THE DEFORMABILITY OF ELASTIC MEMORY SANDWICH COMPOSITES WITH
ELASTIC MEMORY/CONVENTIONAL EPOXY HYBRID FACESHEETS

Submitted by

Allyson Melia Antonio

Department of Mechanical Engineering

In partial fulfillment of the requirements

For the Degree of Master of Science

Colorado State University

Fort Collins, Colorado

Spring 2016

Master's Committee:

Advisor: Donald W. Radford

Susan P. James

Laurence A. Belfiore

Copyright by Allyson Melia Antonio 2016

All Rights Reserved

ABSTRACT

ENHANCING THE DEFORMABILITY OF ELASTIC MEMORY SANDWICH COMPOSITES WITH ELASTIC MEMORY/CONVENTIONAL EPOXY HYBRID FACESHEETS

Shape memory polymer (SMP) composites have the ability to return repeatedly, and with great accuracy, to their cured geometry when heated. By taking advantage of the inherent ability of polymers to exist in a rubbery state at higher temperatures and in a glassy state at lower temperatures, shape memory composites (SMC), which incorporate continuous fiber reinforcement, can accommodate strains up to 5%, compared to the ultimate strain of 1% - 1.5% typical of carbon fibers in aerospace composites. This is possible because the rubbery modulus of an SMP is at least two orders of magnitude lower than its corresponding glassy modulus. The limited lateral stability provided by the matrix in the rubbery state allows the fibers to buckle elastically in sinusoidal waves, called microbuckles, under compressive load. Elastic memory composites (EMC) are a class of SMC that are able to use elastically stored strain energy to exert force, and thereby perform mechanical work. The elastic energy stored by the EMC is not large enough to drive the reverse deformation once cooled to the glassy state, but can be released with applied heat. Because the EMC polymer can be processed into low density foam, the combination of EMC polymer foam with continuous fiber EMC to create sandwich panels, is an attractive one. Although microbuckling is the enabling mechanism for strain accommodation, excessive microbuckling results in either matrix failure (delamination) or fiber breakage. Therefore, the conformability of EMCs is limited by the amount of flexure that can be achieved without incurring permanent damage. Bending an EMC in the rubbery state induces compressive stress that is amplified by the difference in tensile and compressive moduli. Whereas tension is resisted by the fibers, compression is only supported by the matrix. This causes a shift in the location of the neutral stress plane, from the center of the thickness, far toward the maximum tension surface. Additional bending section thickness from adding foam to the EMC to create a sandwich panel, exponentially raises the maximum stress on the compression surface. This leads to microbuckling failure of EMC sandwich panels at much lower deflections than typical solid laminate EMCs. It is hypothesized

that by incorporating permanently bonded conventional carbon epoxy composite plies on the compression surface of the EMC sandwich panel, compression microbuckling failure can be delayed, increasing bending capability. Three base laminate configurations were selected to assess relative deformability in 3-point bending: shape memory only, shape memory with one conventional ply, and shape memory with two conventional plies. To simulate local heating in some specimens, phenolic blocks were bonded to the ends of the foam core and incorporated into the laminate with conventional epoxy, to prevent facesheet shear. The following variables were used to further investigate the viscoelastic behavior of the specimens: bending temperature, deflection rate, and hold time at maximum deflection. Results are presented in the form of force-deflection, rather than stress-strain, as the use of shear end constraint significantly affected the shape of the bent specimens. Global compression facesheet buckling into the foam core caused mid span thinning that was more prominent at higher temperatures. Loading cycle hysteresis due to stress relaxation was recorded at temperatures above and below T_g , being greatest below T_g . It was found, regardless of variables, that the specimens with hybrid elastic memory/conventional epoxy matrix facesheets achieved more than double the deflection of pure EMC.

TABLE OF CONTENTS

ABSTRACT.....	ii
LIST OF TABLES	vii
LIST OF FIGURES	viii
1 INTRODUCTION	1
1.1 Material description	1
1.2 EMC sandwich panels.....	3
1.3 Problem description	4
1.4 Background	8
1.5 Thesis statement.....	13
1.6 Objectives of work	13
1.7 Research approach	13
2 THEORY	15
2.1 Overview of polymer viscoelastic behavior.....	15
2.2 Shape memory polymer behavior	18
2.3 Kinematic model.....	19
2.4 Spring back	22
2.5 Beam bending approximation	23
2.6 Sandwich composite constituent material properties	23
2.7 Sample predictions	24
2.8 Shear end constraints	26
2.9 Failure modes.....	27
2.9.1 Matrix failure.....	27
2.9.2 Core failure.....	27
2.9.3 Fiber failure	28

2.9.4	Sandwich panel failure	29
3	EXPERIMENTAL	30
3.1	Manufacturing	31
3.2	Testing	35
3.3	Elevated temperature stiffness	36
3.4	Bending rate dependence	37
3.5	Incremental bending	37
3.6	Local heating	38
3.7	Damage inspection	38
3.8	Failure microscopy	38
3.9	Profiled foam beam	39
4	RESULTS AND DISCUSSION	40
4.1	Room temperature stiffness	40
4.2	Effects of temperature and end constraint	41
4.3	SM-only comparison	41
4.4	Beam curvature	44
4.5	Effects of deflection rate and hold time	46
4.6	Varied deflection rate at three temperatures	47
4.7	Constant deflection hold	52
4.8	Incremental bending	58
4.9	Deflection at 56°C	59
4.10	Deflection at 80°C	63
4.11	Damage evolution	66
4.12	Foam failure	73
4.13	Sample microscopy	74
4.14	Bent	74

4.15	Restored	79
4.16	Contoured foam.....	82
4.17	Validity of shear constraint	82
4.18	Shape stability	83
5	FUTURE WORK.....	84
6	CONCLUSION.....	85
6.1	Significant findings	85
7	REFERENCES	88
	APPENDIX A	91
A.1.	Sources of error.....	91
A.2.	Manufacturing error	91
A.3.	Load cell temperature sensitivity	92
A.4.	Load frame and test fixture compliance.....	93
	APPENDIX B	96
B.1.	Room temperature stiffness	96
	APPENDIX C	97
C.1.	DSC results of EPON™ Resin 828 mixed with EPIKURE™ Curing Agent 3140 at 45 parts-per-hundred, after postcure	97
	APPENDIX D	98
D.1.	EPON™ Resin 828 Technical Data Sheet	98

LIST OF TABLES

Table 2-1: Numerically derived constitutive parameters for CTD-DP-5.1	22
Table 2-2: Calculated beam section bending properties.	25
Table 3-1: Beam sample descriptions.	34
Table 3-2: Test order of bending rate samples.....	37
Table 4-1: Flexural stiffness at room temperature.	40
Table 4-2: Maximum bending force with rate and temperature variation.	48
Table 4-3: Force reduction at constant deflection.....	54
Table 4-4: Incremental bending results.....	59

LIST OF FIGURES

Figure 1-1: Typical shape memory polymer thermal deformation cycle. [8]	2
Figure 1-2: Polymer states with respect to T_g . [7]	3
Figure 1-3: Notional comparison of laminate properties vs. weight increase. [14]	4
Figure 1-4: Sinusoidal profile of microbuckled fibers in a unidirectional fiber EMC. [18]	5
Figure 1-5: In-plane and out-of-plane fiber micro-buckling. [19]	6
Figure 1-6: Neutral axis shift under compressive stress. [18].....	7
Figure 1-7: Rotation of compression-loaded fibers, resulting in kink band. [19]	7
Figure 1-8: Global buckling failure.	8
Figure 1-9: Conceptual heating zone model of conformable racing seat.[22]	10
Figure 1-10: Localized compression facesheet buckling of a 100% SM sandwich panel. [22].....	11
Figure 1-11: Profiled core sample with one ply of conventional matrix epoxy. [22]	12
Figure 2-1: Kinematic model examples.	15
Figure 2-2: Stress-strain curves.....	16
Figure 2-3: Stress relaxation result. [33].....	17
Figure 2-4: Creep test result. [33]	17
Figure 2-5: Creep strain recovery. [33].....	18
Figure 2-6: Torsional DMA plot of CTD-DP-5.1 [25]	19
Figure 2-7: Four-element constitutive model proposed by Tobushi et al. [24].....	20
Figure 2-8: Viscoelastic lumped-parameter model. [25]	21
Figure 2-9: Ideal geometry of shear and extensional folding. [18]	26
Figure 3-1: Orientation of sandwich cores cut from an SMP foam block.	30
Figure 3-2: SMP foam slices.....	31
Figure 3-3: Sandwich panel layup diagram, side view.	33
Figure 3-4: Cure cycle.	33

Figure 3-5: Available test samples.....	35
Figure 3-6: Test chamber and 3-point bending set-up.	36
Figure 3-7: Local heating with fiberglass heating tape.	38
Figure 3-8: Thickness of profiled foam beam vs. span location.	39
Figure 4-1: Flexural stiffness comparison at room temperature.	41
Figure 4-2: Force vs. Deflection curves by end condition, shape memory plies only.	42
Figure 4-3: 3-L-a @ 42° ~1.2”.....	43
Figure 4-4: 1-L-a @ 42° ~1.0”.....	43
Figure 4-5: Force vs deflection curves by temperature, SM-only. (a) 42°C, and (b) 80°C.	44
Figure 4-6: 1-H-b at 1.0” – Failure onset.....	44
Figure 4-7: 2-L-b at 1.6” – No failure at maximum deflection.....	45
Figure 4-8: 2.5-L-a at 1.6” – No failure at maximum deflection.	45
Figure 4-9: U-3-M-a at 0.6” – Failure onset.	45
Figure 4-10: 4-M-b at 1.3” – Failure onset.	45
Figure 4-11: 5-M-b at 1.5” – Failure onset.	45
Figure 4-12: 6-M-b at 0.8” – Failure onset.	46
Figure 4-13: Force vs. deflection curves at 80°C, with varied deflection rates.	47
Figure 4-14: Force vs. Deflection of 1-M-b.....	50
Figure 4-15: Force vs. Deflection of 2-H-b.	50
Figure 4-16: Force vs. Deflection of 2.5-H-a.....	51
Figure 4-17: Force vs. Deflection of 3-M-b.....	51
Figure 4-18: Force vs. Deflection of 4-M-b.....	52
Figure 4-19: Force vs. Deflection of 5-H-b.	52
Figure 4-20: Bending at 0.1”/min and 56°C.	55
Figure 4-21: Bending at 1.0”/min and 56°C.	56
Figure 4-22: Bending at 0.1”/min and 71°C.	56

Figure 4-23: Bending at 1.0"/min and 71°C.	57
Figure 4-24: Bending at 0.1"/min and 80°C.	57
Figure 4-25: Bending at 1.0"/min and 80°C.	58
Figure 4-26: U-1-H-a – Incremental deflection at 56°C.	60
Figure 4-27: 2-M-b – Incremental deflection at 56°C.	61
Figure 4-28: 2.5-M-a – Incremental deflection at 56°C.	61
Figure 4-29: 3-H-b – Incremental deflection at 56°C.	62
Figure 4-30: 4-L-b – Incremental deflection at 56°C.	62
Figure 4-31: 5-L-b – Incremental deflection at 56°C.	63
Figure 4-32: 1-H-b – Incremental deflection at 80°C.	63
Figure 4-33: 2-L-b – Incremental deflection at 80°C.	64
Figure 4-34: 2.5-L-a – Incremental deflection at 80°C.	64
Figure 4-35: U-3-M-a – Incremental deflection at 80°C.	65
Figure 4-36: 4-M-b – Incremental deflection at 80°C.	65
Figure 4-37: 5-M-b – Incremental deflection at 80°C.	66
Figure 4-38: 6-M-b – Incremental deflection at 80°C.	66
Figure 4-39: Failure progression of 1-H-b.	68
Figure 4-40: Failure progression of U-3-M-a.	70
Figure 4-41: Failure progression of 4-M-b.	71
Figure 4-42: Failure progression of 5-M-b.	71
Figure 4-43: Failure progression of 6-M-b.	72
Figure 4-44: 2.5-L-a at 1.6" at 80°C - No facesheet failure.	73
Figure 4-45: 2.5-L-a at 1.6" at 80°C - Core end shear showing foam shear failure.	74
Figure 4-46: U-3-M-a bent, at up to 25X magnification.	75
Figure 4-47: 4-M-b bent, at up to 25X magnification.	77
Figure 4-48: 5-M-b bent, at up to 25X magnification.	78

Figure 4-49: U-3-M-a restored, at up to 25X magnification.....	80
Figure 4-50: 4-M-b restored, at up to 25X magnification.....	80
Figure 4-51 – 5-M-b restored, at up to 25X magnification.....	81
Figure 4-52: Contoured foam beam before bending.	82
Figure 4-53: Contoured foam beam, bent.	82
Figure 4-54: 2-M-b at 0.5” – Locally heated.	82
Figure 4-55: 2.5-M-a at 0.6” – Locally heated.....	82
Figure 4-56: Beam profile at start of room temperature stability test.....	83
Figure 4-57: Beam profile at end of room temperature stability test.....	83

1 INTRODUCTION

The development of shape memory polymer composites seeks to capitalize on the high stiffness-to-weight ratio, structural tailorability, and possible complex geometry of conventional fiber reinforced composites, paired with the large strain recovery and thermally induced Young's modulus change of shape memory polymers (SMP). The class of SMP composites that are able to use stored strain energy to exert force, and thereby perform mechanical work, are called Elastic Memory Composites (EMC) [1]. The term "elastic memory" is derived from the non-hysteresis reversible change in the elastic modulus of SMPs [2]. Demonstrated applications of EMCs have included space deployable truss booms [3], satellite reflectors [4], and hinges [5]; with potential commercial applications in the recreation, toy, automotive, and construction industries [6].

The work described herein deals with the specific case of composite sandwich panels that are composed of carbon fiber cloth-reinforced facesheets bonded to SMP foam core. The facesheets contain varying numbers of thermosetting SMP matrix plies and conventional epoxy, EPON™ Resin 828 cured with EPIKURE™ Curing Agent 3140 at 45 parts-per-hundred, matrix plies.

1.1 Material description

A shape memory polymer can be either a thermoset or thermoplastic that can be deformed at an elevated temperature to a secondary shape, but will return to its original as-molded shape, unassisted, if heated above its glass transition temperature. The mechanism responsible for this memory effect in an individual polymer may be proprietary, but the commonly accepted notion is a softening or breaking of some fraction, of the secondary chemical bonds above a specified temperature. This allows the reorientation of molecular chains to take place under applied load. If the strain is maintained while the temperature is sufficiently reduced, the bonds or molecular chains re-form or re-solidify, locking in the deformed shape. The strain energy is stored within the deformed polymer, until released by re-heating. This allows large inelastic strains, up to 300-400% [2][6][7], to be recovered. The typical thermal deformation cycle in Figure 1-1 shows the following: Step 1: Load application at high temperature induces strain energy. Step 2: Strain

is maintained as temperature is reduced. However, required applied load drops dramatically with temperature. Step 3a: The strain is recovered, unassisted, with reheating, or Step 3b: The material is constrained and exerts a force on the constraint.

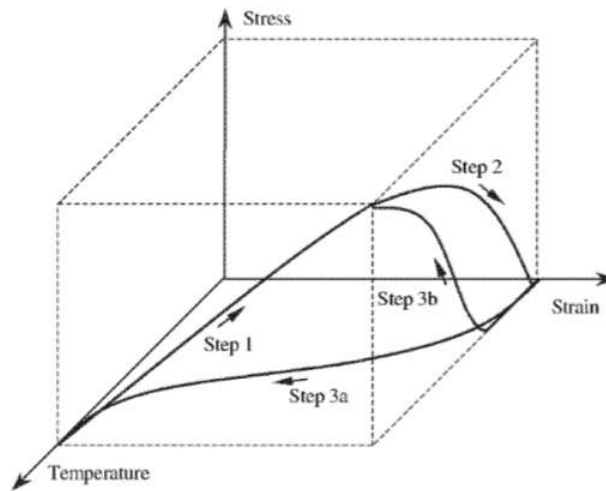


Figure 1-1: Typical shape memory polymer thermal deformation cycle. [8]

An inherent property of polymers is the ability to exist in a rubbery state at higher temperatures and in a glassy state at lower temperatures. “Because the glassy modulus of a polymer is at least two orders of magnitude greater than its corresponding rubbery modulus, the stored elastic stress is not large enough to drive the reverse deformation in the glassy state as the load is removed. As a result, the deformation can be frozen in the glassy state on quenching or after cooling under load to the lower temperatures.” [9]

The shape memory polymer transitions between the glassy and rubbery states over a temperature range, rather than a specific activation temperature, Figure 1-2. The temperature at which the greatest change in modulus occurs is estimated to be the glass transition temperature, T_g [7]. As demonstrated by Hayashi (1993)[10], the T_g and glass transition temperature range can be adjusted to meet the operating conditions by varying the chemical composition.

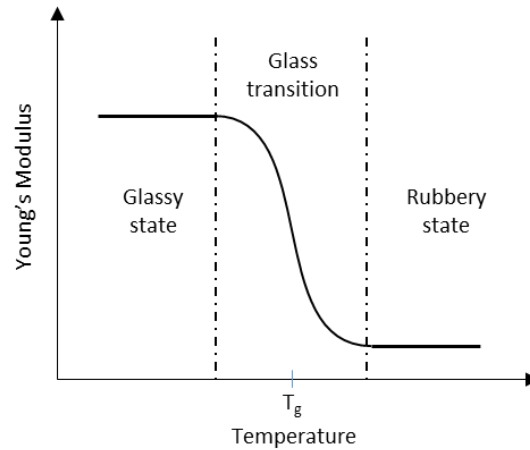


Figure 1-2: Polymer states with respect to T_g . [7]

While capable of large strain recovery, unreinforced shape memory polymers suffer from relatively low strength and low stiffness [11], even in the glassy state. By the introduction of fiber reinforcement, both the in-service structural properties, as well as the storage modulus of the material can be improved [2][12][13]. Since shape memory polymer can be processed with standard composite fabrication techniques, such as wet layup and resin transfer molding, or pre-impregnated into fabric at partial cure (prepreg) [13], it holds great promise of use in many additional applications currently served by conventional polymer composites. With proper design, EMCs have the advantage of adjustability and collapsibility while maintaining the desired composite characteristic of high stiffness relative to weight when glassy. Multiple custom sized parts could potentially be replaced by a single conformable EMC part.

1.2 EMC sandwich panels

The typical composite sandwich structure consists of continuous fiber reinforced polymer facesheets bonded to a relatively thick, but lower density material in the middle. The facesheets provide in-plane axial strength to the outer surfaces of the sandwich, while the middle portion transfers shear between the facesheets and increases the flexural rigidity of the overall section by increasing the thickness. This results in stiff, lightweight parts that can be tailored, via fiber selection and orientation, to provide strength and stiffness aligned with primary load paths. Honeycomb cellular core or structural foam is commonly used

as the material between the facesheets. Figure 1-3 illustrates the potential reduction in weight-to-stiffness ratio by implementing a sandwich structure, over a solid laminate.


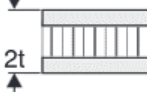
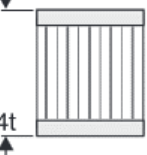
	Solid Material	Core Thickness t	Core Thickness $3t$
			
Stiffness	1.0	7.0	37.0
Flexural Strength	1.0	3.5	9.2
Weight	1.0	1.03	1.06

Figure 1-3: Notional comparison of laminate properties vs. weight increase. [14]

Shape memory polymer is also capable of being processed into low density foam, which has similar, albeit lower mechanical properties, to solid SMPs [15]. The availability of these foams makes it logical to consider the combination of SMP foam with fiber-reinforced SMP, to create EMC sandwich panels. The foam, which can be manufactured from the same base polymer as the matrix epoxy in the facesheets, can contribute to an overall structure with uniform properties with respect to thermo-mechanical response. The obvious advantage to conventional composites offered by sandwich construction can be replicated with SM materials, further expanding the opportunities for implementing EMCs.

1.3 Problem description

The way in which a continuous fiber EMC accommodates strain differs from a solid SMP due to the restriction imposed in the fiber direction. While the SMP matrix maintains its large strain capability at elevated temperature, the conformability of the overall structure is limited by the compression strength and minimum radius of curvature of the fibers.

At elevated temperature, the SMP matrix has considerably softened, and the EMC can be deformed or “packaged” by the application of out of plane load to produce bending. Since the ultimate strain of high

performance carbon fibers, typical of aerospace composite applications, is around 1% - 1.5% [16], but EMCs can accommodate strains up to 5% [16][17][18], the fibers buckle elastically [13] in sinusoidal waves [18], called microbuckles, Figure 1-4, under compressive load. Unlike conventional composites, in-plane microbuckling can occur in SMCs because the matrix in the soft resin state does not produce enough lateral stability to constrain the fiber [17].

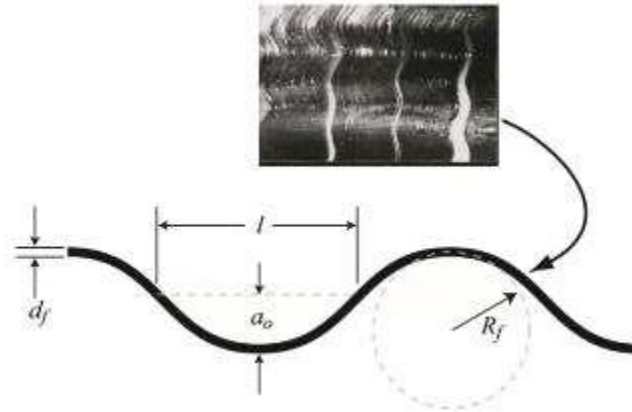


Figure 1-4: Sinusoidal profile of microbuckled fibers in a unidirectional fiber EMC. [18]

Compression induced microbuckles manifest in either the transverse or in-plane orientations, shown in Figure 1-5, where in-plane buckling is the higher energy mode of the two [17]. While microbuckling is necessary to the conformability of shape memory composites, both forms of microbuckling can lead to permanent damage if they exceed the capabilities of the constituent materials. In-plane microbuckling can lead to fiber breakage if the sinusoidal shape results in a bend radius that is too small for the fiber to accommodate [18]. However, the far more common mode is out of plane buckling, due to the lower strain energy required to initiate microbuckling [17], which at increasing amplitude, eventually results in matrix failure in the form of delaminations [18].

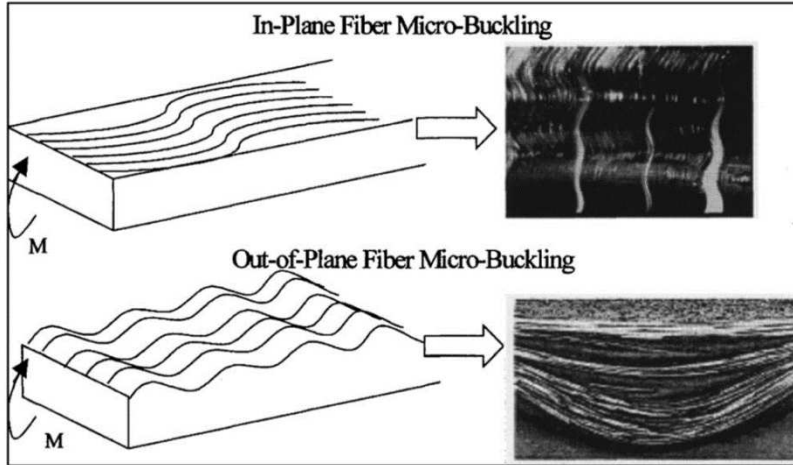


Figure 1-5: In-plane and out-of-plane fiber micro-buckling. [19]

The amplitude of the microbuckles varies from a maximum at the inner surface of the bend to zero at the neutral axis [19]. This is because the bend radius of the innermost surface must be the smallest, with increasing radii through the laminate thickness, and the largest radius at the outer surface, Figure 1-6. If the compression and tension stiffness of the laminate were equal, the neutral axis, defined as a plane in 3D, and an axis in 2D, which is parallel to the bending surface and where the axial stress is zero, would be located in the middle of the thickness. However, the stress required to compress fibers in the microbuckled state is significantly lower than the large stresses required to overcome the axial stiffness of the fibers in tension [18]. This requires the neutral axis to shift toward the outer surface of the bend, as also shown by Figure 1-6, such that moment equilibrium is maintained on both sides of the neutral axis [18].

At high levels of compression, microbuckling can lead to the secondary characteristic response of fiber kinking, which is a known precursor to material failure due to highly localized strain in the region of the kink band [19]. While microbuckling is an elastic instability in the fibers, kinking is a geometric nonlinear response that occurs locally at sites where the fibers are initially misaligned to the load path [19]. In a soft matrix composite, the misalignment can be the result of microbuckling waves, rather than only manufacturing induced fiber misalignment. A kink band, shown in Figure 1-7, is the result of the simultaneous rotation of a band of compression-loaded fibers. This results in laminate compressive failure once the shear yield stress of the matrix material is exceeded [19].

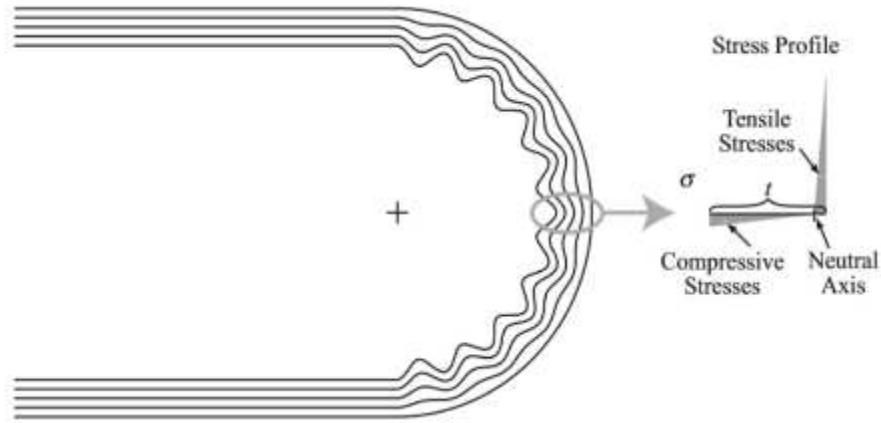


Figure 1-6: Neutral axis shift under compressive stress. [18]

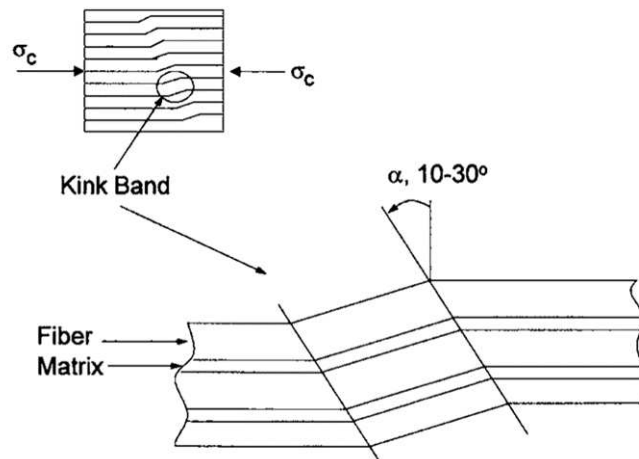


Figure 1-7: Rotation of compression-loaded fibers, resulting in kink band. [19]

The implementation of an EMC as a sandwich structure can further exacerbate the formation of compression microbuckles by increasing the thickness of the laminate that needs to be bent. The limited stiffness of the SM foam core not only forces the compressive stress to be carried nearly exclusively by compression plies located furthest from the neutral axis, but also provides little resistance to transverse buckling amplitude protruding into the core thickness. Lack of a stiff foundation under the compression plies makes it easier for microbuckles to grow in amplitude until global buckling failure occurs, resulting in a single line of fiber fracture through all compression plies.

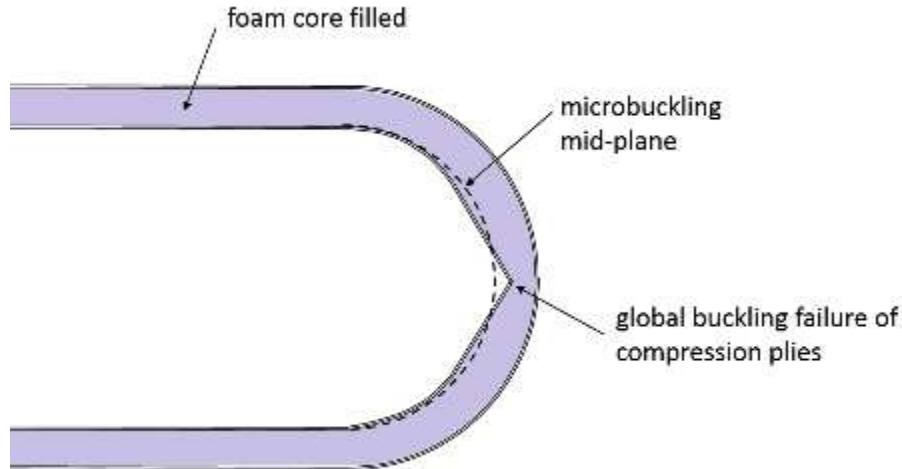


Figure 1-8: Global buckling failure.

1.4 Background

Since it has been established that the mode of failure of a soft matrix composite is excessive fiber buckling, that is manifested as either matrix failure (delamination) or fiber breakage, a method that limits the amount of compressive fiber buckling will improve the conformability of an EMC sandwich panel.

Applying tension to a laminate during bending is one method of reducing compressive load application that was shown to be unsuccessful by Lips et al. [17] and not necessarily helpful by Campbell and Magi [19]. Lips et al. [17] describes bending an IM7 cloth laminate around a mandrel under thirteen pounds of tension (by pulling on ends), caused concentrated kink failure at mid span along the length. Manually constraining the kink formation at this point led to kink formation at other unconstrained locations around the mandrel. By using spring steel in tension behind the sample, rather than tensioning the sample itself, a more uniform pressure was applied, and the specimen was successfully bent 180° around the mandrel [17][17]. The related work presented by Campbell and Magi [19], which includes bending of both tensioned and non-tensioned laminates of the same material, concluded that tensioning does not necessarily delay the onset of microbuckling, or decrease fiber damage.

Campbell and Magi [19] did conclude that the diameter and stiffness of the reinforcing fibers does influence the formation of microbuckles and subsequent kink bands. In an investigation of microbuckling and kinking of unidirectional circular rods in flexure, the comparison of IM7 and T300 reinforcing fibers

showed that the T300 fiber, which has a 40% greater diameter, and an extensional modulus of 20% less than IM7, delayed the formation of microbuckles and subsequent kink bands, until much greater curvatures than the IM7 specimens. While it is of interest to note the influence of fiber selection to the strain capability of a laminate, it was chosen in this work to focus on methods external to changes in the constituent materials.

Similar to the work presented by Lips et al. [17], the addition of an external support to distribute forming pressure is a concept well applied in diaphragm forming of thermoplastic composites. In the work by Monaghan et al. [20], dual diaphragms are installed on both sides of the thermoplastic laminate, and biaxial tension is maintained during 3D forming by clamping around the edges. Experimental forming with several diaphragm materials revealed that a stiffer diaphragm maintains a higher traction force on the laminate, thereby producing a superior surface with no buckling or wrinkling. However, the overall forming pressure required substantially increases with diaphragm stiffness.

The diaphragm forming of thermoplastic sandwich panels has been demonstrated by Schmachtenberg and Strohäcker [21], with panels produced by laminating glass fabric reinforced skins to thermoplastic honeycomb or foam cores. By applying a spring steel sheet on the compression side of the sandwich panel, forming between silicone double-diaphragms produced good 2D bending capability. The authors also chose to heat only one side of the panel to prevent softening of the core. While this work accomplishes good forming ability of fiber reinforced sandwich panels with a softened matrix material, the size of the diaphragm forming apparatus would limit the size of the EMC panels that could be produced. Unlike thermoplastic panels, thermoset polymer-based EMCs cannot be easily bonded or welded together to form larger structures. In addition, the diaphragm forming process is meant to be used once in forming the panel, precluding multiple bending cycles desired in an adjustable, reusable part.

The criteria of an axially stiff material with a small allowable bend radius, that will maintain good traction to the compression surface of the EMC panel, and not require extensive tooling to implement, led to the idea of including a permanently bonded conventional FRP ply on the compression side surface. Because the conventional polymer ply (or plies) is also fiber reinforced, it can be thought of as a potentially

tailorable permanent caul plate, that also serves to increase the functional stiffness of the EMC sandwich when the a part is in use. The conventional thermoset epoxy matrix is still well below its T_g at elevated forming temperatures used for the SMP.

Prior to this study, a mechanical engineering senior practicum project at Colorado State University [22] demonstrated the application of the shape memory sandwich construction on a conformable racecar seat. The shape memory polymer epoxy and SM foam used in that project, CTD-DP-5.1, were the same as those used in this study. The design of the seat, conceptualized in Figure 1-9, featured lateral supports with adjustable regions (highlighted in red) that could be customized to fit a particular driver. The EMC matrix softening at elevated temperature was activated by resistance heating wires (blue lines) embedded in the laminate.

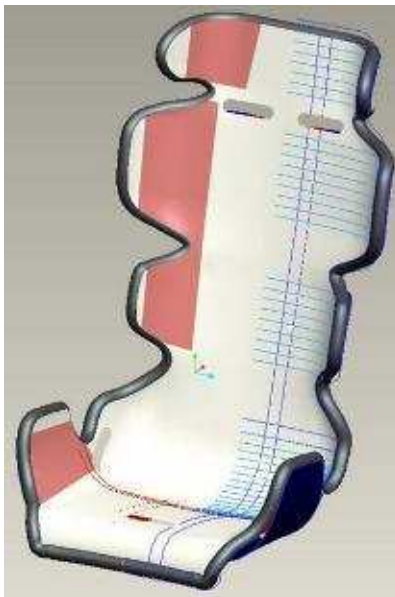


Figure 1-9: Conceptual heating zone model of conformable racing seat.[22]

The conformable seat design incorporated a ply of plain weave carbon cloth containing a conventional epoxy resin matrix (EPON™ Resin 828 cured with EPIKURE™ Curing Agent 3140), as the inner surface ply of the otherwise EMC sandwich laminate [22]. The manufacturability tests performed by the student team demonstrated that a 100% shape memory sandwich panel would fail by compression side facesheet buckling into the core when bent around a mandrel (Figure 1-10). By adding of a compression surface ply

containing conventional epoxy, 828/3140, full bending around the mandrel could be achieved without any local core thinning [22]**Error! Reference source not found..** This increase in capability was also demonstrated in preliminary work, which took place under controlled conditions [23][24].



Figure 1-10: Localized compression facesheet buckling of a 100% SM sandwich panel. [22]

It was observed that adding a ply containing conventional epoxy resulted in compression of the foam core at the center of the panel during bending. The increased pressure required to bend the stiffer laminate exceeded the compression strength of the core, causing thinning. Since thinner core will reduce the moment of inertia of the sandwich panel, and thus reduce the flexural stiffness of the panel in operation, the proposed remedy was an elbow structure at predicted bend locations (Figure 1-11a) [22]. By profiling the core to include a locally thicker region at the center of bending, the minimum required stiffness of the panel can be maintained at all adjustment configurations.

It was further observed that the stiffening of the compression facesheet resulted in increased shear strain in the core, which is most obvious at the ends of the panels. While lack of shear closeouts at the end of EMC panels is helpful to accommodating relative facesheet motion during bending, it results in lower flexural stiffness during structural use. Additionally, shear closeouts may be necessary to prevent exposure of the core to the environment, provide ease of handling, or for aesthetic reasons. In the case of the conformable racing seat, the shear end constraint was not a discrete component, but a consequence of local heating. The material surrounding the heated zone remained at a lower temperature and therefore at a higher stiffness. Shear end constraint due to incomplete heating of a part would also occur with very large structures, for which it would be uneconomical to build a large heating chamber. For these reasons, it is

necessary to investigate the change in the behavior with and without shear constraints or when the panel is locally heated only in the region of bending.

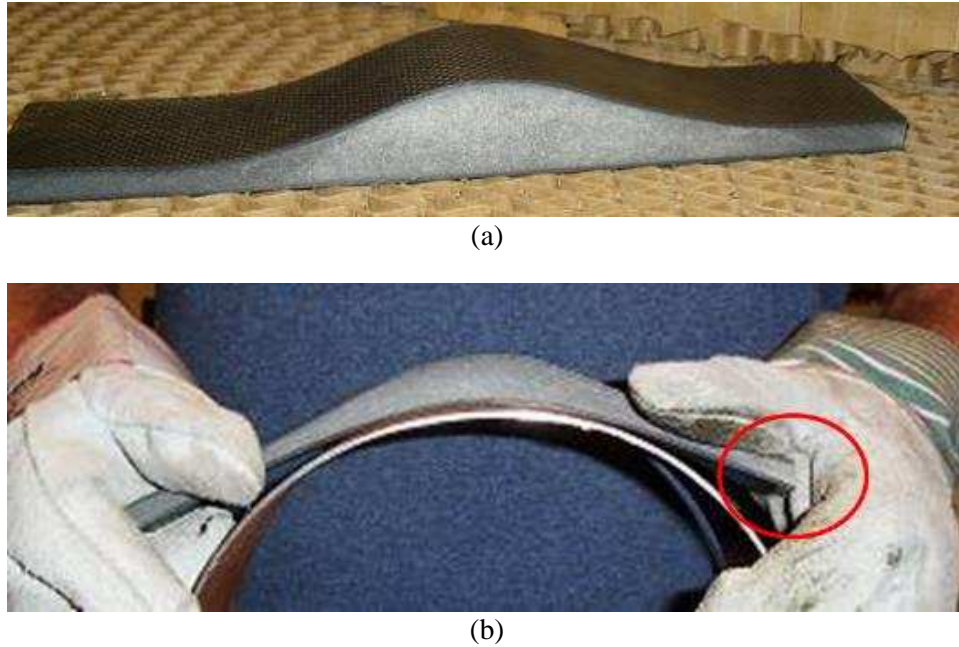


Figure 1-11: Profiled core sample with one ply of conventional matrix epoxy. [22]
(a) Beam in neutral state before bending. (b) Shearing of the core is apparent at the sample end during bending.

Previous work on SMCs and EMCs in the literature primarily focuses on solid laminates which do not have the potential flexural stiffness to weight advantages, nor the inherent drawbacks of incorporating a low compression stiffness foam with an axial reinforcement that fails due to lack of out-of-plane stability. Due to the complex viscoelastic behavior of shape memory polymers, numerous studies have proposed kinematic and mathematical models to predict the response of the solid polymer to thermomechanical cycles, with moderate success [25][26][27]. The additional interaction of the polymer with fiber reinforcements has resulted in general recommendations on the design of SMCs [11][13][19][29], solid laminate behavior prediction models [3][17][28][30][31], and micro-mechanics-based calculation of critical fiber and matrix failure modes [11][13][18][19][29] [31][32]; but has proven exceedingly difficult to predict on the whole with analytical methods. While some behavior of a SMC sandwich panel can be traced back to SMP kinematics and beam bending theory, the implementation portion of SMC sandwich

technology can be currently best addressed by experimental characterization. Documentation of experimental characterization testing for both SMPs and SMC solid laminates are readily available [7][12][17][18][19][25][29][30][33][34].

1.5 Thesis statement

The addition of conventional epoxy matrix plies to the compression surface of a shape memory composite sandwich panel can reduce or eliminate the buckling failure of the compression-side facesheet during large-scale deformation in flexure.

1.6 Objectives of work

Demonstrate and quantitatively compare the improvement in bending capability of shape memory sandwich panels by the addition of conventional matrix plies. Illustrate the viscoelastic response of shape memory composite sandwich panels in flexure with and without conventional matrix reinforcement, and with and without shear end constraints.

1.7 Research approach

This research intends to demonstrate the viscoelastic and geometric response of shape memory composite sandwich panels by subjecting representative sandwich beams to thermo-mechanical variables known to induce viscoelastic response in the neat polymer and shape memory composite solid laminates. The bending capability of the beams is assessed in 3-point bending with and without a varying number of conventional matrix plies. Shear end constraints are implemented in a portion of the beams by bonding phenolic blocks to the ends of the shape memory foam core. Continuous fiber facesheets extend over the bond lines, incorporating the phenolic blocks into the sandwich structure. Due to the highly novel subject of this work, and the limited supply of elastic memory materials, the purpose of the experiments is not to thoroughly characterize the response of the composite. Rather, it intends to provide proof of concept and to document gross trends expected in an application.

Variables identified as most likely to influence the response are:

- Bending temperature

- Number of conventional polymer plies
- Shear end constraints to simulate local heating
- Loading rate
- Hold time at maximum strain

Test specimens are prepared by wet layup of plain weave carbon cloth with commercially available thermoset resin and hardener system, CTD-DP5.1, developed by Composite Technology Development (CTD), Incorporated. Foam core is also produced by CTD, by foaming the DP5.1 epoxy. EPON™ Resin 828 cured with EPIKURE™ Curing Agent 3140 at 45 parts-per-hundred is used as the conventional epoxy. Freestanding post cure for 6 hours at 120°C is performed on the room temperature cured laminate to raise the T_g of the conventional matrix above the maximum test temperature.

Bending tests are performed on an ATS 900 screw drive load frame, with the beam samples and load fixture enclosed in an environmental chamber.

The following observations were used to compare the behavior of the samples:

- Required bending load
- Deflection at failure
- Failure mode
- Core thickness
- Elastic strain component (spring back)
- Loading cycle hysteresis
- Pre- and post-failure stiffness

2 THEORY

The behavior of a shape memory composite sandwich panel in flexure strongly reflects the viscoelastic properties of the shape memory matrix and foam core, but also includes strain and failure modes that are typical of fiber reinforced polymers or sandwich structures. The purpose of this section is to summarize the individual characteristic behaviors that are typically used to describe the complex response of EMC materials.

2.1 Overview of polymer viscoelastic behavior

Polymer materials exhibit a time-dependent response to stress or strain input that is not purely elastic, nor purely viscous. While a linear elastic material is represented in a kinematic model by a spring and a viscous material by a dashpot, viscoelastic materials are typically modeled as some combination of springs and dashpots in series, in parallel, or both.

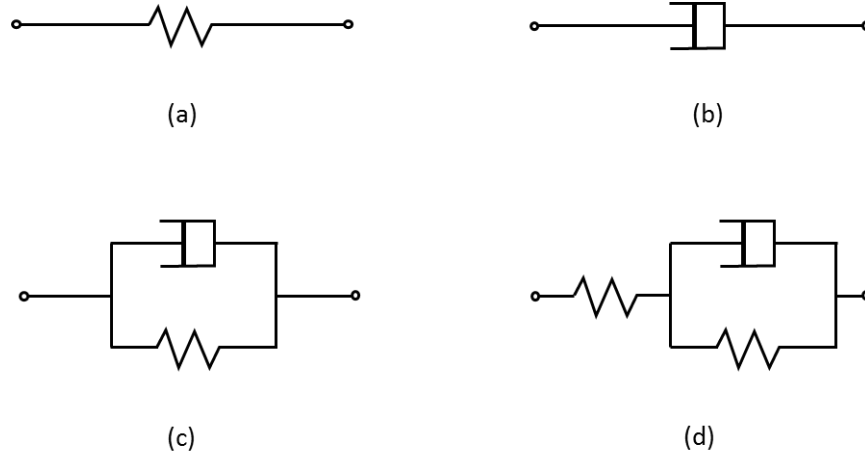


Figure 2-1: Kinematic model examples.

(a) elastic solid "spring", (b) viscous fluid "dashpot", (c) Kelvin solid, and (d) 3-parameter solid.

A purely elastic material is likened to a spring because it strains linearly with increasing or decreasing stress. The strain reaction is instantaneous, and does not change as long as the stress remains constant. All stress applied to the material is stored as strain energy, and is completely recoverable as mechanical work that can be performed by the material as it returns to its unstrained shape. Deformations due to external loads are completely, and instantaneously reversible upon load removal.

A purely viscous material, such as a fluid, and likened to a dashpot, will strain indefinitely in response to applied constant stress. Therefore, the degree of strain response is dependent on the duration of load application. There is no storage of mechanical energy in the viscous material as a result of the strain. When the applied external load is removed, the strain state will remain as-is, and is completely irrecoverable.

The viscoelastic models in Figure 2-1(c) and (d) simulate an initial strain when load is applied, due to the spring, followed by additional time-dependent strain of the dashpot. The time-dependent portion of the strain is creep. If the load is removed after creep has occurred, the initial state of the material is not immediately restored. Over time, the elastic energy stored in the spring acts on the dashpot, leading to creep recovery.

The dependence on time can be demonstrated by the difference in the stress-strain relationship curves in loading and unloading (Figure 2-2). The path of the elastic stress-strain curve indicates that regardless of loading time and rate, the energy input to the material is the same as the energy output. The loop formed by the viscoelastic stress-strain curve indicates the loss of recoverable energy from the material, since more work is applied to cause deformation than is recoverable during strain recovery. For a given material and specified temperature, the amount of irrecoverable work is dependent on the rate of load or strain input, the maximum strain introduced, and the rate of unloading used to measure recovery.

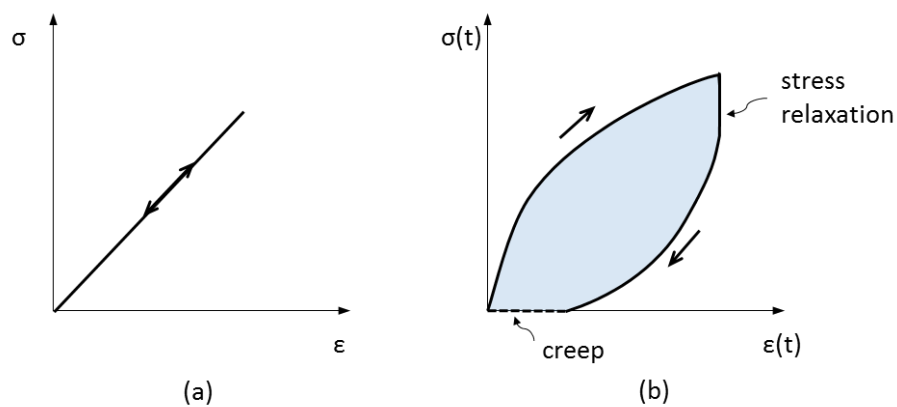


Figure 2-2: Stress-strain curves.
(a) Elastic material and (b) viscoelastic material.

Two time-dependent responses characteristic of viscoelastic polymers, which reduce the recoverable strain energy, are stress relaxation and creep. Since the deformation mechanism requires time for chain uncoiling of the long polymer molecules [35], the degree of response is dependent on the time over which the load or strain is applied. Stress relaxation is best observed as a drop in the stress required to maintain the strain level in a material over time (Figure 2-3). The limit of stress relaxation in a thermoset polymer at $t = \infty$, is due to the presence of permanent bonds between polymer chains, called crosslinks, which are absent in thermoplastics. Crosslinking also limits the maximum creep in a thermoset, and can prevent the polymer chains from uncoiling enough to incur permanent residual deformation.

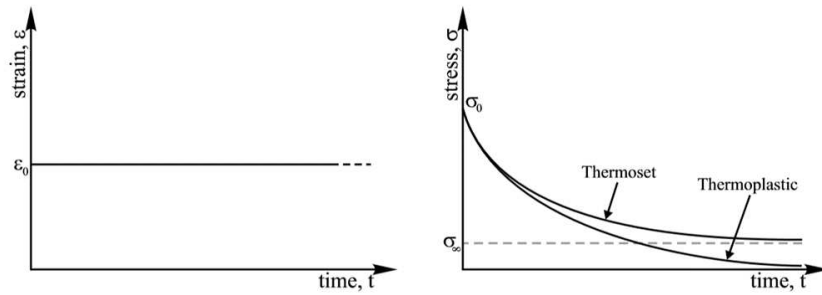


Figure 2-3: Stress relaxation result. [35]

If strain is held constant, and stress is a function of time, modulus must also vary with time [35]:

$$\sigma(t) = \varepsilon_0 E(t) \quad (2.1)$$

Creep is measured as a change in strain over time, under a constant applied stress (Figure 2-4). Similarly, creep strain recovery, after stress is removed, is also used to characterize polymer response.

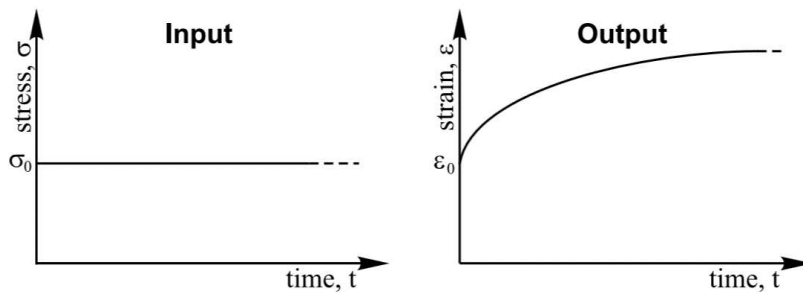


Figure 2-4: Creep test result. [35]

If stress is held constant, and strain is a function of time, then the response is defined by the creep compliance, $D(t)$.

$$\varepsilon(t) = \sigma_0 D(t), \quad (2.2)$$

The creep compliance of a thermoset is governed by both mechanical chain entanglement and crosslinks, but at equilibrium, the behavior is principally due to crosslinks [35].

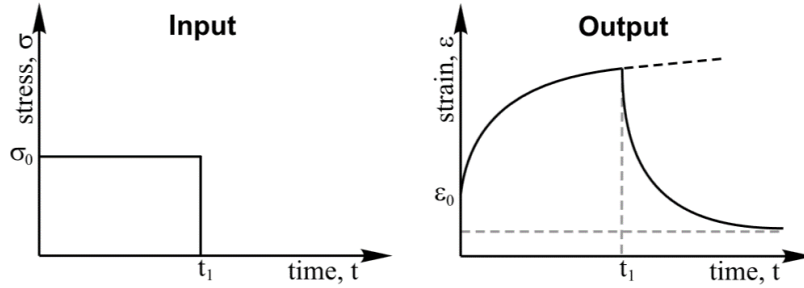


Figure 2-5: Creep strain recovery. [35]

Hysteresis is used to describe both the loss of strain energy input to the material that is dissipated as heat or permanent molecular rearrangement, as well as the rate-dependent delay in response between input and output. As shown in Figure 2-2(b), for a given loading-unloading cycle, the area inside the loop formed by the stress-strain plot quantifies the amount of irrecoverable energy that has been lost to the viscous component of the material response. In the case of a sufficiently crosslinked thermoset, the crosslinks will prevent permanent molecular rearrangement, such that all strain energy is theoretically recoverable, given a slow enough cycle rate.

2.2 Shape memory polymer behavior

When heated above the glassy state, shape memory polymers exhibit viscoelastic behavior similar to other polymers; however, the characteristics of these SMPs make them suitable for active material applications. As stated previously, SMPs have been shown to recover large strains, up to 300-400% [2][6][7]. The strain-recovery cycle is highly repeatable, and recovery occurs autonomously, with only the application of heat. A dramatic change in mechanical properties occurs within the glass transition region, including a decrease in elastic modulus, which is typically around two orders of magnitude. Due to the

significant sensitivity to temperature, a large amount of strain energy can be stored in deformed, then cooled state. This drives an increase in stress required to maintain the strain as the SMP is cooled. The strain energy due to modulus change is so large that it can affect shape stability by inducing spring back, and it can be used to provide actuation to other parts in a system upon reheating.

The T_g of CTD-DP-5.1 EMC epoxy resin, as determined by torsional DMA testing, is considered to be 71°C. From the resulting plot of shear modulus, G , complex shear modulus, G^* , and the ratio of G^*/G in Figure 2-6, it was shown that modulus variations occur throughout a range of temperatures, rather than at a discrete activation value, with the most variation occurring between 20 and 80°C. The T_g of the resin is defined as the peak of the G^*/G curve, which occurs at 71°C [25].

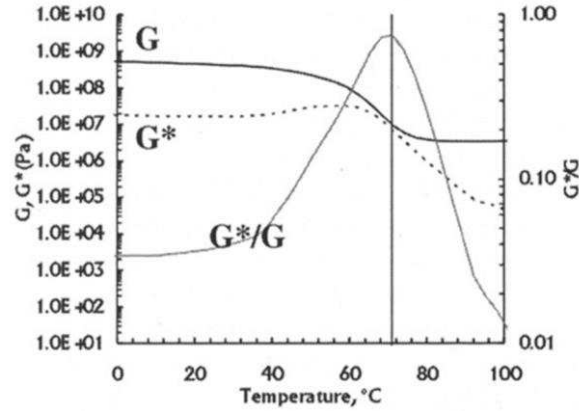


Figure 2-6: Torsional DMA plot of CTD-DP-5.1 [25]

2.3 Kinematic model

As with other polymers, attempts have been made to characterize the viscoelasticity of SMPs with kinematic models. A well-referenced thermo-mechanical constitutive model has been proposed by Tobushi et al. [26], based on testing of thermoplastic shape memory polyurethanes, and forms the basis of many models in the current literature, both thermoplastic and thermoset. In this model, E_1 and E_2 are moduli of linear spring components that govern the elastic response of the material. The dashpot, with viscosity μ , replicates the sensitivity to loading rate, and determines the amount of load applied to spring E_1 . Element μ is effective at all temperatures, although the amount of resistance provided will vary with temperature. The significant component of this model is the slip element, ε_s , which expresses a value of irrecoverable

strain related to internal friction, that is temperature dependent, but not rate dependent. Below the slip initiation temperature the element is completely closed, and causes E_2 to be fully active. Some slip occurs at intermediate temperatures, manifested as irrecoverable strain, and element E_2 is partially loaded. At high temperatures, the slip element is fully open and sliding freely, such that E_2 is not loaded and the deformation stress is governed by only μ and E_1 . Neither the dashpot nor the slip element can store energy for recovery by elastic strain at any temperature.

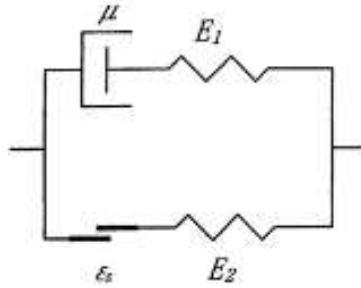


Figure 2-7: Four-element constitutive model proposed by Tobushi et al. [26]

The relationship between ϵ_s and ϵ_c , the creep strain, is expressed by the equation,

$$\epsilon_s = C(\epsilon_c - \epsilon_l) \quad [26] \quad (2.3)$$

where ϵ_l , the critical strain value, and constant C , are dependent on temperature. The stress-strain relationship in the four-element model is expressed as,

$$\epsilon(t) = \frac{\sigma(t)}{E} + \frac{\sigma}{\mu} - \frac{\epsilon - \epsilon_s}{\lambda} \quad [24] \quad (2.4)$$

where μ and λ represent the viscosity and retardation time, respectively.

At elevated temperature, internal friction is small, which results in a large ϵ_l , and strain is easily recovered, reflected by a small C value. Conversely, at low temperature, ϵ_l is small and C is large [26]. Therefore, this equation expresses that at elevated temperatures a large amount of creep strain is both easily produced and recovered, due to low internal friction and although only a small amount of creep may be produced at lower temperatures, a large portion of that creep is irrecoverable because it was produced by overcoming high internal friction.

A lumped-parameter model was proposed by Abrahamson et al.[25], based on tests of the solid CTD-DP5.1 epoxy. This model, Figure 2-8, which also includes four elements, principally differs from other viscoelastic models by including a friction slider element that allows the change in elastic modulus to be activated not only by a change in temperature, but also by induced strain at temperatures below T_g . For the purpose of this research, a key difference between the lumped-parameter model and the previously presented model proposed by Tobushi et al. [26], is the spring, E_t , which provides a constantly present recovery force, meaning no plastic strain can be induced.

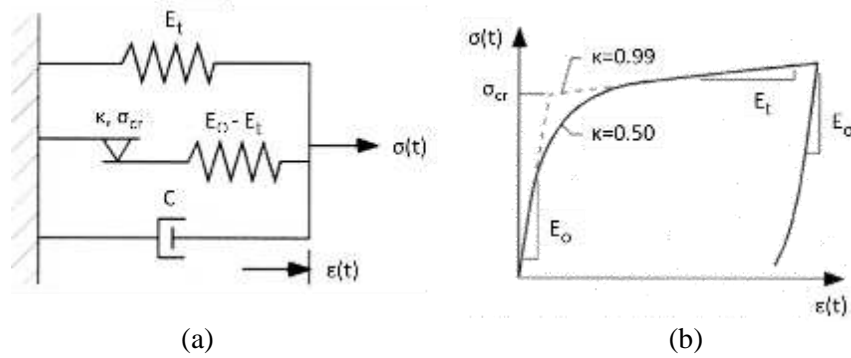


Figure 2-8: Viscoelastic lumped-parameter model. [25]
(a) Spring-dashpot diagram and (b) typical stress-strain curve.

The friction slider also controls the stress-strain relationship at the transition between the two characteristic elastic states, Figure 2-8. The stick-slip stress, σ_{cr} , is highly dependent on temperature, decreasing to zero as temperatures approach T_g . At lower temperatures or low strains, the slider is fully stuck and the response follows the first elastic modulus, E_o . The κ parameter, which is restricted to the range, $0 \leq \kappa \leq 1$, and analogous to a coefficient of friction, controls the rate of the slider's transition between stuck and slipping, while σ_{cr} is the threshold at which the change occurs. Once σ_{cr} is exceeded, the elastic modulus becomes E_t . Equation 2.5 defines the relationship between the parameters, assuming a constant test strain rate, $\dot{\epsilon}_{test}$.

$$\sigma_{n+1} = \sigma_n + E_o \dot{\epsilon}_{test} \Delta t \left\{ \frac{1 + (\text{sgn}(\dot{\epsilon})/\sigma_{cr})[E_t \dot{\epsilon}_{test} n \Delta t - \sigma_n]}{1 + \kappa (\text{sgn}(\dot{\epsilon})/\sigma_{cr})[E_t \dot{\epsilon}_{test} n \Delta t - \sigma_n]} \right\} \quad [25] \quad (2.5)$$

Δt is the numerical integration time step, n is the number of the time step, and σ_n is the stress at the n th time step[25]. The parameters, which vary with material temperature, were derived numerically (Table 2-1), and the model was compared to test data with favorable results.

Table 2-1: Numerically derived constitutive parameters for CTD-DP-5.1

Temperature (°C)	E_o (MPa)	E_t (MPa)	σ_{cr} (MPa)	κ
25	470	3.7	20	0.85
35	410	7.7	13	0.65
45	76	5.5	10	0.15
55	4.8	4.4	0.69	0.10
65	6.2	5.2	0.69	0.05
85	5.4	5.4	—	—

This indicates, that in addition to being temperature dependent, the drop in elastic modulus may also be triggered by the strain level of the material. In this example, the tensile strain around 3% to 5%, which is contrary to the typical assumption that the elastic modulus transition can only occur at temperatures within or above the glass transition region. The published T_g of the CTD-DP5.1 epoxy is 71°C[25], but the strain-activated modulus transition was demonstrated below 45°C, far below the thermally activated transition region.

2.4 Spring back

After a composite panel is formed or bent to the desired curvature and cooled to operational temperature, it is of interest to predict what portion of the strain will be immediately recovered once the strain-inducing constraints are removed. For composites fabricated with CTD-DP5.1 epoxy, geometry is considered stable at room temperature, ~25°C in this work. If the EMC part is to be used as a structural component, the long-term shape stability could significantly affect the performance of the part. While a small amount of spring back has been observed in the unreinforced polymer, as discussed in section 2.2.1, the modulus is so low at storage temperature, that it is unlikely to overcome the internal friction in the polymer.

Once reinforcing fibers are added to the polymer, the fibers do not have an appreciable change in properties within the ~20-90°C temperature range used for SM activation, and maintain their stored strain

energy when packaged. The addition of conventional epoxy plies to the EMC sandwich, to form a hybrid composite, means that not only the fibers, but also the conventional epoxy matrix will store strain energy that resists the deformed shape after cooling. At deformation temperature, the conventional epoxy matrix is still in the glassy state, thus any strain induced in this material is a source of elastic energy.

Elastic spring back observed by Lips et al. [17] during bending tests of IM7 cloth-reinforced CTD-DP5.1 solid laminates averaged roughly 15° , from an initial angle of 180° , where the angle was defined as the inside angle formed by the bend. Furthermore, informal observations revealed additional angle losses up to 15° over a four-day period, for a total loss of 30° .

In the current research, the shape of the bent sandwich panels is not directly measured. However, the remaining load measured by the load cell to maintain the as-bend deflection once the sample is cooled, is considered an indication of the shape instability of the sample. The spring back load will be compared to the number of conventional matrix plies, and is predicted to increase sharply with added plies.

2.5 Beam bending approximation

Although elementary beam theory is not properly applicable for large deflections, the method can be used to indicate the relative bending capability of each sandwich configuration. Comparisons have been made with the calculated location of the neutral bending plane (neutral axis), as well as the calculated bending load, between the selected sample types. Since the samples are expected to fail exclusively in compression, these properties are considered reasonable predictors of relative sandwich beam bending capabilities.

2.6 Sandwich composite constituent material properties

Elastic memory polymer CTD-DP-5.1 neat epoxy has published elastic moduli of $E \approx 100$ ksi below T_g , and $E \approx 1.0$ ksi above T_g [17]. Assuming a 50% volume fraction of T300 plain weave carbon fabric, with a modulus of 32 Msi, to shape memory matrix, the calculated tensile moduli of the shape memory composite lamina are $E \approx 8.05$ Msi below T_g , and $E \approx 8.00$ Msi above T_g . The shape memory matrix is not stiff enough to prevent the fibers from buckling under compressive load. Therefore, the capability of the fibers is

ignored, and the neat epoxy elastic modulus, $E \approx 1.0$ ksi, was used as the compressive stiffness above T_g in prediction calculations.

Manufacturer data for EPONTM Resin 828 cured with EPIKURETM Curing Agent 3140 at 45 parts-per-hundred specifies a tensile modulus of 420 ksi and a heat deflection temperature of 97°C [36]. The conventional epoxy laminate, also at 50% V_f , is assumed to have a moduli of $E \approx 8.21$ Msi at room temperature. This modulus is assumed constant throughout all test temperatures.

Preliminary tension and compression tests of the shape memory foam produced average elastic moduli values of $E \approx 3.40$ ksi at 22°C, and $E \approx 0.02$ ksi at 90°C [22].

2.7 Sample predictions

The comparison of sandwich beam properties is made generically for a temperature below T_g , and for a temperature above T_g , in order to discuss the basic differences in beam performance. Since failure of the beam is expected to occur due to compression of the SM laminae, the distance, c , is calculated from the neutral bending plane of the beam, to the maximum compression surface of the EMC plies. This means that smaller values of c will allow a smaller bending radius at a given beam stiffness, as long as the compression strength of the conventional epoxy plies is not exceeded. Predicted beam properties, from elastic beam theory, are summarized in Table 2-2.

Table 2-2: Calculated beam section bending properties.

Temp	# Conventional Composite Plies	Composition (from compression surface)	# Compression /Tension Plies	Nominal Thickness (in)	^c (to SM Max. Compression Surface) (in)	Bending Moment of Inertia (in ⁴)
< T _g	0	(3)SM, Core, (3)SM	3/3	.310	.155	1.16E-03
	1	(1)CP, (2)SM, Core, (3)SM	3/3	.310	.145	1.16E-03
	2	(2)CP, (1)SM, Core, (3)SM	3/3	.310	.134	1.17E-03
	1	(1)CP, (3)SM, Core, (3)SM	4/3	.320	.132	1.38E-03
> T _g	0	(3)SM, Core, (3)SM	3/3	.310	.295	2.95E-06
	1	(1)CP, (2)SM, Core, (3)SM	3/3	.310	.211	6.29E-04
	2	(2)CP, (1)SM, Core, (3)SM	3/3	.310	.159	9.68E-04
	1	(1)CP, (3)SM, Core, (3)SM	4/3	.320	.219	6.73E-04

CP = Conventional 828/3140, 45 phr epoxy matrix

SM = Shape Memory

The inclusion of conventional composite plies in the sandwich beam reduces the distance from the maximum EMC compression surface to the neutral plane in two ways; first by increasing the overall stiffness of the compression facesheets, and secondly by replacing the outermost EMC plies, which are furthest from the center of the sandwich. Below T_g, which represents the operational temperature of the structural EMC, the change in bending stiffness is minimal, due to the similar elastic moduli of the two epoxy systems. Above T_g, both the location of the neutral plane and the moment of inertia are strongly influenced by including a single conventional epoxy ply to the layup. However, while a similar gain in neutral plane location is achieved by replacing a second ply, the increase in stiffness is less pronounced.

The comparison can be made between replacing a SM ply with a conventional ply and adding a conventional ply to an existing EMC sandwich panel. At elevated temperature, the additional ply adds extra thickness and bending stiffness, but does not affect \bar{y} as positively as replacing an SM ply. Also of importance, is the concern that adding an extra ply creates an asymmetric laminate, affecting structural performance.

2.8 Shear end constraints

Whether due to local heating or edge closeout of the sandwich laminate to prevent exposing the open cell core to moisture, unconstrained shearing of the core throughout the bending region is unlikely in a structural application. The 3-point bend tests conducted on the sandwich beams introduce both bending moment and shear. Testing samples both with and without shear end constraints provides useful data on how the bending progression differs when compression stress on the inner radius cannot be relieved by core shear.

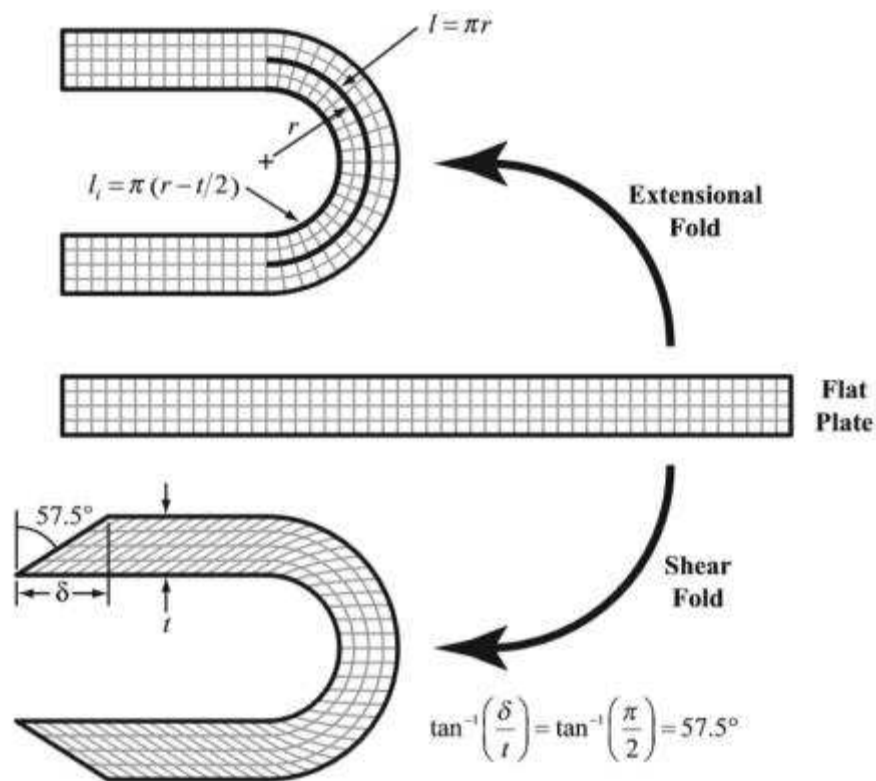


Figure 2-9: Ideal geometry of shear and extensional folding. [18]

The shear fold shown in Figure 2-9, provides an idealized view of flat panel bending with zero shear resistance, assuming that the inner bend radius can be achieved without facesheet failure. The lengths of the inner and outer surfaces remain constant because the difference in curve length at the bend results in through-thickness shear, and a difference in length at the panel ends. The extensional fold that is also shown, does not shear at the ends, however it assumes that the panel is capable of shortening or lengthening

in the bend region, in response to induced compressive and tensile stresses. While a change in length may be possible for the solid SM epoxy, the carbon fibers in the current sandwich beams prevent elongation of the facesheets, even when the matrix is softened at elevated temperatures. Some localized compression buckling may occur on the inner plies before matrix failure, but not to the extent required to facilitate extensional folding.

2.9 Failure modes

Failure morphology of individual test specimens must be identified and documented in order to assess and improve the flexural capabilities of EMC and EMC/conventional epoxy matrix hybrid sandwich structures. The primary failure modes associated with EMCs and sandwich panels are discussed in the following paragraphs.

2.9.1 Matrix failure

The matrix of an SMC is most susceptible to failure in tension or shear, resulting in delamination of the plies. Although the solid epoxy is capable of recoverable strains up to 400% [2][6][7], the strain restrictions imposed by the addition of significantly stiffer carbon fibers, limits the allowable composite strain to around 5% [16][17][18]. The fiber microbuckling motion that allows SMCs to achieve higher effective compression strains, relies on matrix shearing between the fibers, and a lower fiber volume fraction lessens the amount of strain required. A fiber volume fraction of 40% is recommended for EMC laminates in order to allow fiber motion without causing matrix failure [17][32], whereas typical carbon reinforced composites contain around 60%. The plain weave fabric utilized in laminate preparation includes transverse tows that both restrain large global buckling delaminations due to matrix failure, and serve as local strain intensifiers, by preventing strain distribution by fibers held beneath the tows.

2.9.2 Core failure

Foam failure initiates when excessive tensile, compressive, or shear strain causes tearing or crushing of the cellular structure. DP5.1 foam is open celled, meaning that thin ligaments of polymer maintain a lattice-like network that is permeable by other materials. Testing performed on a similar thermoset foam,

TEMBO® 3XE, which is a trademarked proprietary foam also produced by Composite Technology Development, demonstrated full strain recovery from up to 80% compression in multiple cycles [15]. Shear is assumed to be the primary strain that can initiate core failure in the beam samples. Within the range of bending allowed by the test fixture, shear strain to failure of the core is not believed to be a limiting failure mode.

2.9.3 Fiber failure

As discussed in section 1.3, the carbon fibers are the stiffest component of the sandwich structure, and due to their extremely high aspect ratio, are highly susceptible to compressive failure. The incomplete lateral stability provided to the fibers by the SM epoxy above T_g , allows some amount of compressive strain to be accommodated by sinusoidal microbuckling of the fiber, which is a bending deformation mode, not an axial strain [18]. Although fiber microbuckling is the primary mechanism that allows SMC materials to achieve high bending strains, if the strain limits of the fiber is exceeded composite failure will occur [30]. If the strain limit is assumed to be due to the allowable curvature of the microbuckled fiber, then the effective strain can be calculated from the maximum curvature induced by the sinusoidal shape [18].

The maximum fiber curvature occurs at the peak, or trough, of the sinusoid and can be calculated by

$$R_f = \frac{\lambda^2}{\pi^2 a_o} \quad [18] \quad (2.6)$$

where λ is the micro-buckle wavelength, and a_o is the amplitude. The effective extensional strain due to fiber bending is given by,

$$\epsilon_{effective} = \frac{1}{1 + \frac{4}{\pi^2} \left(\frac{\lambda}{a_o} \right)^2} \quad [18] \quad (2.7)$$

By combining equations (2.6) and (2.7), the maximum effective strain that can be accommodated by a microbuckled fiber can be calculated by,

$$\epsilon_{effective} = \frac{1}{1 + 4\pi^2 \left(\frac{R_f}{\lambda} \right)^2} \quad [18] \quad (2.8)$$

for a known or experimentally determined allowable fiber curvature.

However, this effective strain calculation assumes the fiber is free to microbuckle at an ideal wavelength. In application, microbuckling is limited by fiber volume fraction, which is directly related to the amount of matrix shear strain required for fiber motion, as well as geometrically induced buckling initiation sites, such as edges of overlapping tows in woven fabric, and regions of fiber misalignment due to manufacturing. The process of weaving also introduces kinking to the fibers at the overlap locations, further reducing the compressive strength of individual fibers. In testing, failure due to excessive fiber bending may be visible on the compression surface as a line of fiber fracture through individual tows, and may or may not be accompanied by delamination.

Woven fabrics are commonly used to improve ease of handling during composite fabrication, as well as provide in-plane geometric stability transverse to loading, due to containing fibers oriented at 90° to the load path. Bending tests documented by Gall et al. [11] on fabric reinforced EMCs, showed that while the bend in a tow weaved under a transverse tow provided a favorable nucleation site for buckling, use of plain weave carbon fabric provided more consistently dispersed initiation sites as opposed to a few “highly favorable” sites in a satin weave.

2.9.4 Sandwich panel failure

The failure of the sandwich panel can occur as either a single component failure, as discussed in the previous paragraphs, or as a global failure, only made possible by the sandwich configuration. Global failure modes include disbonding of the core/facing interface, indentation failure under concentrated loads, and global buckling of the compression facesheet into the core [37]. While one mode of failure may occur initially, because that mode can then trigger and interact with other modes, the final failure mode can be completely different [37].

In 3-point bend testing of typical non-SMC, sandwich panels the force-displacement output can indicate the type of failure that has occurred. If the force decreases slowly and continuously, core indentation failure is indicated. Force spontaneously dropping is typical of delamination [38].

3 EXPERIMENTAL

The size of the EMC sandwich panels used in testing were limited by the available materials, and the maximum span of the 3-point load fixture. Additionally, it was decided to uniformly heat the entire test sample, which required enclosure in a heating chamber.

The foam block that yielded the core material is shaped by the walls of the enclosure in which foaming of the epoxy takes place. The upper surface rises unconstrained, not unlike a loaf of bread, and it is known that the bottom of the block has the highest density, with a decreasing density gradient through the height. To reduce the difference in density between samples, the foam was sliced in sheets parallel to the foaming direction (Figure 3-1). Therefore each sample contained foam from both the upper and lower portions of the block.

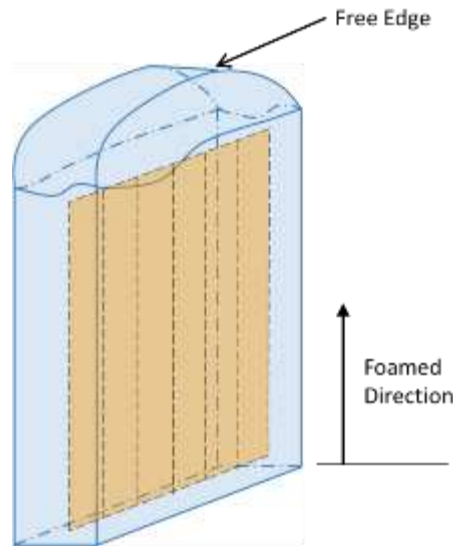


Figure 3-1: Orientation of sandwich cores cut from an SMP foam block.

To promote core shear over core compression, it is desirable to make the beam samples as long as possible, to keep the flexural stiffness of the beam lower than the compression stiffness of the foam. However, the maximum span of the 3-point loading rollers is 7.5 inches. Since variations in strain through the depth of the beam are assumed to be minimal, a nominal width of 1.0 inches was chosen to simplify beam calculations.

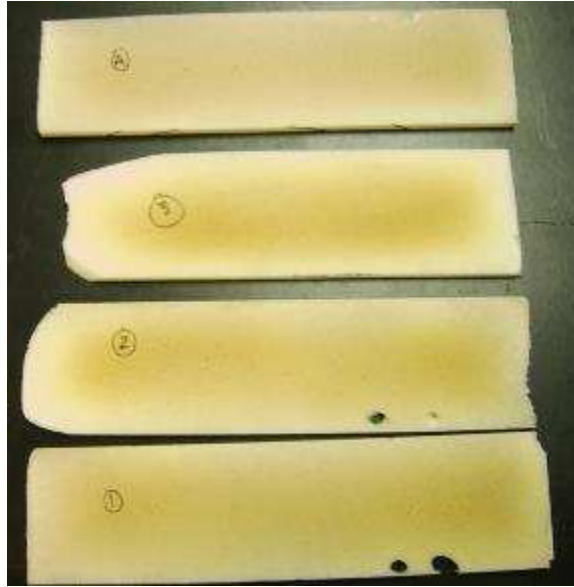


Figure 3-2: SMP foam slices.

3.1 Manufacturing

The trademarked TEMBO® thermoset shape memory resin and hardener system, CTD-DP5.1, was developed and provided by Composite Technology Development (CTD, Lafayette, CO). Open cell foamed blocks of DP5.1 were also provided by CTD. To produce core for the beam samples, a single foam block was sliced into 0.25-inch thick sheets with an industrial foam cutter. EPON™ Resin 828 cured with EPIKURE™ Curing Agent 3140 at 45 parts-per-hundred produced conventional epoxy behavior where needed. Plain weave T300 carbon fabric, 5.6 oz/ sq yd, provided continuous fiber reinforcement oriented at 0°/90° to the length of each beam.

Sandwich samples were prepared by wet layup in six-sample plates and had open core ends or were closed-out with phenolic blocks. Phenolic blocks an inch in width and 0.25" thick were bonded to the ends of the foam sheets with 828/3140, for a total beam length of about 10". Open-ended samples were 9" in length. The carbon cloth was impregnated with shape memory resin over the length of the foam and with 828/3140 over the phenolic blocks. In samples with hybrid compression-side facesheets, shape memory resin was replaced by 828/3140 epoxy in one or more outer plies. One ply of un-sized peel ply was applied to the upper surface of the laminate to bleed off excess resin and cotton breather was used to provide an airflow path to the vacuum port. Once foam core was included in the laminate, a thick steel plate, which

spanned between the phenolic blocks, was used to protect the core from being compressed by vacuum pressure when the curing epoxy produced exothermal heat. Loose phenolic blocks were used to support the steel plate above lay ups without shear end constraints. Although, fiber volume fraction was not strictly controlled during layup, it is assumed to be around $V_f = 50\%$, based on typical layup procedure.

Samples were initially cured under vacuum pressure at room temperature, about 20°C, for at least 20 hours. The 828/3140 required a free-standing post cure at 120°C for six hours to generate a T_g above the test temperatures, a requirement which was had been established by previous DSC testing. Analysis was not performed on the proprietary materials provided by CTD. However, it was verified with CTD that exposure to the post cure process would not damage the EMC epoxy or foam. A diagram of the laminate stack up, relative to the flat tool surface is shown in Figure 3-3.

The step-by-step procedure for sample manufacture is as follows:

1. Bond foam core to phenolic blocks with conventional epoxy (if applicable). Cure at room temperature, unconstrained, for 24 hours.
2. Lay-up conventional epoxy plies (if applicable). Cure at room temperature, under vacuum bag, for 24 hours.
3. Lay-up compression-side shape memory plies. Cure at room temperature, under vacuum bag, for 24 hours.
4. Bond core to compression facesheet. Cure at room temperature, under vacuum bag, for 24 hours.
5. Lay-up tension-side shape memory plies. Cure at room temperature, under vacuum pressure, for at least 20 hours.
6. Freestanding post cure for 6 hours at 120°C.

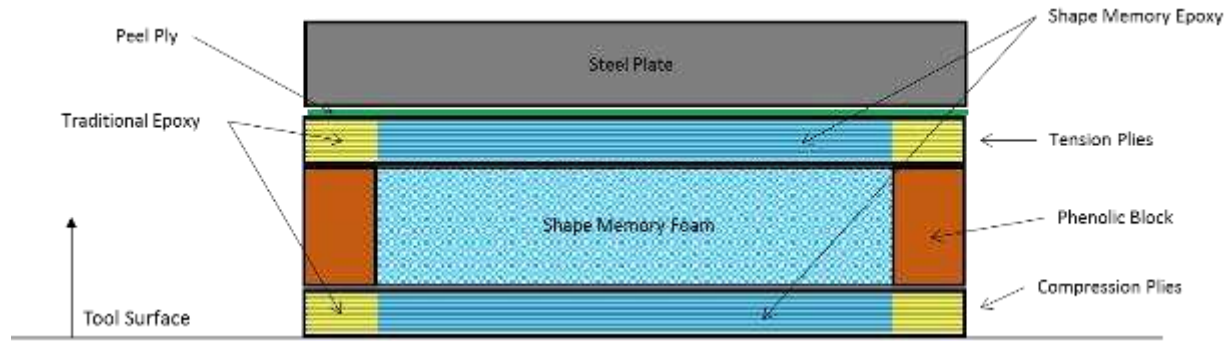


Figure 3-3: Sandwich panel layup diagram, side view.

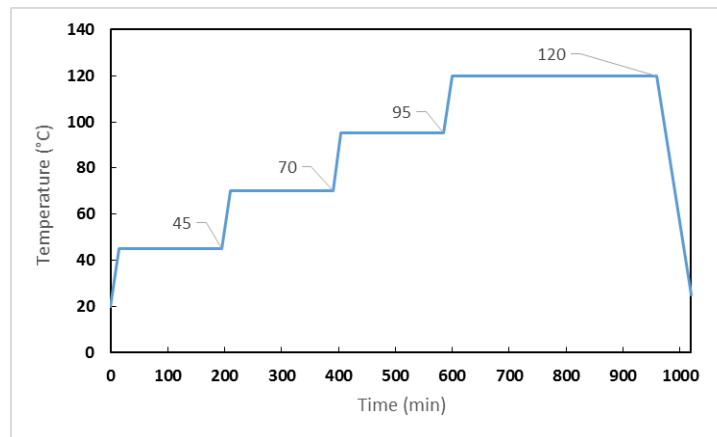


Figure 3-4: Cure cycle.

Cured sandwich plates were mounted with double-sided tape, onto a sacrificial MDF board that was clamped to the worktable of a vertical mill. The tension surface of the samples was always placed adjacent to the MDF board. Plates were parted into 1" wide beams with a 1/4" diameter solid carbide end mill. Cutter speed was set to 1300rpm, with a 1.5 inch per minute automatic feed rate. Cutting was started with a Kennametal (uncoated solid carbide) end mill, and sample sets 6, 5, and 4 were parted in this way. Midway through parting Set 3 the beam edges were becoming progressively rougher, especially the foam. At this time, the cutter was replaced with an OSG (titanium coated solid carbide) of the same size. The remainder of Set 3, and sets 2.5, 2, and 1 were sequentially completed. Each plate typically yielded six samples, however some samples were discarded due to large defects (bubbles) in the core, which were identified during layup.

Based on facesheet composition and end condition, samples from each plate are identified in the following table.

Table 3-1: Beam sample descriptions.

Sample Set	Number of Replicates	Number of Conventional Composite Plies	Composition	Number of Compression/Tension Facesheet Plies	End Condition
1	6	0	(3)SM, Core, (3)SM	3/3	Open
2	6	1	(1)CP, (2)SM, Core, (3)SM	3/3	Open
2.5	3	2	(2)CP, (1)SM, Core, (3)SM	3/3	Open
3	6	0	(3)SM, Core, (3)SM	3/3	Phenolic
4	6	1	(1)CP, (2)SM, Core, (3)SM	3/3	Phenolic
5	6	2	(2)CP, (1)SM, Core, (3)SM	3/3	Phenolic
6	7	1	(1)CP, (3)SM, Core, (3)SM	4/3	Phenolic

CP = Traditional 828/3140, 45 phr epoxy matrix

SM = Shape Memory

Sample sets 1 and 3, which contained only shape memory plies, were deemed baseline groups of the open and shear end constrained beams, respectively.

A note about sample labeling convention:

While the numerical label identifies the foam slice and the laminate components, the uppercase letter (L, M, or H) refers to the original intended test temperature (Low, Medium, or High). The “C” indicates the compression or top side (when mounted in the bending fixture), which is the face that was manufactured in contact with the tool surface, and in practice appears at the bottom of the laminate stack up diagram. “B” stands for “bottom”, referring to the denser lower portion of the foam block. During testing, the “B” end of the sample was always placed on the left side of the center loading roller, as viewed in test assembly photos. Photos documenting as-bent beam profiles are also taken at this orientation.

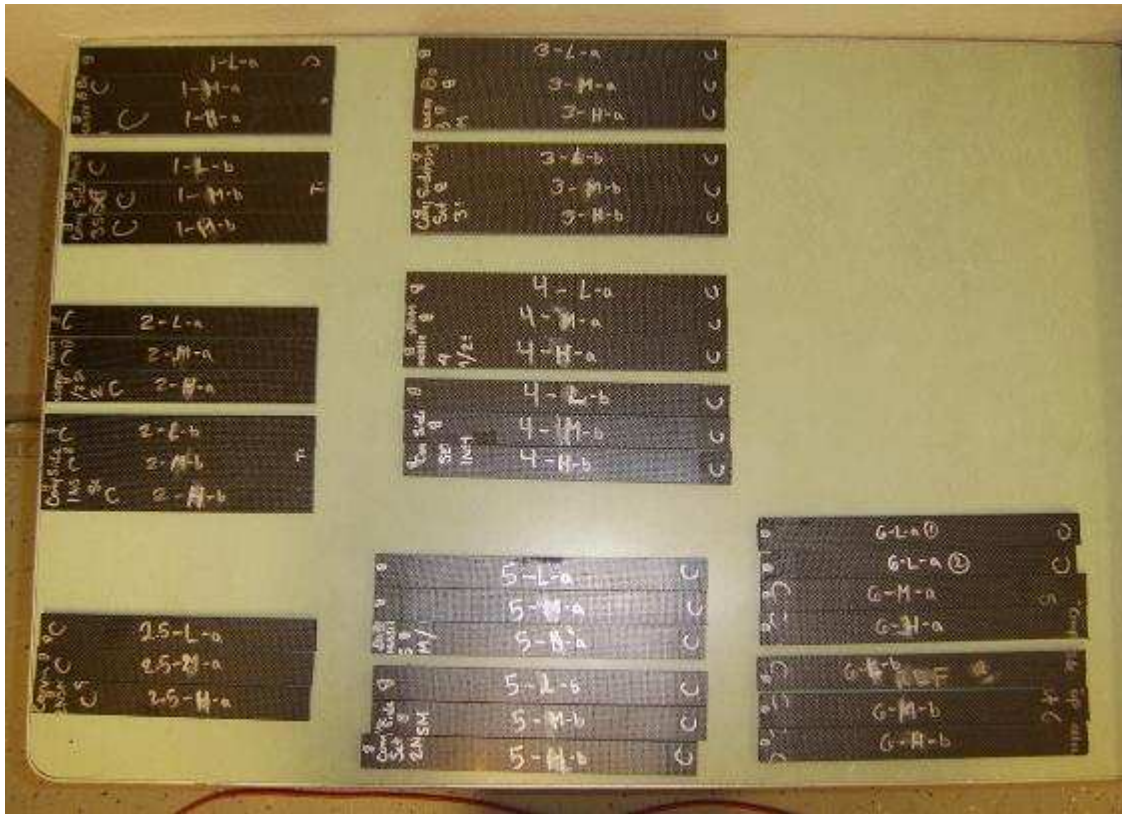


Figure 3-5: Available test samples.

In order to increase the data generated with the available samples, some samples from Set 1 and from Set 3, which had symmetric facesheets, were flipped over and used for additional tests. The rationale behind the reuse is that failure occurs due to compression buckling of the fibers, but does not degrade the tension strength of the plies. Beam samples that were reused in this manner gained an additional “U” designation.

3.2 Testing

To simulate the packaging of the shape memory composite in a measureable manner, a 3-point bending test was used to simplistically represent the high point of a single sided mold, or a mandrel that is used to shape the composite, while intermittent support is provided on the other side. The distance between the two lower 0.5” diameter rollers is 7.5”. The center loading roller is 2.0” in diameter.

The cured shape memory epoxy requires temperatures within the glass transition region, or higher, in order to achieve high strains without damage. This required a temperature control enclosure to be installed around the bending fixture.

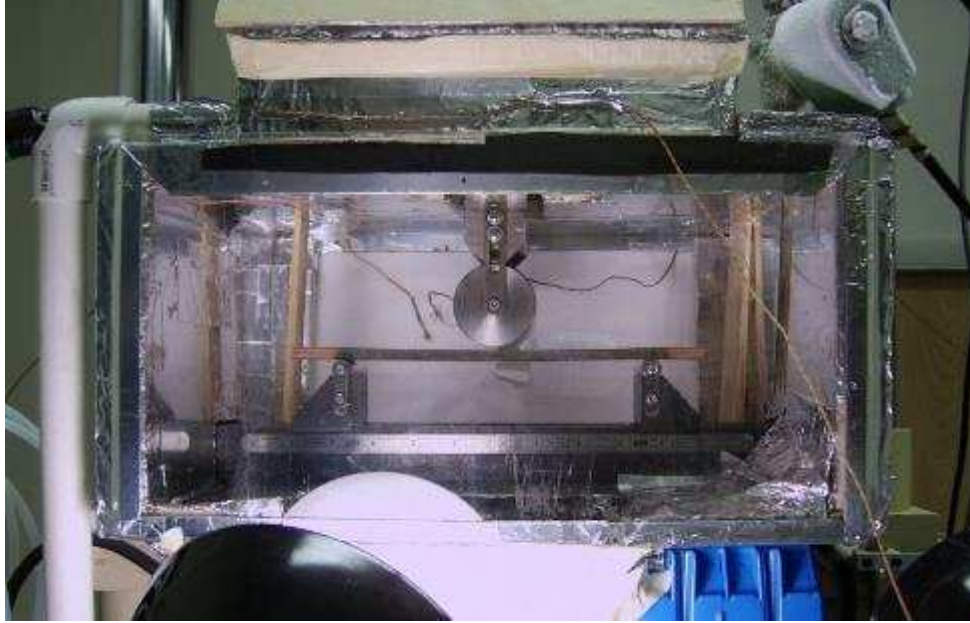


Figure 3-6: Test chamber and 3-point bending set-up.

To facilitate rapid cool down, thereby reducing overall test times, liquid nitrogen vapor was injected into the enclosure. The location of the injection point was chosen to avoid the heating element and air recirculation port, but maximize the distance from the sample, promoting uniform cooling. Two thermocouples were installed in the chamber. The free air thermocouple was used as input to the LabVIEW software program that controlled the heater and liquid nitrogen inlet valve. The second thermocouple was positioned in contact with the upper roller surface, and used in comparison with the free air thermocouple output to monitor the heating state of the large mass components.

A combined compliance measurement of the load frame and test fixtures was performed with isotropic aluminum and steel beams. The details of the measurement and calculations can be found in the Appendix.

Prior to testing, width and thickness of each sample was measured at the beam center, as well as the ends of the foam core section. Pre-test, room temperature stiffness was recorded by loading the samples to a total deflection of 0.045 inches, at a rate of .005"/min.

3.3 Elevated temperature stiffness

Samples with the lowest load to failure, those with shape memory plies only, were put through a load-unload cycle at 42°C, 56°C, and 80°C. Samples were heated and held at test temperature for a minimum

of 10 minutes to reach thermal equilibrium, followed by loading at 0.1"/min. to a deflection of the maximum deflection allowed by the bend fixture. Maximum deflection was approximately 1.65", but varied due to individual sample thickness. Deflection was measured from first contact of the loading roller with the upper surface.

Due to unexpected early failure of samples bent at 42°C, the test temperatures were updated to 56°C, 71°C, and 80°C, in a second round of stiffness testing. Samples that did not fail before the maximum fixture-allowed deflection was reached, were retested at 1.0"/min loading rate. At least one sample from each laminate configuration was tested.

3.4 Bending rate dependence

To observe the change in response due to bending rate and temperature, one sample of each type was loaded to a deflection of 1.0", first at a rate of 0.1"/min, then at 1.0"/min. Samples were held at 1" deflection for 10 minutes before unloading at the same rate. Tests were performed at 56, 71, and 80°C. Samples were tested in the order indicated by the table below. If failure was achieved, the subsequent tests were cancelled for that sample.

Table 3-2: Test order of bending rate samples.

Test Order	1	2	3	4	5	6
Temperature (°C)	56	71	56	71	80	80
Load Rate (in/min)	0.1	0.1	1	1	0.1	1

3.5 Incremental bending

Samples were heated and held at a test temperature of 56°C or 80°C for a minimum of 10 minutes, followed by loading at 0.5"/min. to an initial deflection of 0.5". Heating elements were then turned OFF, and the sample was immediately cooled to room temperature by adding liquid nitrogen vapor to the test chamber. Once cooled, the load application roller was removed at 0.1"/min until the applied load returned to zero. The sample was removed from the fixture in the as-bent shape and inspected for indications of failure. If damage to the laminate was not apparent, the test was repeated to a deflection of 0.1" further

than the previous cycle, until failure was observed. Between loading cycles, samples were heated to 90°C for 10 minutes and allowed to cool to room temperature on a flat surface. Mid span thickness was measured with a dial caliper before re-testing.

3.6 Local heating

Two sandwich beams with conventional epoxy plies, but without phenolic shear constraints, were loosely wrapped with woven fiberglass heating tape about the middle seven inches and heated to approximately 85°C, measured at the surface of the upper face sheet. Load was applied at 0.1"/min. The first sample, from Set 2, was deflected 0.5 inches. The second sample, from Set 2.5, was deflected 0.6 inches. The bent shape was retained by cooling with liquid nitrogen vapor. The room temperature samples were removed from the fixture, and resulting curvature was photographed.

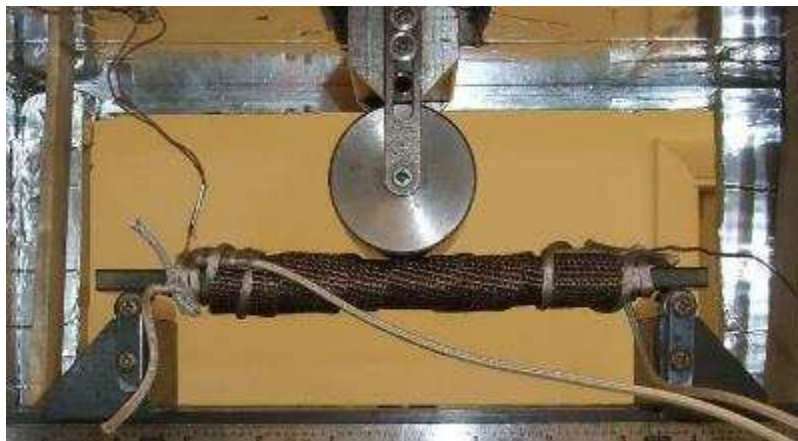


Figure 3-7: Local heating with fiberglass heating tape.

3.7 Damage inspection

Samples were heated to 90°C for 10 minutes to relax any residual stress, and a final post-test thickness mid-span thickness measurement was taken. Room temperature stiffness was measured by loading to 0.045" at .005"/min.

3.8 Failure microscopy

One sample of each from sets 3, 4, and 5, which had been previously tested to failure at 80°C, was reloaded at 0.5"/min and 80°C, and frozen in the bent shape. Samples 4 and 5, which contained one and

two conventional resin plies respectively, were frozen at 1.6” deflection, and Sample 3 at 1.2” of deflection. The deflections chosen were the highest each sample had experienced in testing. The damaged middle sections were cut out with a diamond abrasive cutting wheel on a water cooled tile saw and then wet sanded with 100, 400, and 800 grit sandpaper. 25X magnified photos of the polished surfaces were taken, first in the bent state and secondarily in the stress relaxed state.

3.9 Profiled foam beam

A single sample with profiled core, 0.25” thick on the ends and increasing to maximum thickness of 0.35” at mid-span, was loaded at room temperature and at 80°C for comparison to the flat beams. The facesheet composition of the sample was the same as Set 4, with one conventional epoxy matrix ply on the upper surface. All thickness increase was added to the tension side of the sample, while the compression surface remained level. Foam was cut by hand, so thickness is approximate.

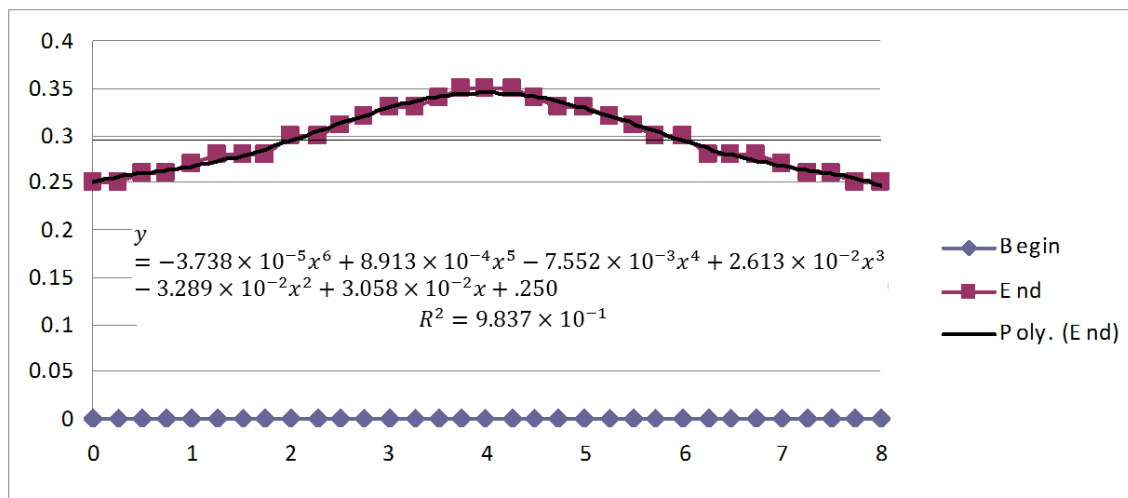


Figure 3-8: Thickness of profiled foam beam vs. span location.

4 RESULTS AND DISCUSSION

4.1 Room temperature stiffness

The room temperature ($\sim 25^{\circ}\text{C}$) stiffness of the beam configurations were compared at very low deflection, approximately 0.05". To prevent accidental overloading, and negate the possibility of viscous effects on the stiffness measurement, deflection was performed at 0.005"/minute. Table 4-1 and Figure 4-1 summarize these results. Note that beams from Sample Set 1 are considered the baseline of open-ended samples, and likewise Sample Set 3 is the baseline of shear-constrained samples. The data of the shear constrained sample sets contained more than twice as much scatter as their open-ended counterparts, as shown by the plot in Figure 4-1.

Table 4-1: Flexural stiffness at room temperature.

Flexural Stiffness (lbf/in) Pre-Test - Room Temperature (Scaled to 1" nominal width)						
Set	End Condition	Composition	# of Replicates	Average (lbf/in)	Standard Deviation	% Baseline
1	Open	(3)SM, Core, (3)SM	6	164.5	7.4	100%
2	Open	(1)CP, (2)SM, Core, (3)SM	6	179.8	5.2	109%
2.5	Open	(2)CP, (1)SM, Core, (3)SM	3	175.3	5.5	107%
3	Phenolic	(3)SM, Core, (3)SM	6	154.9	11.6	100%
4	Phenolic	(1)CP, (2)SM, Core, (3)SM	6	146.4	19.5	95%
5	Phenolic	(2)CP, (1)SM, Core, (3)SM	6	134.7	16.0	87%
6	Phenolic	(1)CP, (3)SM, Core, (3)SM	6	138.4	18.8	89%

CP = Traditional 828/3140, 45 phr epoxy matrix

SM = Shape Memory

Stiffness comparisons at room temperature and in the very low deflection range were expected to reflect the trend predicted with elastic beam bending theory in Table 2-2. The shape memory and conventional epoxies produce approximately the same stiffness at room temperature, although the T300 fiber dominates the properties. Due to the high variation in the stiffness values of the end-constrained beams, and the limited number of samples available, a statistical difference in stiffness due to adding shear end constraints was not shown.

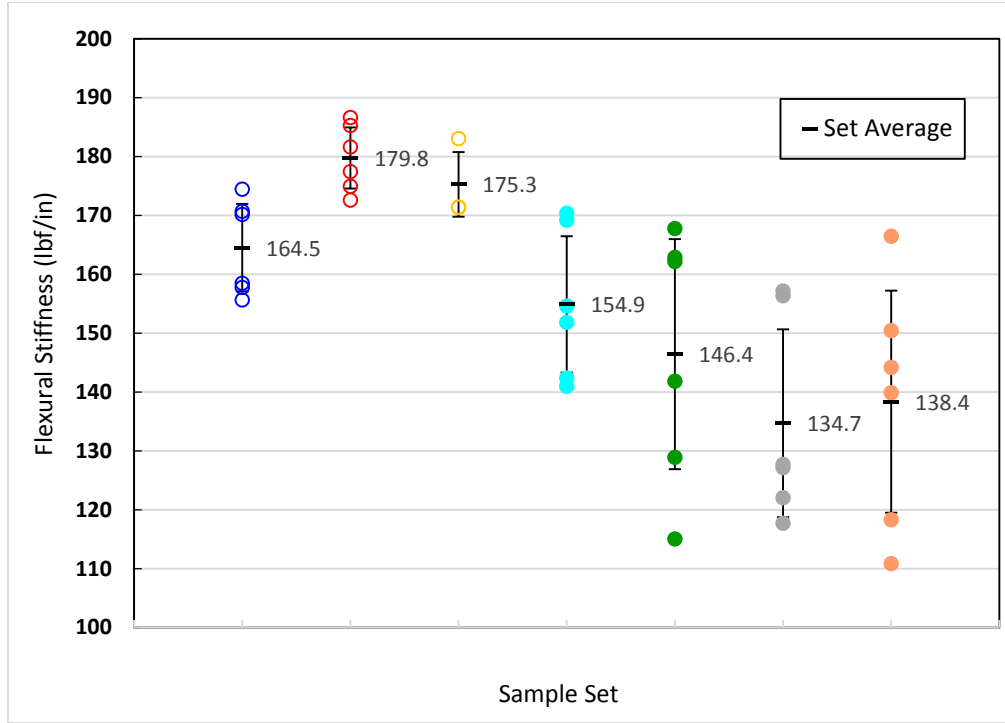


Figure 4-1: Flexural stiffness comparison at room temperature.

4.2 Effects of temperature and end constraint

The load required to bend the samples was highly dependent on the test temperature due to the modulus transition that occurs as the shape memory material enters or exceeds the glass transition region. Stiffness variation within temperature ranges that remained above or below the transition region was not directly studied, but appeared to be negligible. The end condition of the beams also influenced the required load, but more significantly affected the as-bent curvature and the failure mode. For the purpose of this work, failure is defined as incurring irrecoverable damage. Although some beams were considered “failed”, all were still capable of some bending resistance due to intact lower plies.

4.3 SM-only comparison

Beams containing the same ply stack up, symmetric with only shape memory plies, but with either open ends or shear constrained ends, are compared. These samples represent the baseline condition, shape memory only, globally heated and locally heated. The differences between results are attributed solely to temperatures and end constraints. The force vs. deflection plots in Figure 4-2 illustrate that although end

constraints affect the maximum values, the profiles remain similar. The selected test temperatures are below (42°C), within (56°C), and above (80°C) the glass transition region.

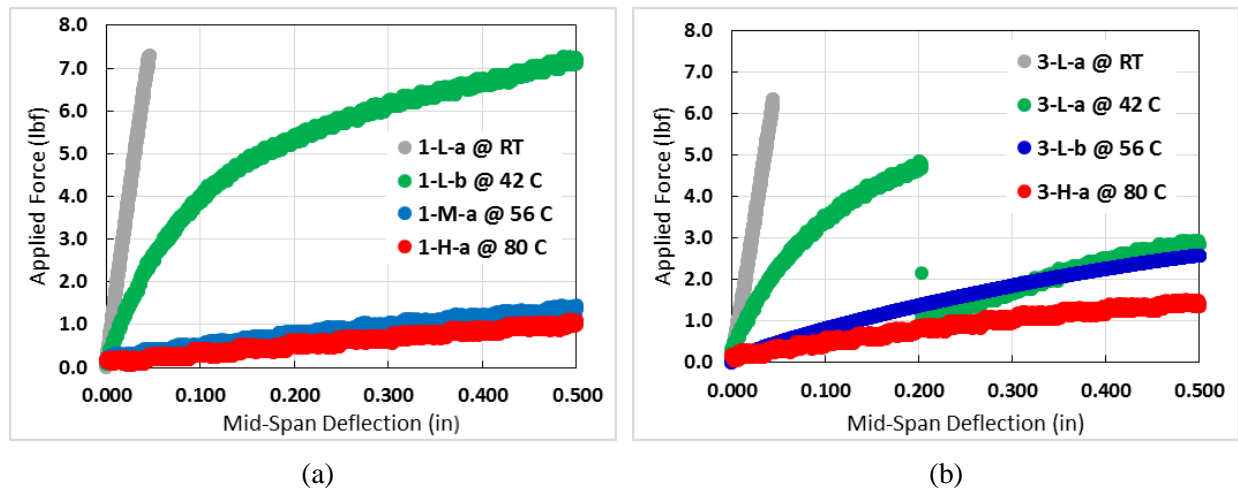


Figure 4-2: Force vs. Deflection curves by end condition, shape memory plies only.
(a) Open-ended beams, and (b) Shear constrained beams. Room temperature (~25°C) bending was performed at .005"/minute, and heated tests were at 0.20"/minute.

While there is an increase in force to bend the end constrained beam at 80°C, the load curve comparison at 42°C shows a lower initial stiffness. The most obvious difference caused by end constraints was an apparent failure of 3-L-a at 0.20" of deflection. The corresponding open-ended beam, 1-L-b, deflected over 0.5" without damage. After the abrupt load drop at failure, the upper plies were observed to gap away from the load cylinder, in Figure 4-3. However, the beam was still capable of carrying some load.

As discussed in Paragraph 2.8, the upper skin is unable to shorten under compressive load, due to the reinforcing fibers, and buckles globally into the core, creating a much tighter bend radius at the center of the beam. This makes it evident that the localized failure is not a result of the load cylinder crushing the upper plies.

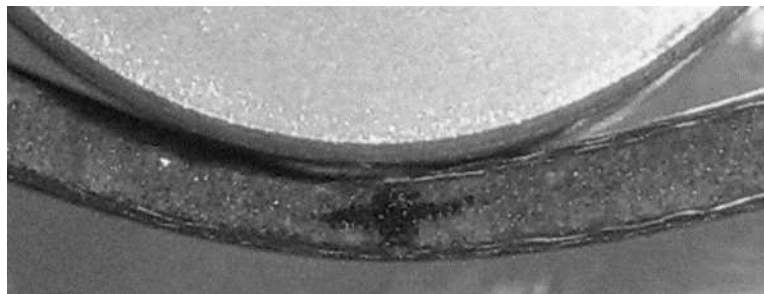


Figure 4-3: 3-L-a @ 42° ~1.2".
Failure occurred at approximately 0.20", based on force vs. deflection data.

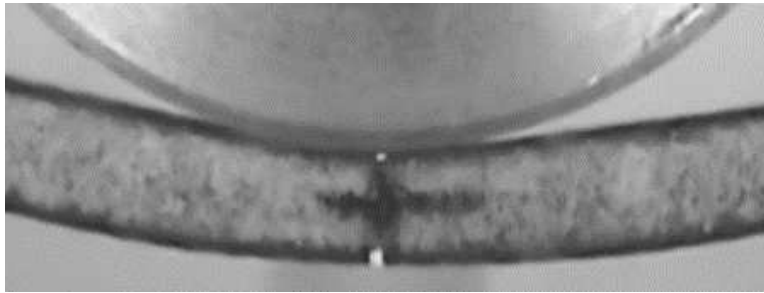
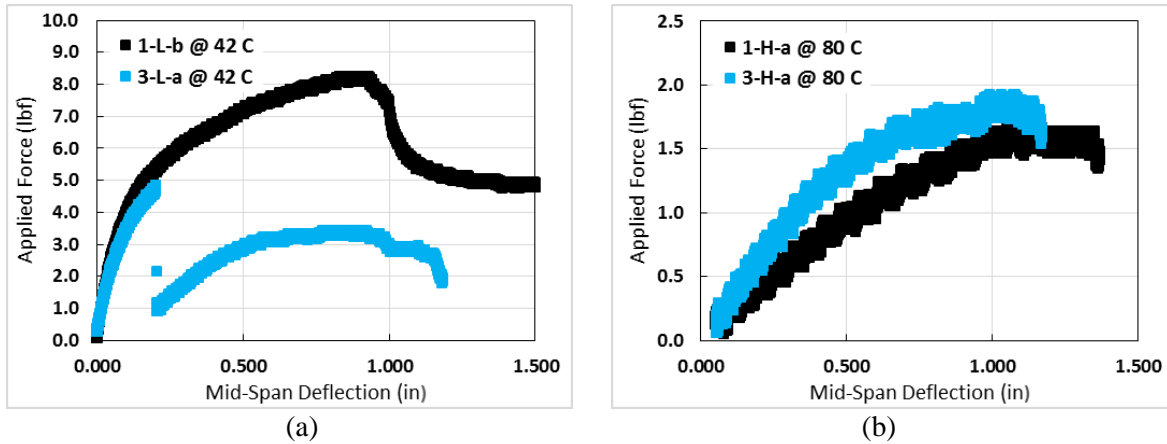


Figure 4-4: 1-L-a @ 42° ~1.0".
Immediately after failure, based on force vs. deflection data.

Due to unexpectedly early failure of Sample 3-L-a, at just 0.20" of deflection when bent at 42°C, the test temperatures were modified to 56°C, 71°C, and 80°C in subsequent tests. It was assumed that the lower temperature reduced the strain to failure of the matrix, such that fiber or tow movement to accommodate bending was significantly restricted. Since the end constraints prevent the facesheets from unloading through core shear, more fiber microbuckling is required in the upper facesheet to achieve a given deflection, compared to an open-ended beam.

Figure 4-5 shows the full force vs. deflection curves of the test temperature extremes, 42°C and 80°C. At 80°C, both beams deflect over 1" without failure. At 42°C, both load curves indicate a failure event just prior to 1" of deflection. Although the capability of 3-L-a had been significantly reduced by the first failure, it carried additional load at increasing deflection until the second failure. The similarity of the deflection at failure of the two beams suggests a common failure mode.

While the potential for failure at such a small portion of the test fixture travel, 0.20" of 1.6" available, was considered unacceptable for comparing beam bending capability, it should be noted that the 0.20" of deflection that was achieved prior to failure would be considered extremely flexible for a conventional sandwich panel.

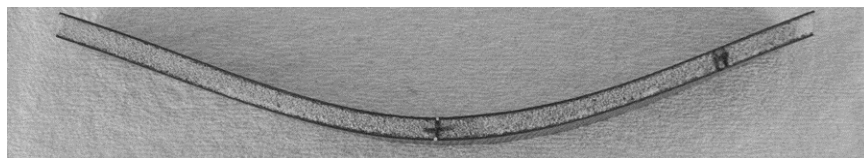


**Figure 4-5: Force vs deflection curves by temperature, SM-only.
(a) 42°C, and (b) 80°C.**

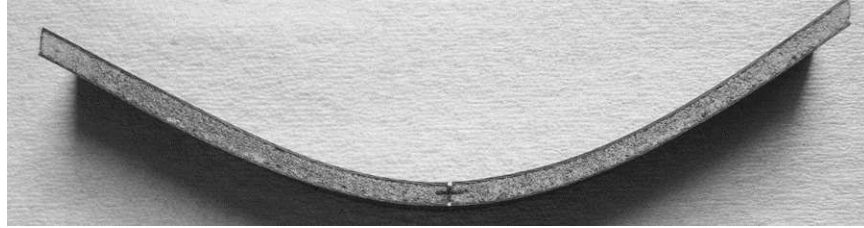
4.4 Beam curvature

Although the following photos were taken toward the end of testing, in all test stages the differences in curvature between the beam configurations were noted. These images are included here to better visualize the bending load results and failure modes that will be discussed in subsequent sections. The characteristic curvature of each beam type did not vary with bending temperature or rate. Force vs. Deflection data associated with these photos is found in Section 4.10.

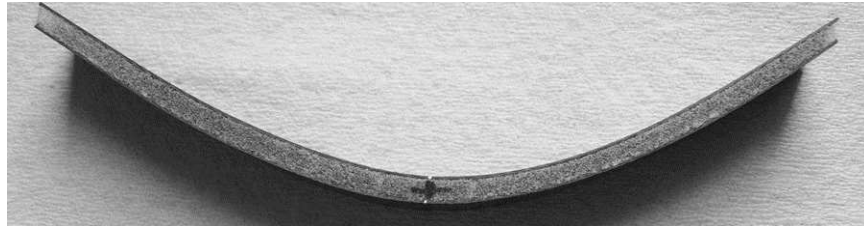
The characteristic shape of each sample type, when bent, is compared in Figure 4-6 through Figure 4-12. The differences in resulting curvature are primarily the result of the beam composition, and are most easily compared after bending at 80°C and subsequent cooling to lock in the shape. Depending on the beam type, some samples reached the maximum deflection allowed by the load fixture without observable failure, either visually or by Force vs. Deflection curve examination.



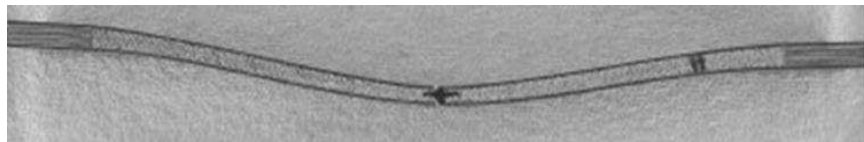
**Figure 4-6: 1-H-b at 1.0” – Failure onset.
Shape memory only**



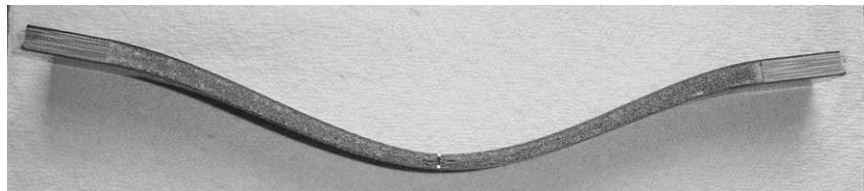
**Figure 4-7: 2-L-b at 1.6" – No failure at maximum deflection.
One conventional matrix ply.**



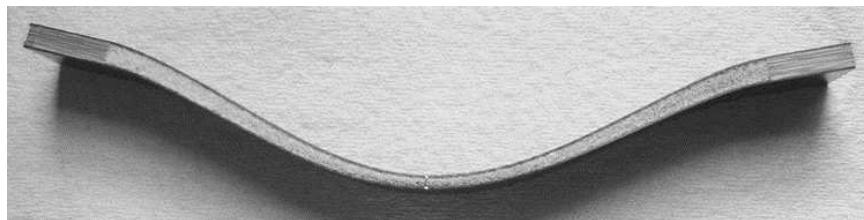
**Figure 4-8: 2.5-L-a at 1.6" – No failure at maximum deflection.
Two conventional matrix plies.**



**Figure 4-9: U-3-M-a at 0.6" – Failure onset.
Shape memory only with shear constraint.**



**Figure 4-10: 4-M-b at 1.3" – Failure onset.
One conventional matrix ply with shear constraint.**



**Figure 4-11: 5-M-b at 1.5" – Failure onset.
Two conventional matrix plies with shear constraint.**

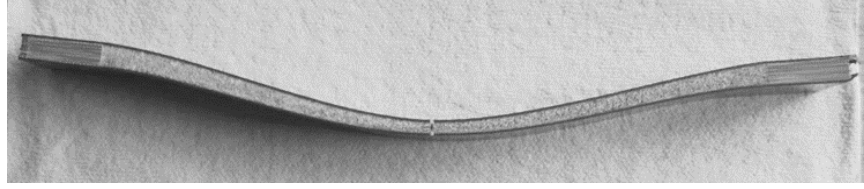


Figure 4-12: 6-M-b at 0.8" – Failure onset.

One conventional matrix ply added to compression surface and shear constrained. (Facesheets are no longer symmetric.)

Notice that the open-ended beams exhibit little to no mid-span thinning, while each of the shear-constrained beams is clearly thinner in the center where the foam has compressed. Furthermore, the center bend radius of the open-ended beams is larger and extends toward the ends of the beam, and end shear is prominent in the foam. As discussed in section 2.8, if a flat panel is folded and the inner and outer lengths remain equal, then compressive and tensile bending stresses can be relieved by through-thickness shear. Adding phenolic blocks prevents through-thickness shear, which otherwise results in the greatest strain at the ends. As deflection advances, the compressive stress in the upper facesheet overcomes the limited buckling stability provided by the core, and the facesheet begins to buckle globally, with the amplitude of the buckling wave causing mid-span core compression. The resistance of the core increases as it is compressed, limiting the amplitude of the wave. If bending continues and the compressive modulus of the core prevents the mid-span peak from growing, then the buckling wavelength begins to shorten and inverse peaks develop near the ends of the beam. The inverted peaks apply tension to the core, rather than compression, as they grow. A distinguishing feature of the shear-constrained samples is the reversed bending curvature caused by these end peaks, in the region close to the phenolic blocks. In locations of the greatest reversed curvature, it appears that the foam may be locally thickened as a result of tension.

4.5 Effects of deflection rate and hold time

In the interest of reducing test time, shape memory only samples from Set 1 and Set 3 were loaded at several deflection rates, at 80°C, and the resulting Force vs. Deflection curves were compared. Figure 4-13 compares the data collected. By comparing the results of loading at 0.05"/min and at 0.5"/min, where one rate is an order of magnitude faster than the other, it was concluded that the force required to bend at 80°C

is not highly dependent on deflection rate and that 0.02"/minute is unnecessarily slow. Ply failure did not occur at 80°C, when the shape memory epoxy was softest and least able to support the fibers, thus it was assumed that increasing the deflection rate at lower temperatures was also reasonable.

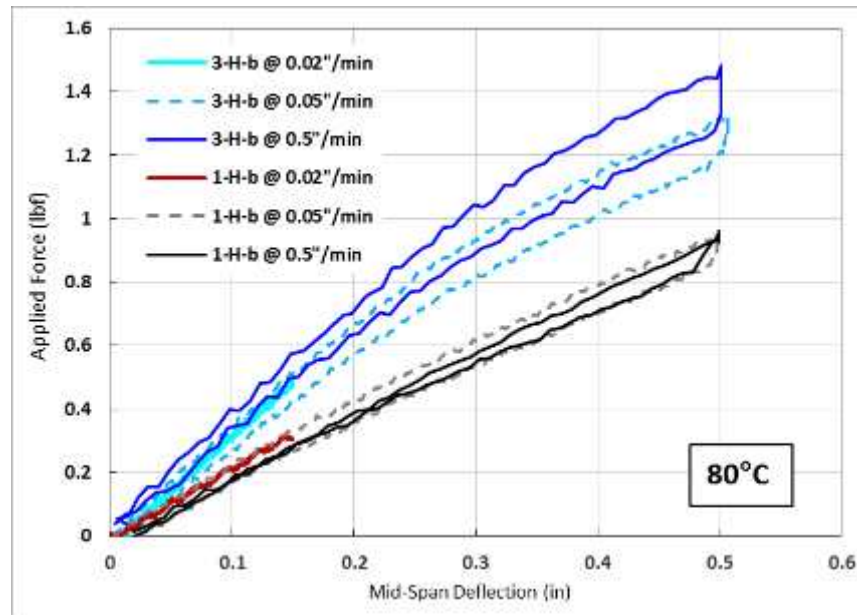


Figure 4-13: Force vs. deflection curves at 80°C, with varied deflection rates.

Stress relaxation was observed during the time the load frame was stopped, which was only about two minutes during the tests of Sample 3-H-b, and between five and eight minutes during the tests of Sample 1-H-b. The difference in loading and unloading curves generated hysteresis loops when the data was plotted, indicating that the sample beams do not exhibit a purely elastic response to load application. If the load were to continue to drop to zero over a longer hold time, the response would be considered viscous.

4.6 Varied deflection rate at three temperatures

The effect of load application rate on “perceived stiffness” was evaluated at 56°C, 71°C, and 80°C. The loading rates chosen were 0.1"/min and 1.0"/min. In the cases of 1-M-b and 3-M-b, because the samples with only SM facesheets should be symmetric, these were further tested upside-down once they had failed. Table 4-2 summarizes the maximum forces recorded during load application.

Table 4-2: Maximum bending force with rate and temperature variation.

	Maximum Applied Force (lbf) During Deflection From 0.0" to 1.0" (Scaled to 1" Nominal Width)								
Temperature (°C)	56			71			80		
Bend Rate (in/min)	0.1	1.0	% force increase	0.1	1.0	% force increase	0.1	1.0	% force increase
1-M-b	2.80	4.45	59%	1.66	1.74	5%	1.62*	1.85*	15%
2-H-b	2.95	4.51	53%	1.92	2.00	4%	1.84	1.92	5%
2.5-H-a	3.09	4.66	51%	2.03	2.15	6%	1.98	2.10	6%
3-M-b	2.68	4.34	62%	1.88	1.9 ⁺	2%	1.84*	1.81*	-2%
4-M-b	4.05	5.57	37%	2.64	2.88	9%	2.40	2.59	8%
5-H-b	3.66	4.90	34%	2.60	2.73	5%	2.39	2.50	5%

*Sample failed in previous test and was reused upside down.

⁺3-M-a was substituted in this test due to failure of 3-M-b in previous test.

Test results were significantly affected by bending rate at 56°C, and minorly affected at 71°C and 80°C. The data supports the conclusion that bending stiffness is rate dependent, and that faster rates require application of greater force, for a given temperature. At 56°C, beams with higher percentages of SM material were more sensitive to bending rate, with 1-M-b and 3-M-b requiring ~60% higher maximum forces to bend at 1.0"/min than at 0.1"/min. Substitution of SM plies with conventional plies caused decreased sensitivity to bending rate, commensurate to the number of plies replaced.

The addition of conventional plies at 56°C had a greater effect on end-constrained beams than on their open-ended counterparts. Whereas the the open-ended configuration was 6% (from 59% to 53%) less sensitive to bending rate with one conventional ply, the replacement of one SM ply with a conventional ply in an end-constrained configuration resulted in force increase percentage reduction from 62% to 37%. At 71°C and 80°C, the data did not support an increase or decrease in sensitivity to bending rate due to the addition of conventional plies. At all temperatures and all rates the force required to bend the beams was increased by the inclusion of conventional plies in the facesheets. Two beam failures occurred during this set of tests, both at 71°C, and both in SM only beams. 1-M-b failed at 0.1"/min and was not tested at 1.0"/min. 3-M-b failed at 1.0"/min after a successful test at 0.1"/min. A correlation between bending rate

and beam failure was not demonstrated, but beams with conventional epoxy plies were shown to have superior resistance to bending failure over SM only.

The Applied Force vs. Mid-Span Deflection plots in Figure 4-14 through Figure 4-19 group the load profiles per sample, and compare the effect of loading rate at each test temperature. Solid lines identify force application at 0.1"/minute, and dotted lines indicate 1.0"/minute. Solid and dotted lines representing the same test temperature are plotted in identical colors for easier comparison. The time at constant 1.0" of deflection was 10 minutes. Loading and unloading were performed at the same rate. Load frame vibration during initial reversal is blamed for noise in the data, which is especially prominent in the plots of 2.5-H-a and 5-H-b.

As summarized in Table 4-2, although the force required for bending increases at a faster deflection rate, this increase is only substantial at 56°C, which is below T_g . However, stress relaxation occurs during the time the deflection is held at 1.0", and the applied force to maintain constant deflection drops to a value similar to the 0.1"/min curve prior to load frame reversal. At 71°C and 80°C, some stress relaxation did occur at 1.0" of deflection, but the beam response is far more elastic. The decrease in area within the hysteresis loop indicates the immediacy of the material response, which was altered little by the rate of bending.

A comparison of the unloading curves of open-ended beams loaded at 0.1"/min and at 56°C, to the like loaded shear-constrained beams, indicates that the shear-constrained configuration produces a more elastic response because the slope of the unloading portion of the curve is more linear. The curves of shear-constrained beams display an inflection point around 0.4" of deflection, which is not present for the open ended beams. This curve inflection is most prominent in 3-M-b, which implies that its cause is alleviated by adding conventional plies.

1-M-b and 3-M-b had the least amount of residual strain during unloading at 71°C and 80°C, which was surprising since the conventional plies were expected to contribute to elastic response. In fact, adding conventional plies resulted in a widening of the hysteresis loop, indicating a greater difference in measured flexural stiffness between loading and unloading, and a more viscous response. Since the viscosity of the

polymers is the same in different beams if tested at the same temperature, the change in response must be the result of how the strain occurs in the beam. It is believed that the addition of conventional plies causes more strain to be induced in the foam core at a given deflection, than with less, or no, conventional plies.

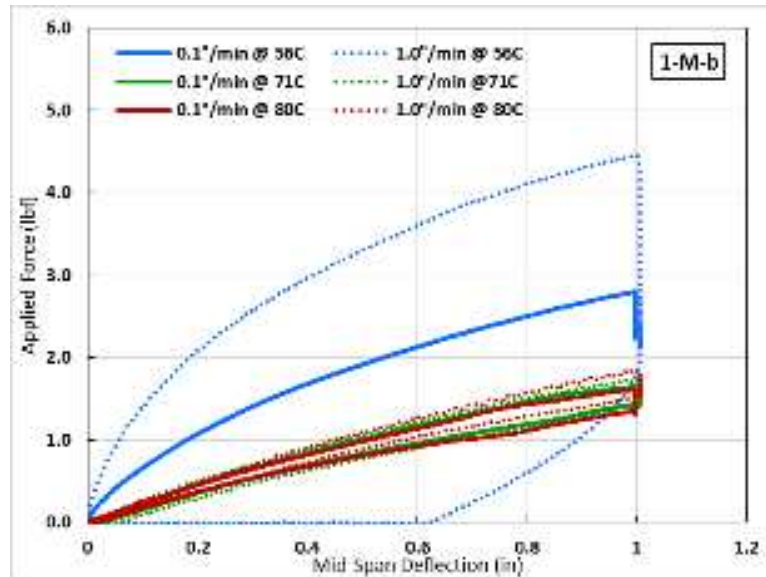


Figure 4-14: Force vs. Deflection of 1-M-b.

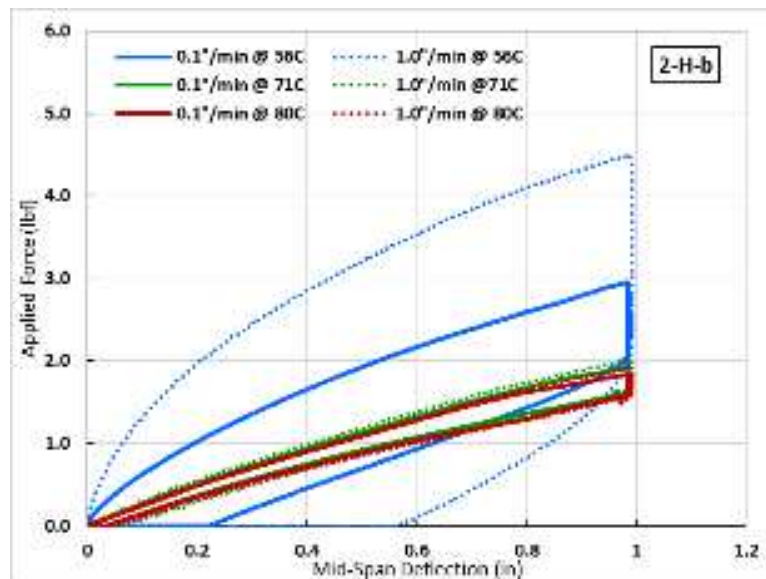


Figure 4-15: Force vs. Deflection of 2-H-b.

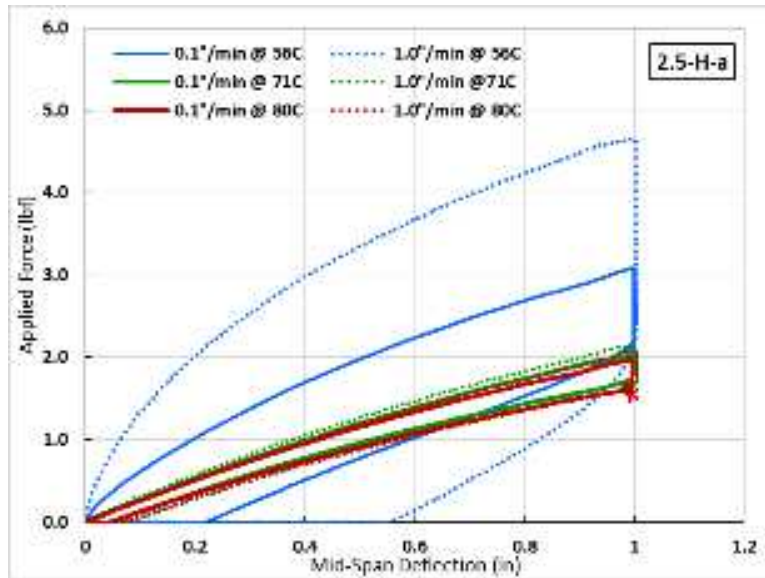


Figure 4-16: Force vs. Deflection of 2.5-H-a.

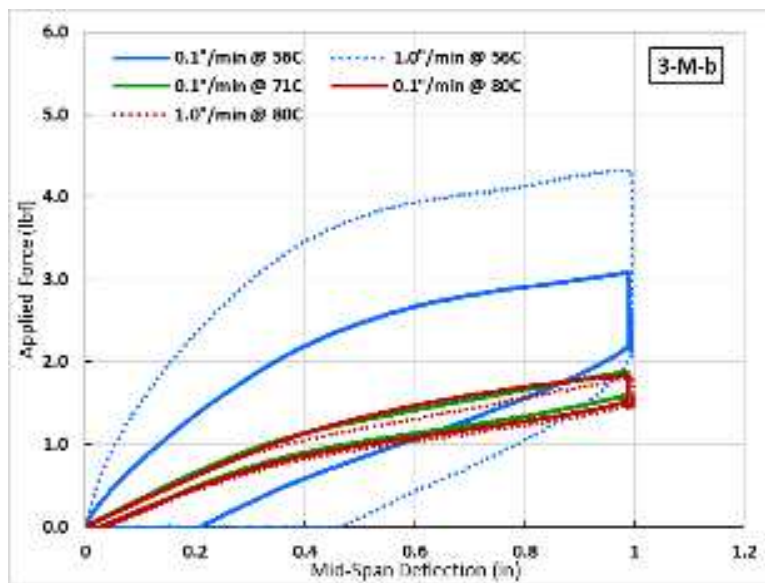


Figure 4-17: Force vs. Deflection of 3-M-b.

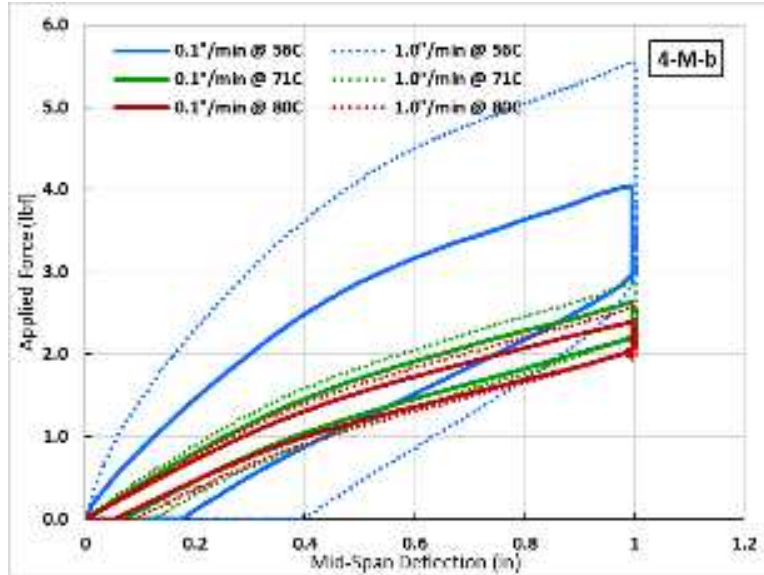


Figure 4-18: Force vs. Deflection of 4-M-b.

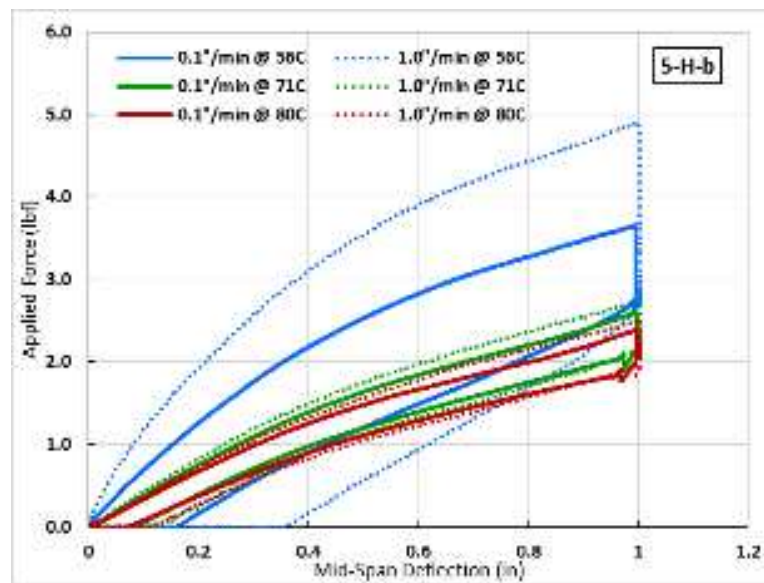


Figure 4-19: Force vs. Deflection of 5-H-b.

4.7 Constant deflection hold

The generation of hysteresis loops in the Force vs. Deflection plots indicates a time-dependent component in the reaction of the beams to applied load. Significant reductions in force were observed in all tests when samples were held at constant deflection for any length of time. It was of interest to re-plot the load-unload curves of the samples discussed in Section 4.6 versus time, to compare the effects of beam composition and temperature. These plots are shown in Figure 4-20(a)(b) through Figure 4-25(a)(b). The

hold time of 10 minutes at 1.0” was selected after reviewing the load curves of initial tests. Stress relaxation results in a time dependent reduction in applied load at constant deflection, but as mentioned in Section 0, the redistribution of strain that occurs during stress relaxation is limited in thermoset polymers by the limits of chain stretching, such that the force will reach an equilibrium value and not go to zero. Table 4-3 summarizes the applied force recorded at the start and end of the 10 minute hold. The percent reduction of applied force from starting value, % Drop, is used to compare the amount of strain energy that is lost due to stress redistribution within the SM materials.

The force recorded at the start of the hold is strongly influenced by the viscosity of the SM material in the sample, whereas the force at the end of the hold is primarily due to the temperature-dependent elastic modulus. If the deflection was held long enough for the applied force value to completely stabilize, then this modulus could have been measured. As is, after 10 minutes, the force vs. time plots in Figure 4-20(a)(b) through Figure 4-25(a)(b) show the applied force approached, but did not achieve equilibrium.

Stress relaxation occurs under maintained applied force, as a result of strain redistribution within the material, occurs over time. At higher temperature the internal friction of the polymer is lower, so stress relaxation occurs quicker but less stress relaxation occurs overall because the material was less resistant to strain during bending. At lower temperature more stress relaxation can occur because viscosity prevents strain from propagating easily within the material. Over time, the internal friction of the material can slowly be overcome.

Since the forces at the end of the 10 minute hold vary little between deflection at 0.1”/min and deflection at 1.0”/minute, there is no stored energy gain due to bending at a quicker rate unless the beam can be frozen before stress relaxation occurs. Deflection at quicker rate does require more applied load at all temperatures, which could be a concern if the beams were larger or stiffer.

While the results at 71°C and 80°C appear similar in comparison to 56°C, the open-ended beams had nearly the same Start and End forces, while the end-constrained beams still differed between 71°C and 80°C. Shear end constraints or local heating requires the upper and lower facesheets to more fully interact, whereas foam shear in the open-ended configurations can accommodate independent behavior. The force

required to bend and hold end-constrained beams is more dependent on temperature than it is for open-ended beams.

In the force vs. deflection plots, the near-immediate non-linear drop in load at the beginning of the hold is attributed to viscous resistance of the SM material to motion. Hence the rapid drop once the load frame is stationary. The linear portion of the hold curve is attributed to stress relaxation that requires time to respond to applied load. The length of the transition region between the initial load drop and the linear portion is longer at lower temperatures, taking up about half the hold time at 56°C, about a third at 71°C, and approximately a fourth at 80°C.

Table 4-3: Force reduction at constant deflection.

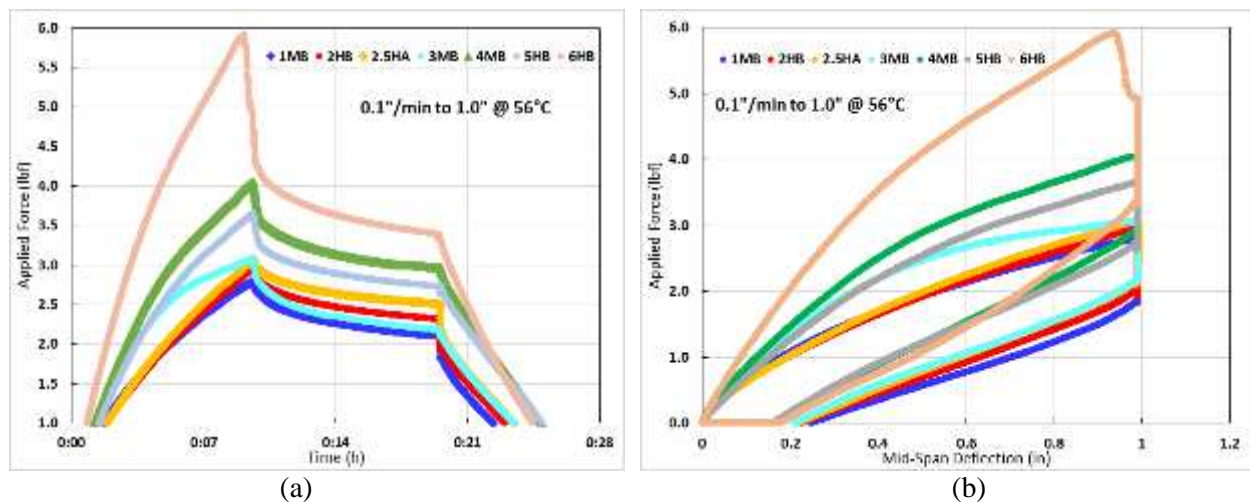
Load Drop During 10 Minute Hold at 1.0" Deflection (lbf)										
Sample	Load Rate	56°C			71°C			80°C		
		Start	End	%Drop	Start	End	%Drop	Start	End	%Drop
1-M-b	0.1"/min	2.8	2.1	25%	1.7	1.4	13%	1.6*	1.3*	19%
	1.0"/min	4.5	2.1	53%	1.7	1.4	18%	1.9*	1.5*	18%
2-H-b	0.1"/min	3.0	2.2	27%	1.9	1.7	9%	1.8	1.7	8%
	1.0"/min	4.5	2.2	52%	2.0	1.7	17%	1.9	1.7	14%
2.5-H-a	0.1"/min	3.1	2.5	19%	2.0	1.9	9%	2.0	1.8	8%
	1.0"/min	4.7	2.4	48%	2.2	1.8	16%	2.1	1.8	16%
3-M-b	0.1"/min	2.7	2.2	18%	1.9	1.6	14%	1.8*	1.5*	20%
	1.0"/min	4.3	2.1	51%	no test			1.8*	1.5*	19%
4-M-b	0.1"/min	4.1	3.0	27%	2.6	2.3	14%	2.4	2.1	11%
	1.0"/min	5.6	3.0	46%	2.9	2.2	23%	2.6	2.1	20%
5-H-b	0.1"/min	3.7	2.7	26%	2.6	2.3	11%	2.4	2.2	8%
	1.0"/min	4.9	2.7	45%	2.7	2.2	21%	2.5	2.1	18%

*Sample failed in previous test and was reused upside down.

At 56°C the curves of 4-M-b and 5-H-b have a distinct separation, with 4-M-b obviously higher than 5-H-b. This is contrary to the assumption that 5-H-b should be the stiffer beam due to one more conventional epoxy ply in the compression facesheet. The difference in bending stiffness was believed to be caused by more thinning of the foam in 5-H-b, which can be seen in a similar beam in Figure 4-11. At 71°C and 80°C the load curves of 4-M-b and 5-H-b lie almost on top of each other, which indicates that foam thinning is not the only cause, and that heating beams at or above T_g reduces this effect. In comparison, the open-

ended beams 1-M-b and 2-H-b exhibited the opposite effect. At 56°C, the curves of the two specimens are more similar in values than they are at higher temperatures.

Sample 3-M-b is known to have failed in the 0.1"/min deflection at 71°C, however, there is not an obvious indication of the failure event in Figure 4-22(a)(b). Failure was determined visually. Load frame induced noise in the deflection data is observed in plots of all tests in this figure, but the remainder of the load curve is consistent with prior test runs. Likewise, Sample 1-M-b failed during 1.0"/min deflection at 71°C, but the failure event is not apparent in Force vs. Deflection plot in Figure 4-23(a)(b). Conversely, the plot of this sample in Figure 4-24(a)(b), where it is reused for testing upside down, displays uncharacteristic waviness. However, the unusual noise in the data, shown in the subsequent test in Figure 4-25(a)(b), makes it likely that an issue with data signal was the cause. Initial failure in SM-only beams always occurred in the matrix, rather than fiber breakage. Therefore, as long as the failed facesheet of the re-used beam was only loaded in tension, the results should not be compromised.



**Figure 4-20: Bending at 0.1"/min and 56°C.
(a) Force vs. Time, and (b) Force vs. Deflection.**

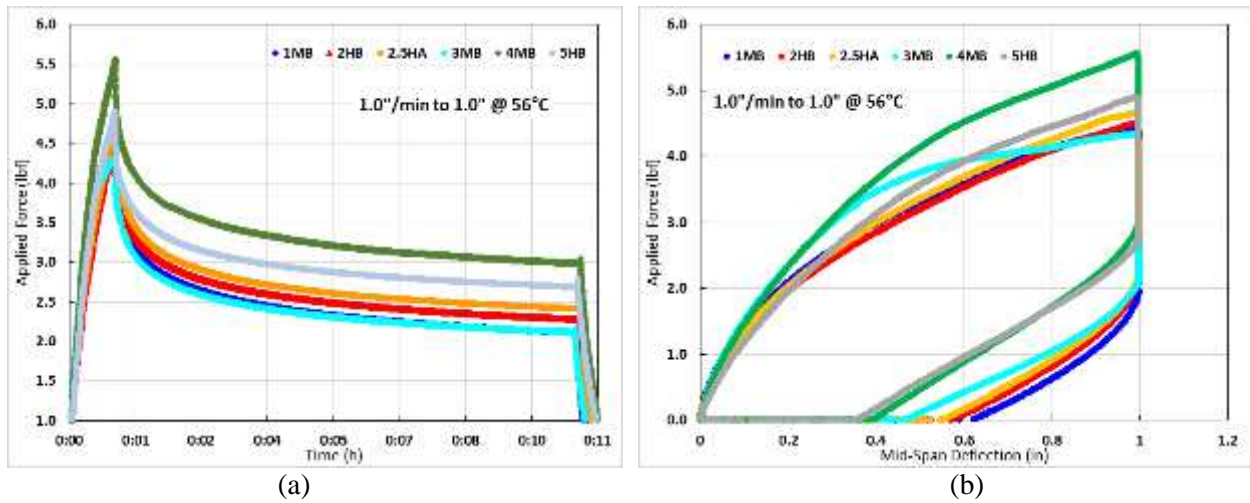


Figure 4-21: Bending at 1.0"/min and 56°C.
(a) Force vs. Time, and (b) Force vs. Deflection.

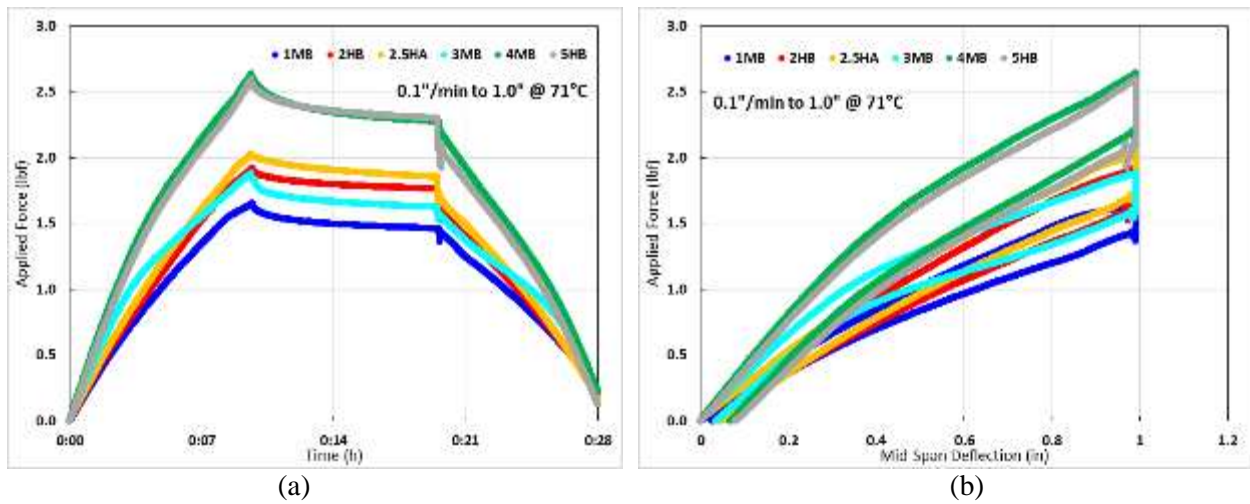


Figure 4-22: Bending at 0.1"/min and 71°C.
(a) Force vs. Time, and (b) Force vs. Deflection.

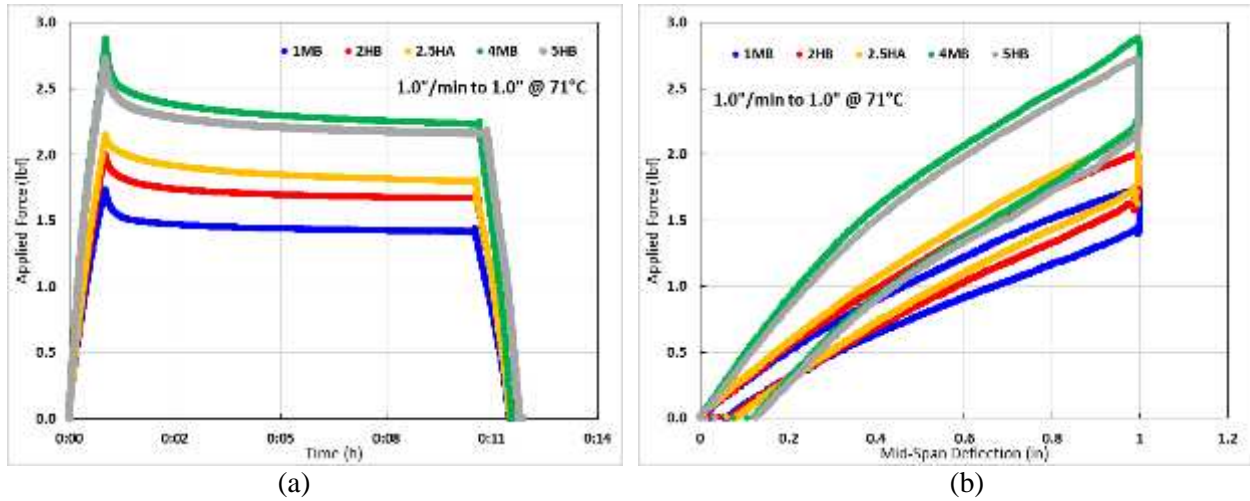


Figure 4-23: Bending at 1.0"/min and 71°C.
(a) Force vs. Time, and (b) Force vs. Deflection.

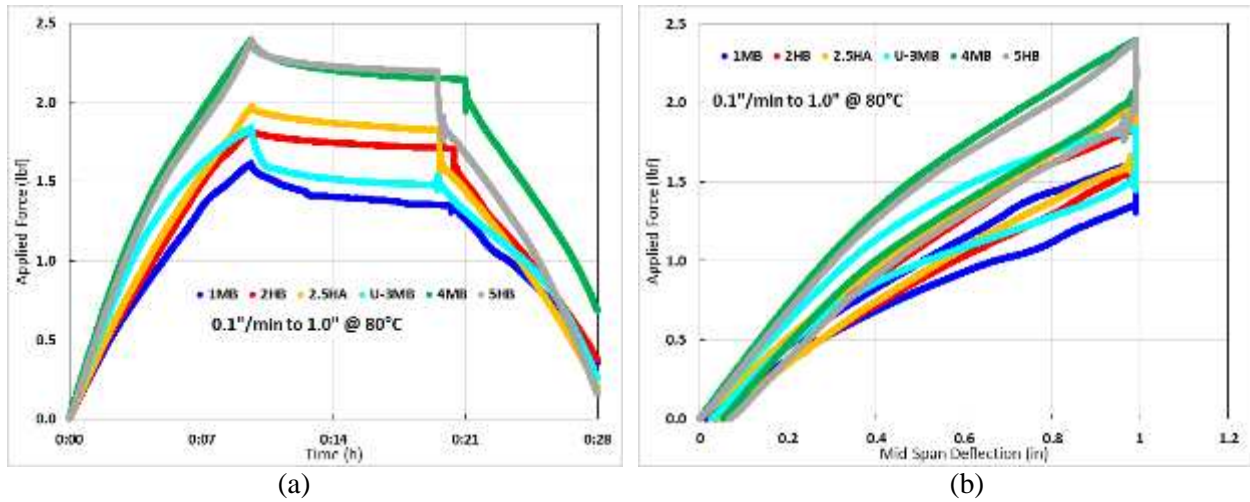
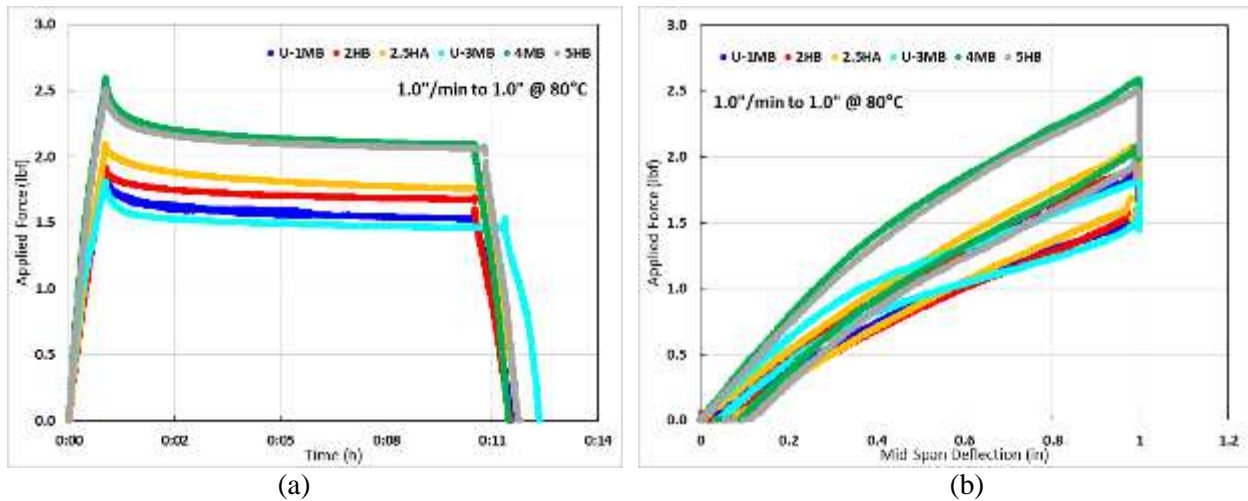


Figure 4-24: Bending at 0.1"/min and 80°C.
(a) Force vs. Time, and (b) Force vs. Deflection.



**Figure 4-25: Bending at 1.0"/min and 80°C.
(a) Force vs. Time, and (b) Force vs. Deflection.**

4.8 Incremental bending

By loading the beams in 0.1" increments and freezing the shape, three objectives were investigated: visual inspection for failure under the loading cylinder, residual force after cooling bent beams to room temperature, and consistency of force vs. deflection data in multiple bend-freeze-restore cycles. It was assumed that measuring the residual force when the beam was cooled to ~20° would be a good indication of how much spring back would occur without applied load, however, because liquid nitrogen was used to rapidly cool the samples, super cooling often occurred and prevented accurate measurement. Instead, shape stability is discussed briefly in Section 4.18. Since the SM epoxy and conventional composites are not considered subject to fatigue, repeated loading and restoring in increments of increasing deflection should result in coincident force vs. deflection curves unless failure occurs. Photos of beam curvature at 80°C were previously presented in Section 0. Additionally, photos documenting damage progression as specimens were loaded after failure are found in Section 4.11. Since the purpose of these tests was to intentionally cause failure in each specimen, separate sets of specimens were used for tests at 56°C and at 80°C.

Table 4-4 summarizes the results of incremental bending tests. Beams from Set 2 and Set 2.5 did not fail although deflected to the full travel of the bending fixture, approximately 1.6". The results clearly

demonstrate that substituting conventional plies into the SM beam delays or prevents compression failure during bending. The maximum load provides an indication of the ultimate capability of the beams prior to failure. If the beam failed during testing, the Max Force reflects the highest force recorded during the failure increment. If no failure occurred, the Max Force is the highest value recorded throughout all tests, and the deflection increment where it was recorded is indicated in parentheses. Although beams were deemed to fail once any irreversible damage had occurred, because load could still be supported, it was not unusual for forces greater than the Max Force to be observed in deflection increments beyond failure.

Due to limited availability, a specimen from Set 6 was tested only at 80°C. Although the configuration in Set 6 produces a thicker and heavier beam that is stiffer at room temperature, the deflection to failure is poorer than replacing one SM ply with a conventional ply, as in Set 4. While it would be tempting to add a conventional ply onto an existing SM-only laminate in order to increase deflection, this appears to be an inadequate solution.

Table 4-4: Incremental bending results.

56°C			80°C		
Specimen	Failure Deflection Increment (in)	Normalized Max Force in Failure Increment (lbf)	Specimen	Failure Deflection Increment (in)	Normalized Max Force in Failure Increment (lbf)
U-1-H-a	1.3	5.84	1-H-b	1.0	1.66
2-M-b	did not fail	(1.4") 5.87	2-L-b	did not fail	(1.6") 2.27
2.5-M-a	did not fail	(1.4") 8.87	2.5-L-a	did not fail	(1.6") 2.37
3-H-b	0.6	4.36	U-3-M-a	0.5	1.44
4-L-b	1.5	5.93	4-M-b	1.3	2.96
5-L-b	1.6	6.47	5-M-b	1.5	3.35
--	--	--	6-M-b	0.8	3.37

4.9 Deflection at 56°C

The load curves at 56°C show less coincidence between deflection increments than at 80°C due to a higher sensitivity to differences in test temperature below T_g . The test chamber set point temperature was reached and held for 10 minutes prior to testing, but ambient room temperature and number of previous test run that day affected fluctuation about the set point, typically $\pm 1^\circ\text{C}$. Since samples were photographed and restored in batches between bending increments, successive tests were often hours or days apart. While

similar temperature fluctuation occurred during 80°C testing, differences in bending force were less significant.

Failure initiation was detected on U-1-H-a at 1.3” and the force vs. deflection plot in Figure 4-26 displays the expected force reduction in subsequent deflection cycles. The curves from 1.3” to 1.6” show an increasing amount of creep during unloading as the beam remains in contact with loading roller. In the 1.6” increment, the spring back is about 0.15 inches.

Neither 2-M-b nor 2.5-M-a, shown in Figure 4-27 and Figure 4-28, failed during testing, although a reduction in bending force in increments 1.5” and 1.6” occurred, similar to U-1-H-a. An increase in creep was observed at higher deflections, approximately 0.05 inches at 1.6” deflection. The similarities between the three open-ended beam figures, where load curves at specific deflection increments were or were not coincident, further supports the assumption that variations in test temperature caused load-restore cycle inconsistencies. All specimens were bent to the same increment before being inspected, photographed, and restored for bending to the next deflection level.

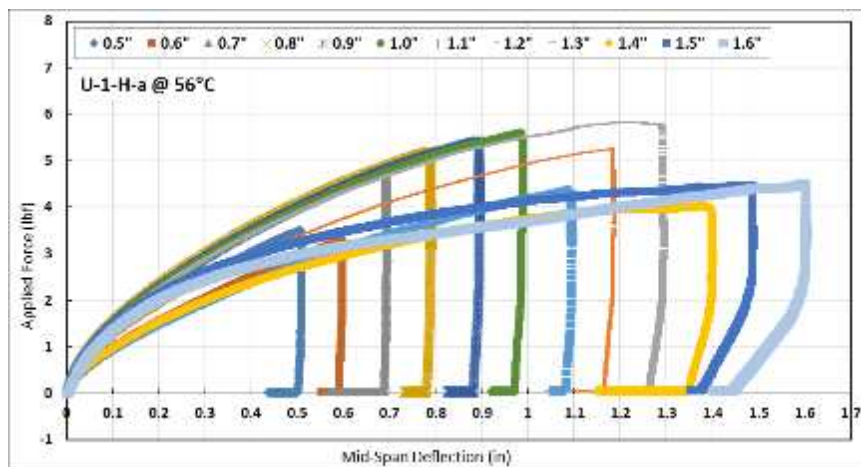


Figure 4-26: U-1-H-a – Incremental deflection at 56°C.

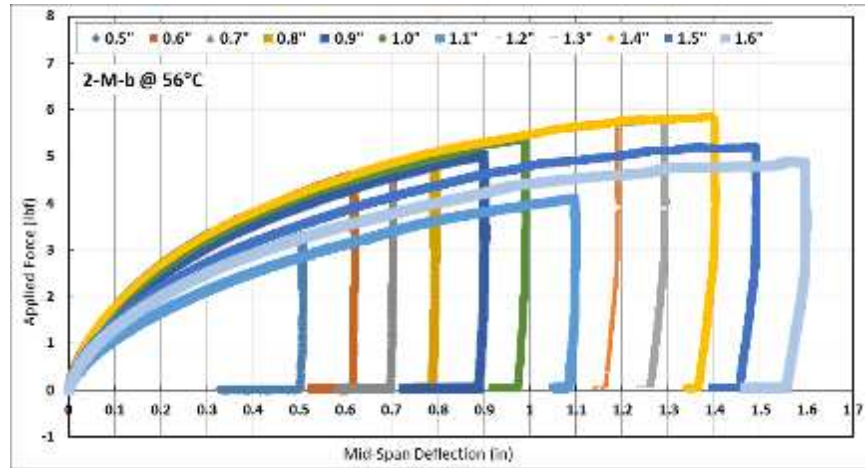


Figure 4-27: 2-M-b – Incremental deflection at 56°C.

3-H-b failed at only 0.6” deflection, after which the force vs. deflection curves in Figure 4-29 show a distinct bow, with an inflection point at 0.6 inches. Creep during unloading is prominent in the curves at deflections of 1.0 inches and greater, with a maximum of ~0.12 at 1.6”.

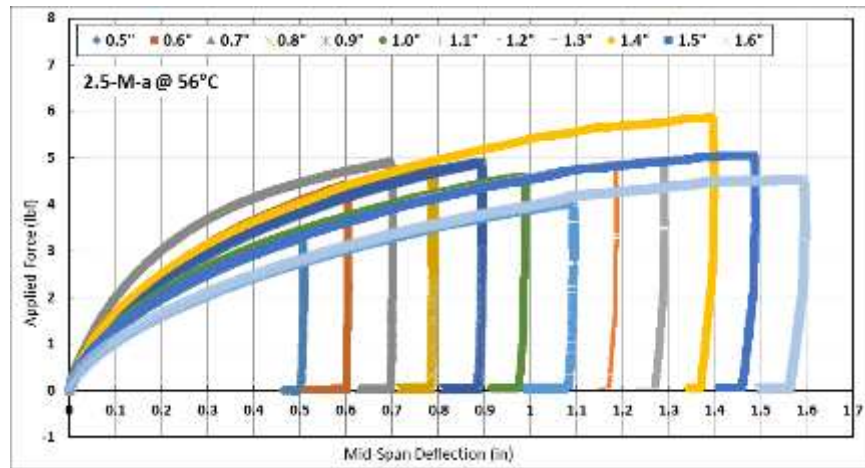


Figure 4-28: 2.5-M-a – Incremental deflection at 56°C.

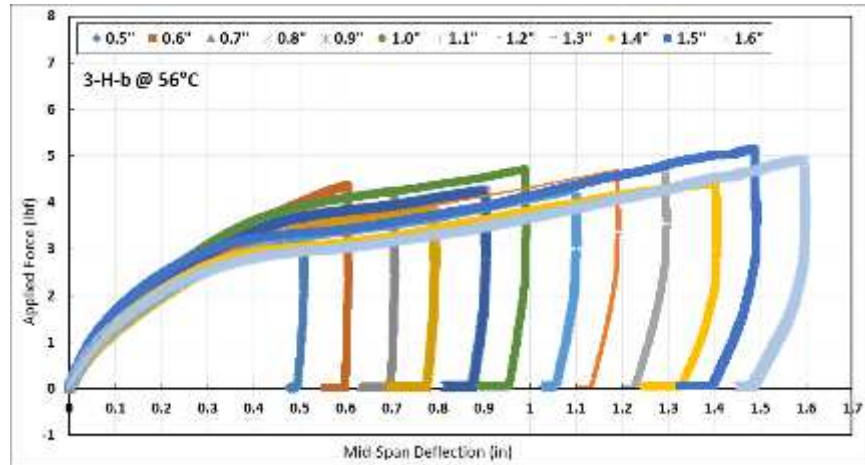


Figure 4-29: 3-H-b – Incremental deflection at 56°C.

Inclusion of a second conventional ply in 5-L-b only delayed failure for an additional 0.1 inch of deflection over 4-L-b, but required about 0.5 lbf to achieve the same deflection. In both samples, creep became noticeable in unloading (≥ 0.05 inches) at about the 1.0" deflection increment. Waviness was observed in the 1.5" and 1.6" load curves of all end-constrained beams tested at 56°C. This is possibly the result of beam slippage on the end rollers at higher beam curvature, as this did not appear perfectly equal on both ends. Due to a set point entry error during the 0.8" increment of 5-L-b, the test temperature was $\sim 70^{\circ}\text{C}$, resulting in an unusually low load curve.

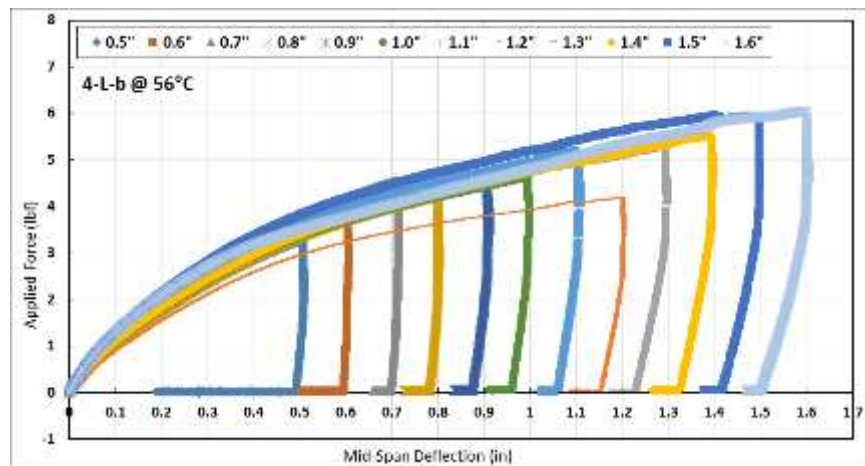


Figure 4-30: 4-L-b – Incremental deflection at 56°C.

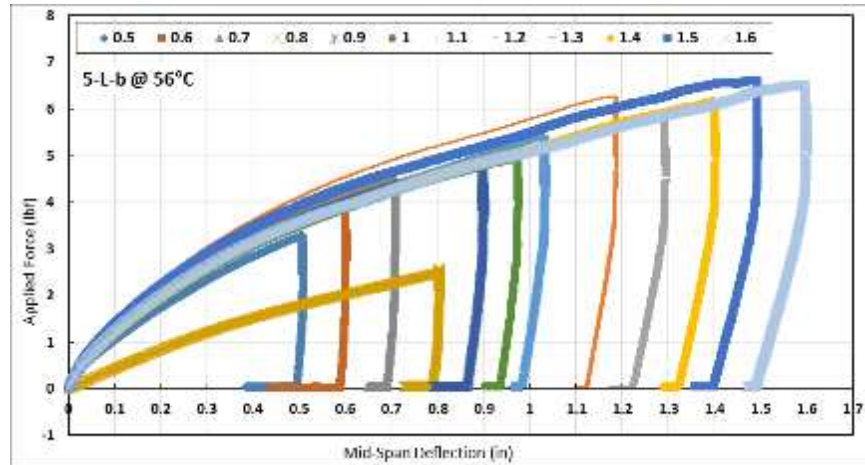


Figure 4-31: 5-L-b – Incremental deflection at 56°C.

4.10 Deflection at 80°C

Beam failure at 80°C always occurred at lower deflection values than at 56°C. Force vs. deflection curves were more consistent between load-restore cycles than shown in the previous section. The characteristic waviness observed in higher deflections at 56°C occur at lower values in the following figures. Creep that was prominent in Figure 4-26 of U-1-H-a was negligible in tests of 1-H-b. None of the force vs. deflection figures give an obvious indication that failure has occurred. As in testing at 56°C, the samples from Set 2 and Set 3 did not fail, due to containing conventional plies.

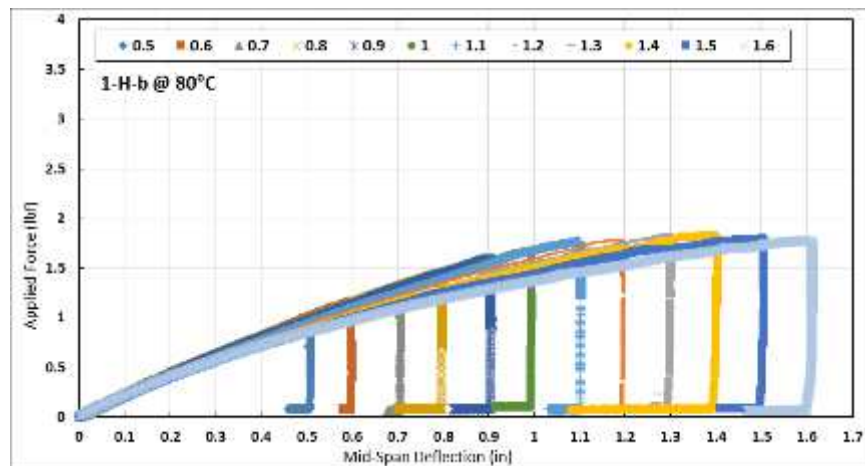


Figure 4-32: 1-H-b – Incremental deflection at 80°C.

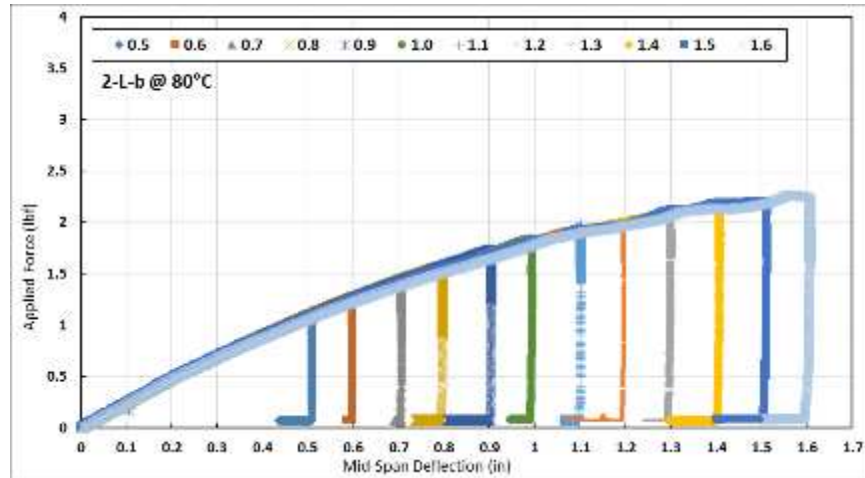


Figure 4-33: 2-L-b – Incremental deflection at 80°C.

Shear-constrained beams tested at 80°C, Figure 4-35 through Figure 4-37, have a more distinct inflection at about 0.3 inches, which is not present in similar tests at 56°C. It was observed during testing that initial deflection measured on the compression facesheet is a result of foam compression prior to global beam bending. At higher temperature, the compression modulus of the foam is lower and more mid-span thinning occurs relative to deflection value. The linear portion of the curve is typical of constant cross section beam bending.

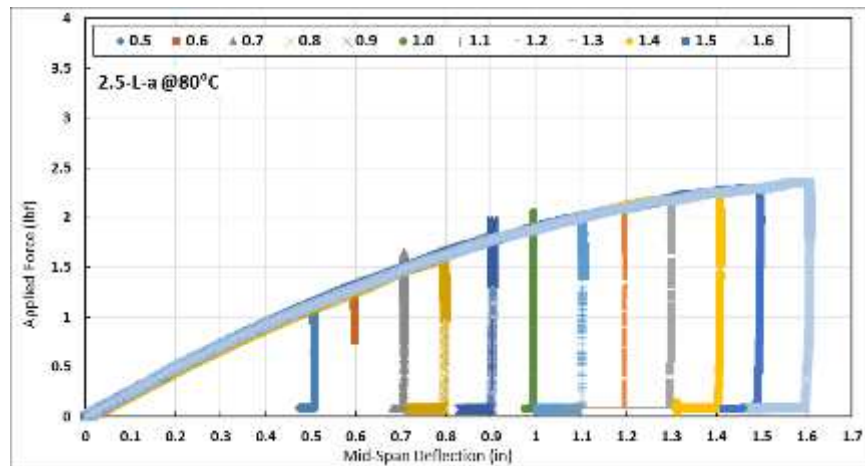


Figure 4-34: 2.5-L-a – Incremental deflection at 80°C.

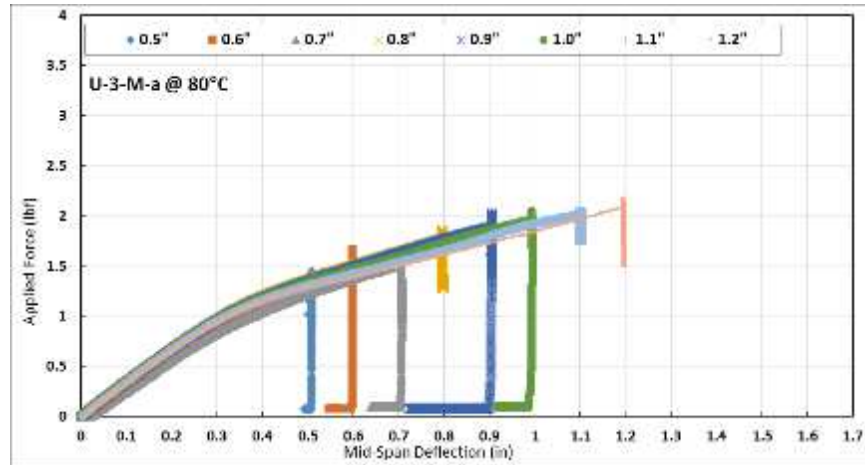


Figure 4-35: U-3-M-a – Incremental deflection at 80°C.

Although U-3-M-a produced a sharper inflection in the curve than 3-H-b, in Figure 4-29, Figure 4-35 shows only minor bowing after failure at 0.5". This may be because all load curves are post failure. The additional conventional ply in 5-M-b adds 0.2 inches of deflection over 4-M-b. Since the conventional plies do not soften at significantly within the test temperatures, beams bent at 56°C and 80°C both require ~0.5 lbf of additional force to deflect the second conventional ply to the maximum curvature values.

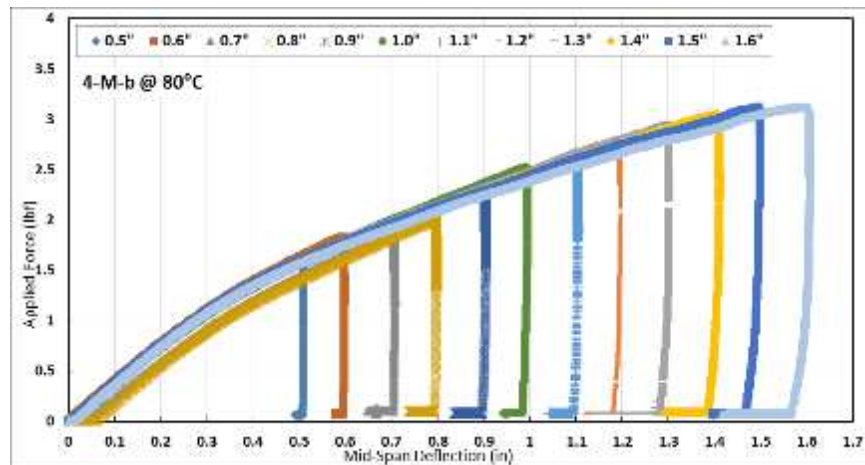


Figure 4-36: 4-M-b – Incremental deflection at 80°C.

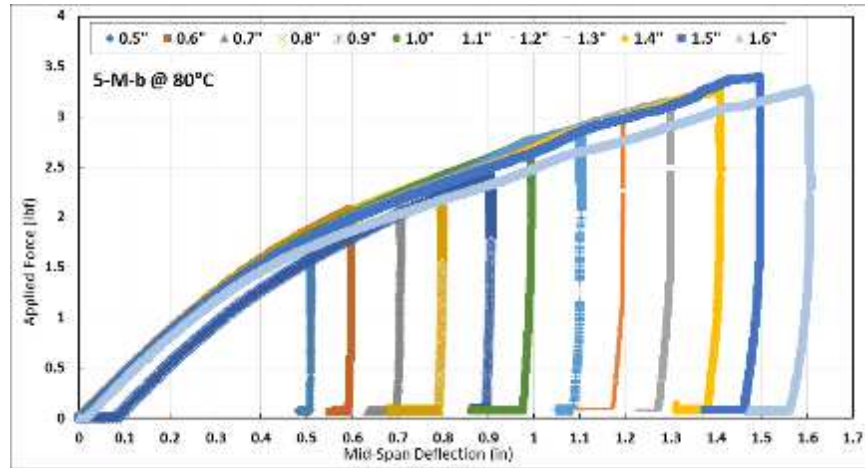


Figure 4-37: 5-M-b – Incremental deflection at 80°C.

Set 6 has shown little added bending benefit over the SM-only beam, and is easily outperformed by Set 4, as it fails at only 0.8". Higher load values are still recorded in successive tests, as full conventional ply failure has not occurred. The 6-M-b was thicker than the other configurations, requiring greater force to bend.

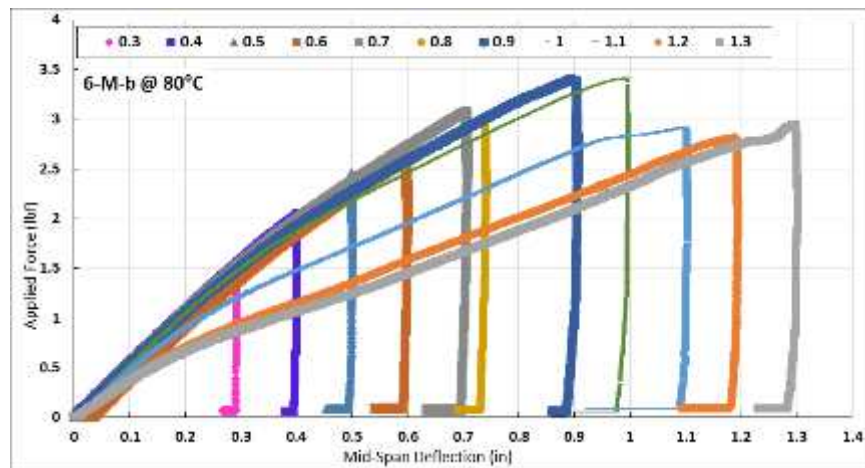


Figure 4-38: 6-M-b – Incremental deflection at 80°C.

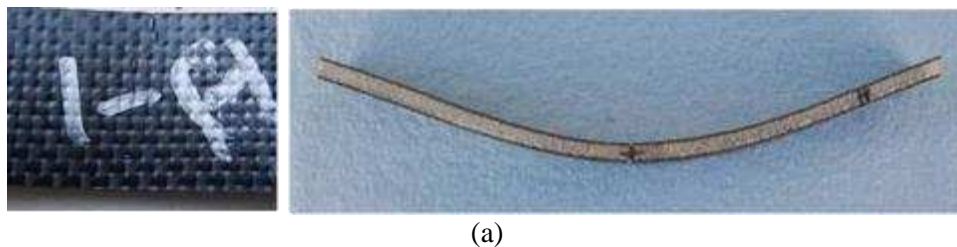
4.11 Damage evolution

Figure 4-39 through Figure 4-43 document the progression of failure of beams loaded incrementally at 80°C. Progression at 56°C was also documented, but is not included here because similar, but more pronounced, characteristic behaviors of each beam type were observed at 80°C. The force vs. deflection plots for these specimens are in Section 4.10. Beams from Set 2 and Set 2.5 are not included here because

failure was prevented by the included conventional plies. Photos were taken at 0.1” increments of deflection, once failure onset was observed. Curvature was set by rapid cooling with liquid nitrogen vapor to allow inspection under the center load cylinder.

In all specimens failure occurred as out of plane buckling of axial tows that initiated at the edge of an overlapping transverse tow. The failure region of SM-only beams is diffused around the mid-span and appears to be a general softening of the facesheet under the load cylinder. As failure progresses, the entire length between transverse tows buckles, resulting in large buckle amplitudes. The effect of shear end constraints is seen by comparing 1-H-b and U-3-M-a in Figure 4-39 and Figure 4-40, respectively. The mid-span thickness of 1-H-b remains nearly constant throughout failure progression, resulting in a larger center bend radius, compared to U-3-M-a. The “H” marking on the right side of each beam can be used to compare foam shear about 1 inch away from the beam end. Clearly, the end constraint of U-3-M-a prevents shear within the bending region, whereas the “H” on 1-H-b was increasingly distorted. The failure region of U-3-M-a is initially diffuse, but becomes concentrated on a single transvers tow as the bend radius of the upper facesheet rapidly decreases.

Since failure, as it is defined in this work, does not immediately extend across the entire width of the beam, it is understandable why the beams may be able carry loads higher than the maximum force recorded before failure initiation. The axial fibers on the exposed upper surface of the beam are also most susceptible to out of plane buckling, whereas adjacent tows in the same ply, but woven under a transverse tow, are further constrained against buckling because they are held between the lower ply and the transverse tow. These unbuckled tows may not be fully loaded when failure initiation occurs.



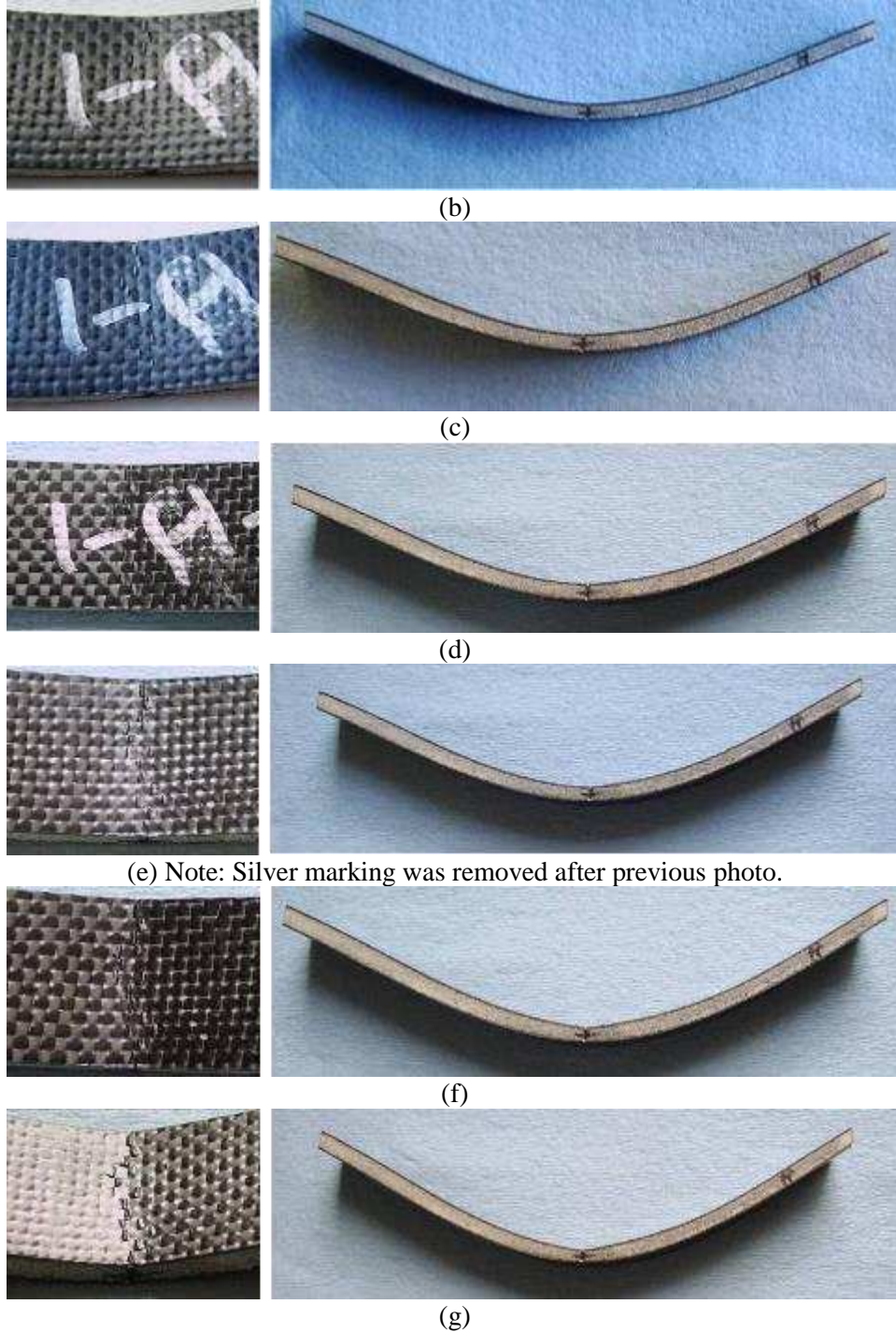


Figure 4-39: Failure progression of 1-H-b.
 (a) 1.0", (b) 1.1", (c) 1.2", (d) 1.3", (e) 1.4", (f) 1.5" and (g) 1.6". Beam 1-H-b was loaded in 0.1" increments of deflection at 80°C and was observed to display failure initiation at 1.0".



(a)



(b)



(c)



(d)



(e)

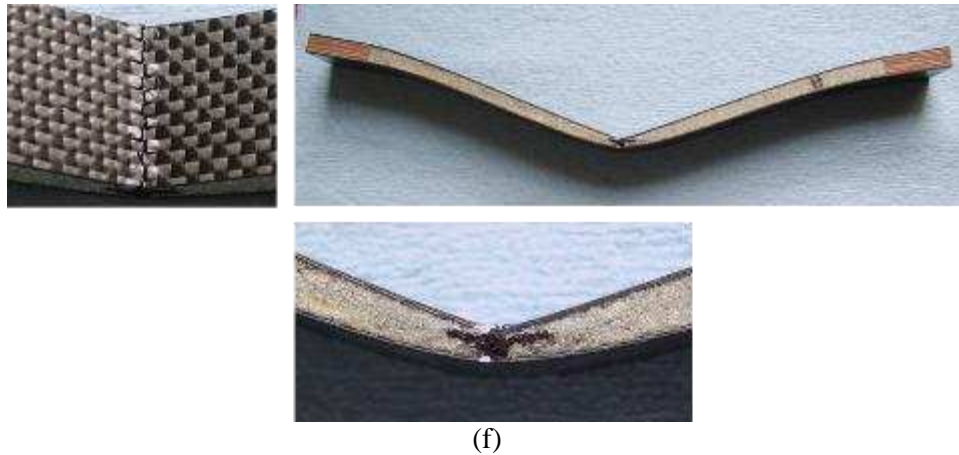
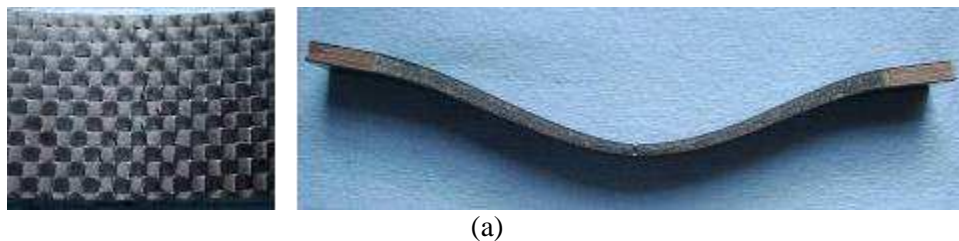


Figure 4-40: Failure progression of U-3-M-a.
(a) 0.6", (b) 0.7", (c) 0.8", (d) 0.9", (e) 1.0" and (f) 1.2". Beam U-3-M-a was loaded in 0.1" increments of deflection at 80°C and was observed to display failure initiation at 0.6". Photo was not taken at 1.1" deflection. (Note: Sample designation with "U" prefix indicates the beam was being reused upside down.)

The failure of beams with conventional plies caused smaller amplitude tow buckles than seen in the SM-only photos. Initially, only a part of a tow would buckle, appearing to initiate at voids caused by the cloth weave. The short and tightly grouped buckles formed mainly along the beam centerline and were rougher to the touch than buckles formed on the SM ply. The display of failure of 5-M-b was more conservative than that of 4-M-b, producing only sharp, tiny microbuckles. The progression from initiation to solid buckled line required only one additional deflection increment, compared to two or three increments in 4-M-b. The center of 5-M-b is noticeable thinner, allowing a larger bend radius. This indicates that the two conventional plies acted as a stiffer caul plate on the SM materials, allowing the beam to deflect further than with one conventional ply. However, a portion of the additional deflection is due to foam thinning, which would cause the beam to have a lower moment of inertia at room temperature, and means a less stiff structural part in application.



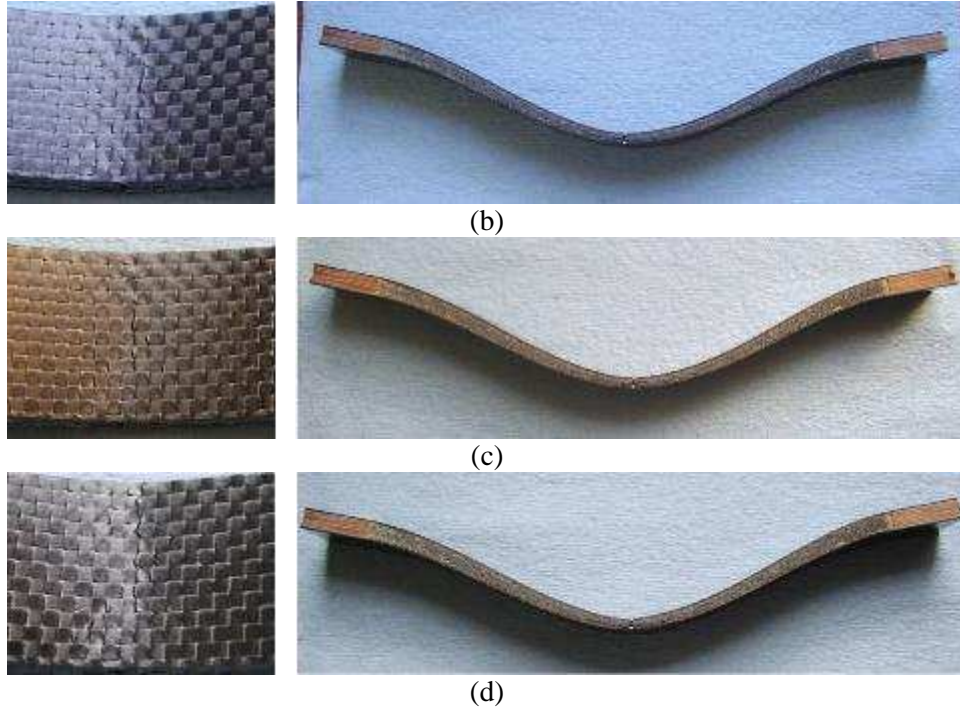


Figure 4-41: Failure progression of 4-M-b.
(a) 1.3", (b) 1.4", (c) 1.5" and (d) 1.6". Beam 4-M-b was loaded in 0.1" increments of deflection at 80°C and was observed to display failure initiation at 1.3". Beam center thickness was 0.166" at failure initiation.

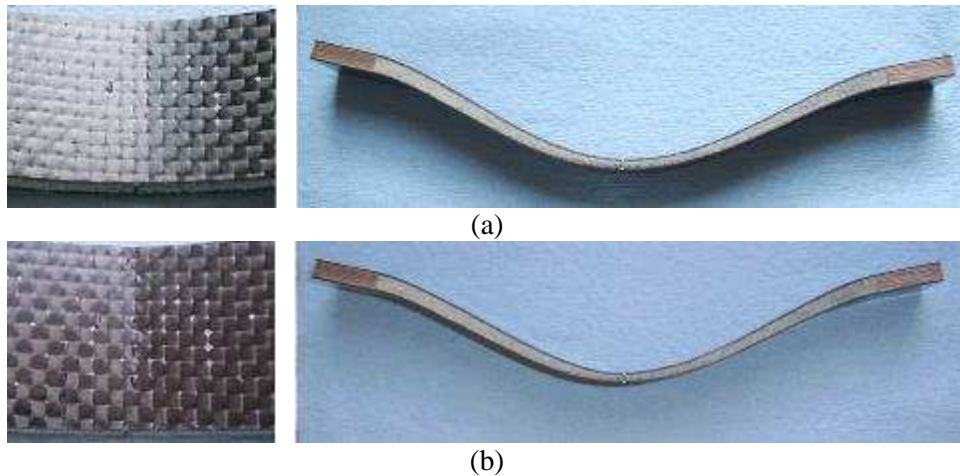


Figure 4-42: Failure progression of 5-M-b.
(a) 1.5" and (b) 1.6". Beam 5-M-b was loaded in 0.1" increments of deflection at 80°C and was observed to display failure initiation at 1.5".

6-M-b was expected to allow deflection similar to 4-M-b since one conventional ply is incorporated. The failure displayed by 6-M-b was more likened to 5-M-b, distinct lines of sharp tow buckles. From the

first observation, the line of buckles extended across the entire width of the facesheet, and was the most brittle in appearance. The thickness at mid-span was closest to 5-M-b when measured at low deflections.

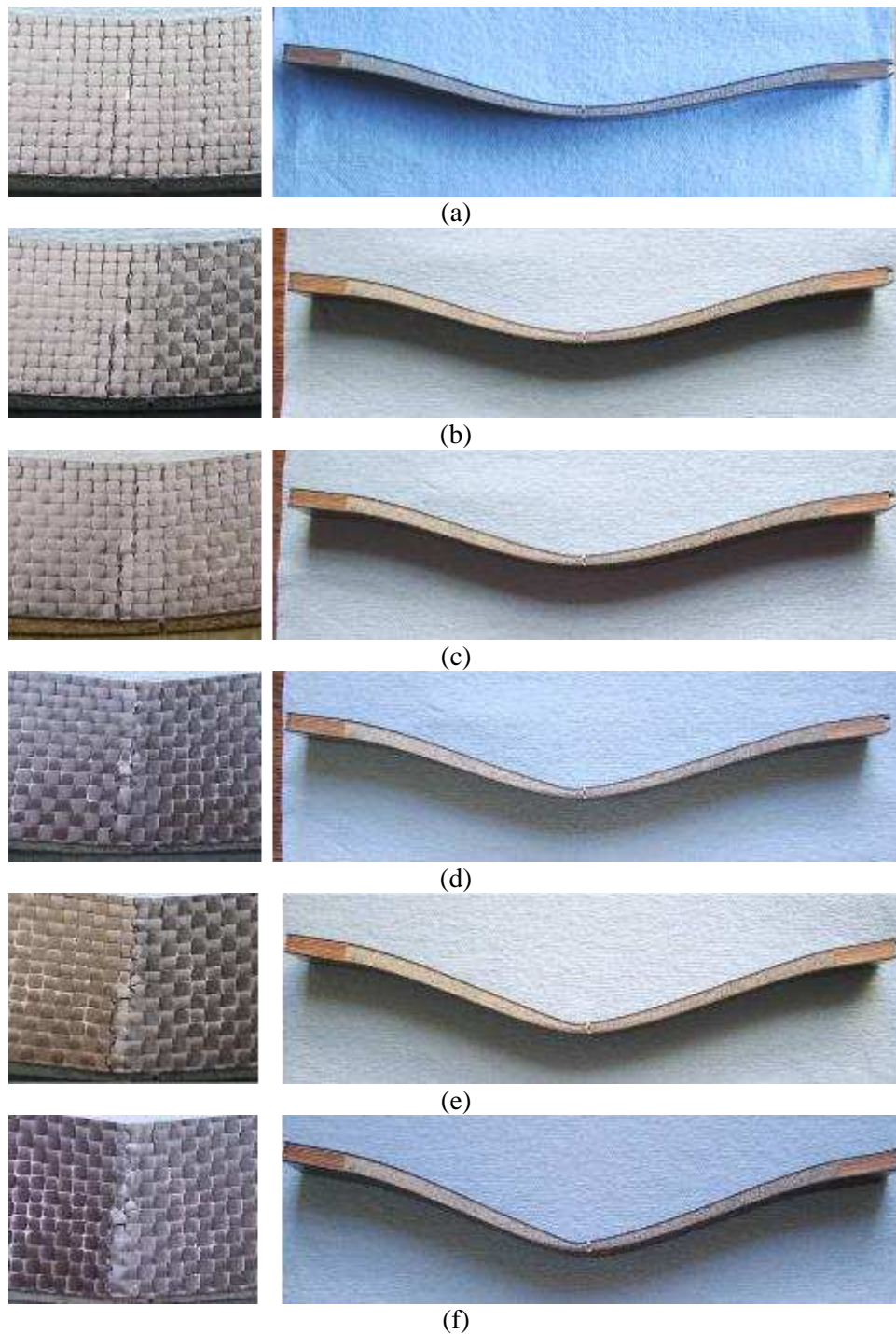


Figure 4-43: Failure progression of 6-M-b.
(a) 0.8", (b) 0.9", (c) 1.0", (d) 1.1", (e) 1.2" and (f) 1.3". Beam 6-M-b was loaded in 0.1" increments of deflection at 80°C and was observed to display failure initiation at 0.8".

4.12 Foam failure

Much discussion has focused on failure defined as microbuckling of fibers under compressive loading of the facesheets. As the lowest modulus component of the sandwich configuration, both in flexure and extension, the stress to shear or compress the foam is much lower than required to affect any other materials. While foam allowables are not studied in this work, the foam must survive bending in order to be effective in a structural application. It was noted that the end constrained beam with two conventional composite plies had the most foam thinning of all configurations, as deflection by foam compression required less force than bending the stiffened facesheet. A strain limit beyond which the foam is permanently crushed must be avoided. Bending at temperatures below 80°C resulted in greater mid-span thickness by increasing foam compressive modulus.

2.5-L-a was deflected to 1.6" in incremental bending, as discussed in Section 4.10, and was considered not failed throughout all deflection cycles. The maximum deflection curvature of this beam, shown in Figure 4-44, displays a high degree of foam shear at the ends. A close-up view of the end in Figure 4-45 shows the formation of a crack where the foam has torn near the upper facesheet. No fiber buckling occurred, but irrecoverable damage was caused.



Figure 4-44: 2.5-L-a at 1.6" at 80°C - No facesheet failure.

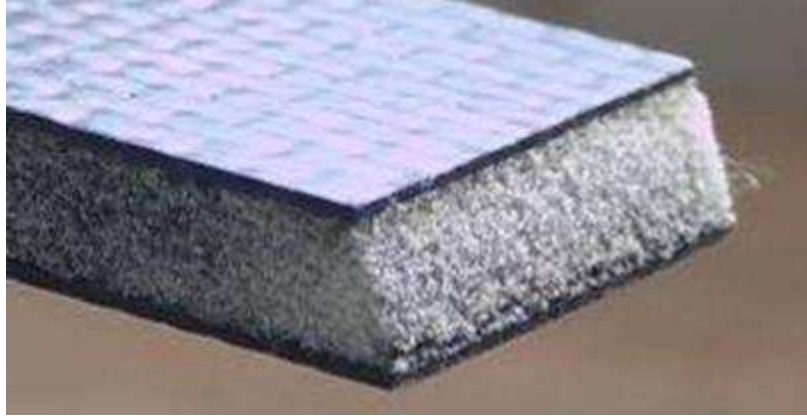


Figure 4-45: 2.5-L-a at 1.6" at 80°C - Core end shear showing foam shear failure.

4.13 Sample microscopy

Cross section photographs at 25X magnification are presented first in the as-bent state, then in the stress relaxed state. U-3-M-a is shown deflected to 1.2", 4-M-b to 1.6", and 5-M-b to 1.6" at 80°C, which is the highest deflection each sample experienced in prior testing.

Under magnification, a thin grey line is observed between the SM and conventional epoxy plies in the upper facesheets of 4-M-b and 5-M-b. Since no chemical interaction is believed to take place between the conventional and SM epoxies, this is believed to be a resin rich layer created when the SM ply was laid up on the already cured conventional epoxy ply, and the tows were not free to nest completely. The most visible example is of 5-M-b while bent, in Figure 4-48(b). After restoring 4-M-b, a similar line can be seen in Figure 4-50(b). Voids along this line may have formed where air was trapped in the epoxy during layup or where fibers were incompletely wet out at tow overlaps. Voids act as failure initiation sites and cracks extend from the voids into the neat resin, although it seems to be secondary failure to the fiber buckling. U-3-M-a does not have the same type of line since all plies were consolidated at the same time.

4.14 Bent

Out of plane ply buckling is present in all three beams in both the upper and lower facesheets. The largest amplitude fiber buckles, which were readily visible on the top ply during testing, were used to identify failure in the samples. All samples also show compression buckling in the lower facesheet under magnification. It is assumed that after failure of all upper plies, the neutral bending surface of the beam

shifts to within the lower plies. It is of interest to note that although 5-M-b has progressed only 0.1” beyond failure initiation, the lower facesheet compression buckles are most prominent in that beam. Compression buckles appear to initiate at perpendicular tow overlap locations.

U-3-M-a, the SM only beam, exhibited the most localized upper ply failure, although bending was taken 0.6” beyond failure initiation. This should have provided ample deflection increments to propagate delamination, if it were likely to occur. In Figure 4-46(b), two upper plies show tow breakage and fiber separation adjacent to the buckle location. The SM matrix appears to have softened enough to allow fibers in the damaged tows to move independently, producing a frayed appearance at the broken edge. The lower facesheet in Figure 4-46(c)-(d), displays a more diffuse failure zone, with buckling at two weave overlap locations. The buckling amplitude in the lower plies is less prominent than in the other two samples. Delamination appears to occur within the tow, rather than between plies.

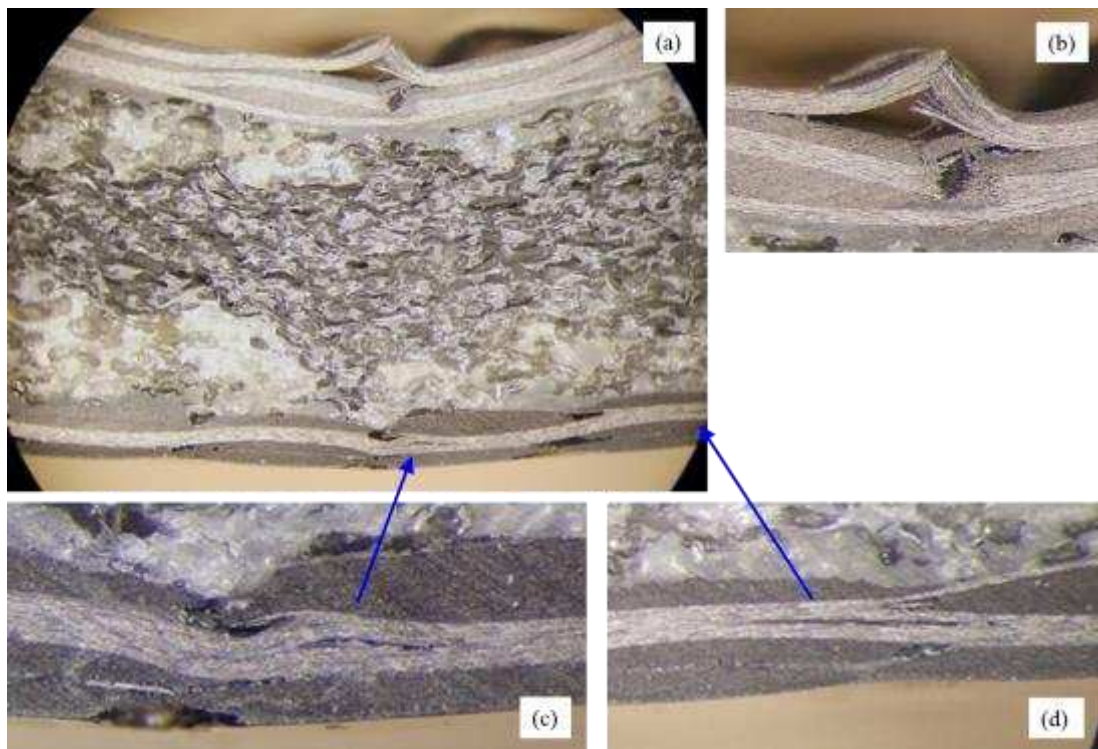


Figure 4-46: U-3-M-a bent, at up to 25X magnification.

(a) Full view of beam cross-section at mid-span, (b) fiber “peak” formed in axial surface tow at midspan, and compression failure of second ply, (c) compression buckling delamination of lower facesheet, and (d) additional delamination of lower facesheet away from mid-span.

Both 4-M-b and 5-M-b show brittle failure of the top ply, with cracking, delamination, and fiber debris present. Unlike U-3-M-b, fibers stay together in a tow bundle and do not separate once the tow is severed. The top facesheet of 4-M-b in Figure 4-47(b)-(c) has two distinct failure locations, which are not at adjacent. In Figure 4-47(b), micro buckles have formed in the upper two plies due to the axial tows being misaligned with the compression load as they weave over and under the transverse tows. A crack has formed in the transverse tow between the buckles, where it appears the matrix has failed to resist shear in the fiber bundle, resulting in delamination. The buckle in the upper surface tow has progressed to the formation of a kink band, with distinct lines transverse to the thickness, where the fibers have bent. The buckle in the second ply tow is more gradual, with larger bend radii, and some delamination of the fibers has occurred. The fiber motion of the two tows provides a side-by-side comparison of buckling in a conventional matrix (top ply) and buckling in a shape memory matrix (second ply).

The ply damage in Figure 4-47(c) is a complete severing of the axial tow, with no indication of ductile fiber buckling prior to fracture. Very little delamination is evident. At the crack location, the axial fibers of the upper two plies are in direct contact, and a portion of the SM tow has remained attached to the NSM tow as it buckled and cracked. It may appear that some of the conventional epoxy has wet the fibers on the adjacent SM ply, but since the conventional epoxy is cured before layup of the SM plies, epoxy bleed and mixing is considered unlikely. Several loose pieces of broken tows are stuck under the delaminated upper ply, but the fibers in this debris remain adhered together, indicating highly brittle ply cracking.

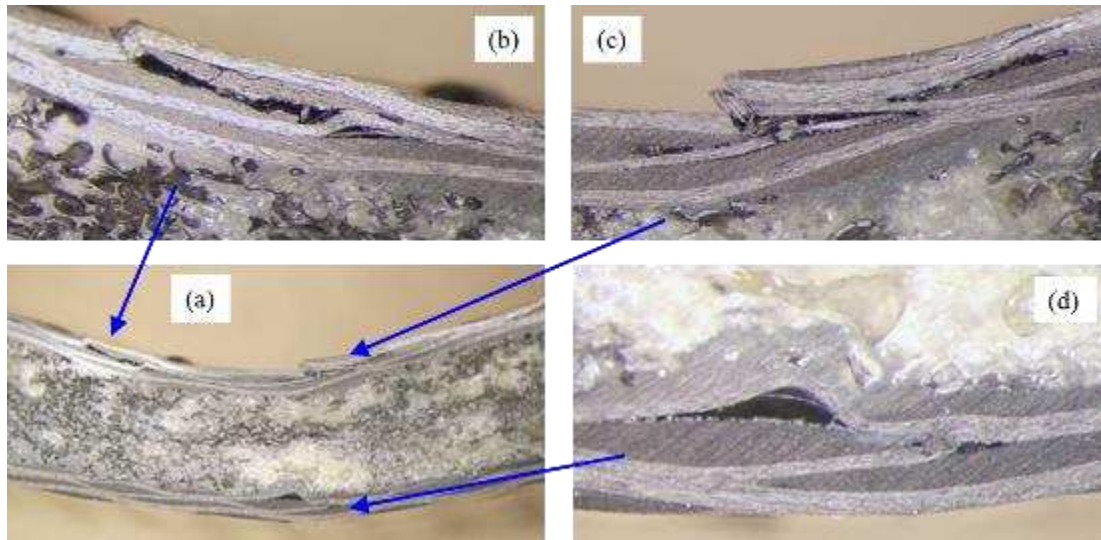


Figure 4-47: 4-M-b bent, at up to 25X magnification.

(a) Full view of beam cross-section at midspan, (b) compression buckling of axial tows, and delamination between first and second plies, (c) brittle failure of upper facesheet, (d) lower ply local compression buckling delamination.

A large compression buckle is immediately obvious in the lower facesheet ply closest to the core. The height of the buckle is believed to correspond to compression loading over a very small amount of deflection and time, such that the load caused local ply failure at the weakest point, rather than being distributed over several microbuckling locations. Compression stress is accumulated in the conventional epoxy ply during deflection. Brittle failure of this ply is followed by immediate buckling of the underlying SM plies, which shifts all accumulated compression load to the lower facesheet. It is this near-instantaneous load application that causes a large buckle to form at the weakest site. The neutral bending surface in a beam with failed upper facesheet is approximately midway through the thickness of the lower facesheet due to the low stiffness of the foam core. The through thickness location of the large buckle delamination and adjacent smaller amplitude buckle in Figure 4-47(d) correlates well with this assumption.

The failure of the upper facesheet of 5-M-b in Figure 4-48 is highly brittle, with both transverse cracking, observed in the upper ply, and inter-ply cracking and delamination, between the first and second plies, and between the second and third plies. The axial tow of the second conventional epoxy ply appears to be unusually wavy, due to multiple delamination locations. A large chunk of displaced fiber has separated from the top ply and appears to be folded over in Figure 4-48(b).

An unusually large bubble in the core is encircled in red in Figure 4-48(a). Since the void is not located at the center of the beam or between the upper and lower facesheet failure locations, it is assumed to have no impact on the test results.

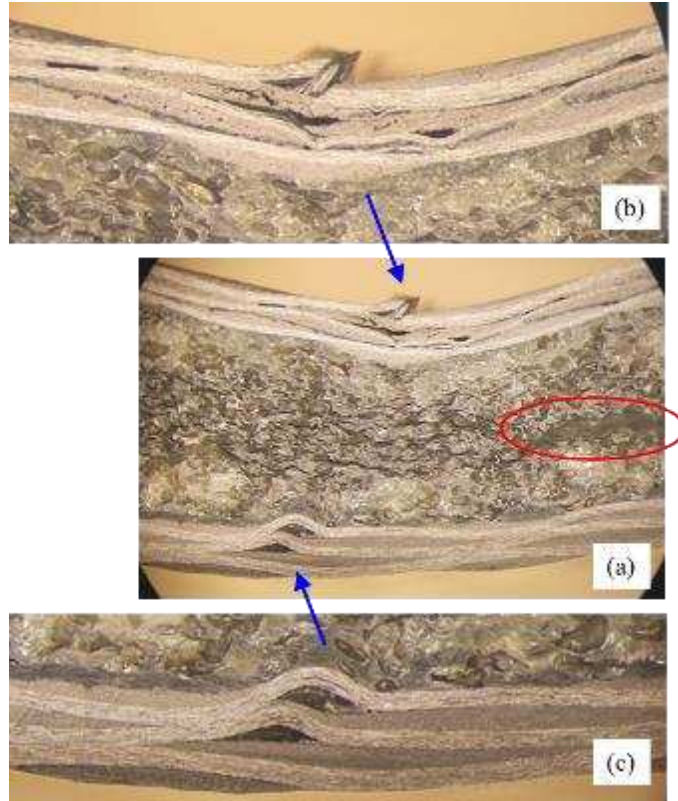


Figure 4-48: 5-M-b bent, at up to 25X magnification.

(a) Full view of beam cross-section at mid-span, and apparent large void in foam (encircled), (b) concentrated mid-span failure, axial tow "peak" and delamination between first and second plies, and between second and third plies, (c) compression buckling and delamination of two lower plies.

The two plies of lower facesheet shown in Figure 4-48(c) have buckled in compression. Each is approximately equivalent in amplitude to the single buckle in the lower facesheet of 4-M-b. This may correspond to double the stored compression stress in the upper facesheet before failure, because 5-M-b contains two conventional epoxy plies, versus one conventional ply in 4-M-b. The two ply buckles are located at transverse tow weave locations, which provide an inherent buckling initiation site caused by misalignment to the compression load. Unintentional alignment of the plies during layup placed the two initiation sites nearly on top of each other, which further weakens the second ply after failure of the first. Due to weave orientation, the through thickness location of the axial tows falls within the upper half of the

facesheet thickness. Some delamination within the tows is visible, indicating a ductile fiber buckling motion.

4.15 Restored

The amount of epoxy infiltration could be more accurately assessed once the samples were restored. Based on purely visual observation, the SM epoxy has filled about 20-35% of the total 0.25" foam thickness of the three samples pictured in Figure 4-49 through Figure 4-51. At elevated temperature, the low viscosity SM epoxy is not believed to impede shear in the foam, however the filling of the open cells would limit the beam thinning due to compression under the loading roller.

Of the three samples, U-3-M-a in Figure 4-49 shows the least amount of damage after being restored. The flatness of the plies and only minor displacement of the broken tows makes failure difficult to detect at room temperature. Without magnification, only a small dark spot on the upper facesheet, shown in Figure 4-49(b), is visible on the beam cross-section. The dark spot is created by delamination of the bent and broken fibers. On the lower facesheet, the buckled and delaminated ply is nearly invisible in Figure 4-49(c).

Voids in the epoxy at the tow overlap locations are prevalent throughout the lower facesheet pictured in Figure 4-49(a), but are not present in the upper facesheet. If this is common for all beams in Set 3, compression resistance was likely reduced when the samples were loaded right side up, but upside down loading is believed to be minimally affected due to fiber-dominated tension capability. It would have been prudent to perform microscopic inspection of offal produced during the sample trim process prior to testing to identify defects that could affect test results.

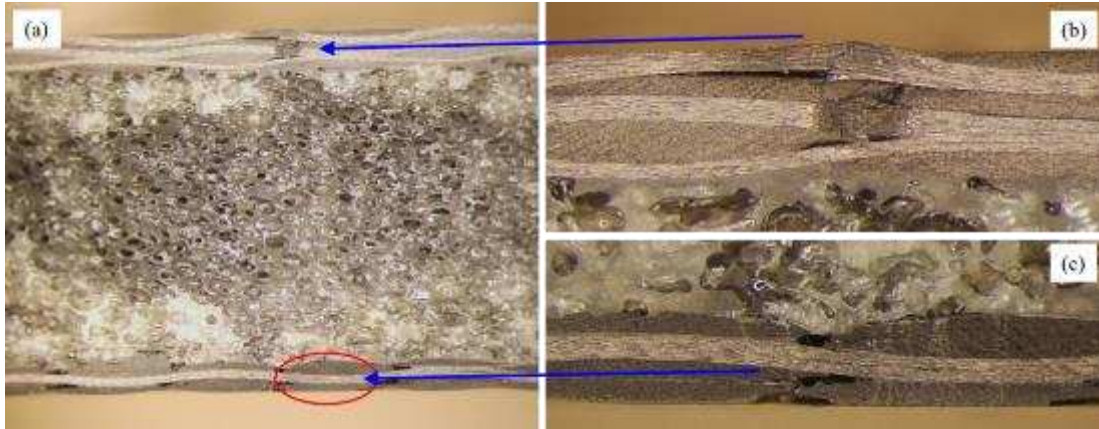


Figure 4-49: U-3-M-a restored, at up to 25X magnification.

(a) Full view of beam cross-section at mid-span, (b) upper facesheet shows dark region where fibers are bent or broken, (c) lower facesheet delamination is difficult to detect after restoring.

The severed edge of the upper facesheet of 4-M-b in Figure 4-50(b) prevents the top ply from being fully restored to a flat surface. This discontinuity makes it easier to detect a damaged area without magnification. A crack line is clearly visible when the beam is viewed from the top down. The other delamination on the upper facesheet, encircled in Figure 4-50(a), restores nearly flat, with only a thin dark line visible on the cross-section. The large delamination in the lower facesheet, which was unmistakable when bent, is nearly invisible in the restored state. Foam cells above this delamination appear to be filled with shape memory epoxy, which is visible as a bright white area above, and to the right of the delamination. No obvious change in behavior is attributed to the filled cells.

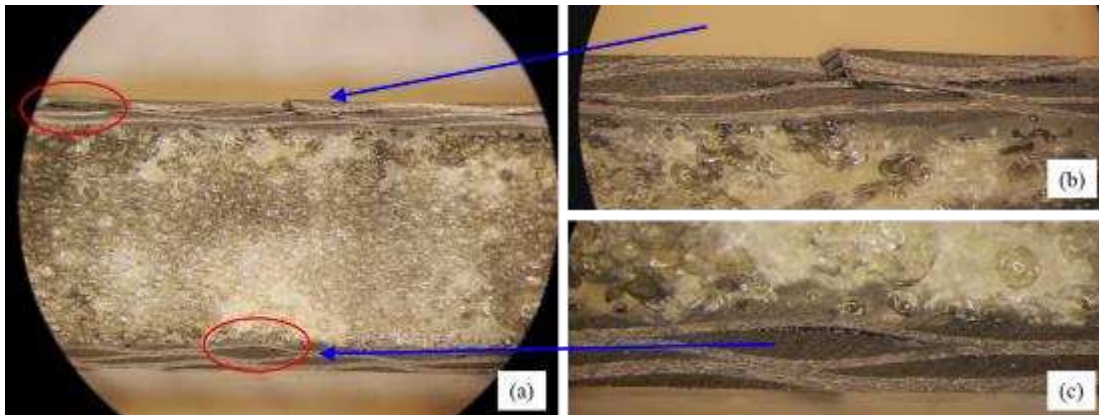


Figure 4-50: 4-M-b restored, at up to 25X magnification.

(a) Full view of beam cross-section at mid-span with damage locations identified, (b) axial tow "peak" on upper facesheet, (c) lower facesheet delamination.

The restored upper facesheet of 5-M-b remains raised at the cracked ply location, shown in Figure 4-51(b). Multiple delamination locations prevent the fibers from returning to their original positions. Delaminations formed within the transverse tows of the conventional epoxy plies, rather than within the axial tows, as seen in the SM plies. The chunk of brittle fiber on the topmost ply in Figure 4-48(b) is still partially attached, but the ply is clearly incapable of carrying load in that area.

The large foam bubble observed in the bent cross-section, is identified in Figure 4-51(a) with an arrow, where it has returned to an ovaloid shape and is more clearly visible. Previously, it was difficult to determine whether this void region was a compressed bubble or a crack. During sample manufacturing, large bubbles were seen, some over an inch across. Foam was sanded to 0.25" before layup and no obvious bubbles were seen in the surfaces of the foam sheets used.

The two lower facesheet compression buckles of 5-M-b in Figure 4-51(c) have not completely closed and are still clearly visible in the cross-section without magnification. It is unclear, but likely, that this is related to the incomplete flattening of the upper facesheet, because the tension facesheet of all samples should be of the same composition.

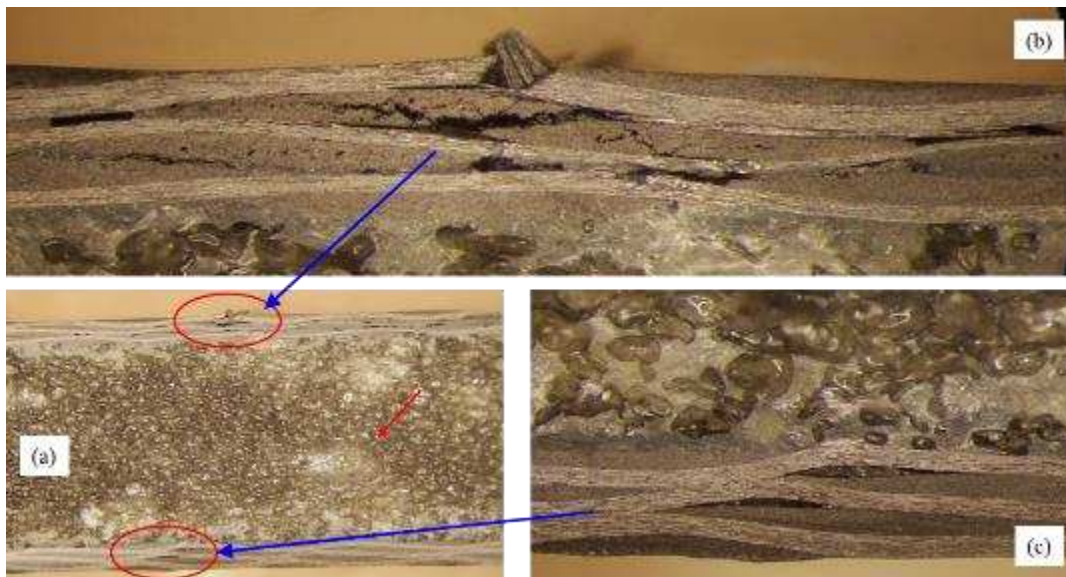


Figure 4-51 – 5-M-b restored, at up to 25X magnification.

(a) Full view of beam cross-section at midspan with damage locations circled, (b) delaminated ply on upper facesheet remains slightly raised, (c) lower facesheet delaminations are not fully closed.

4.16 Contoured foam

Since foam thinning is known to occur when the beams are bent, this demonstration showed that by predicting the amount of compression that would occur at a specific deflection, it was possible to design a foam profile that would compress to the desired thickness. If bending zones were identified in a real part, the same foam can be used throughout with locally increased thicknesses, rather than substituting a different material in these zones to prevent compression.

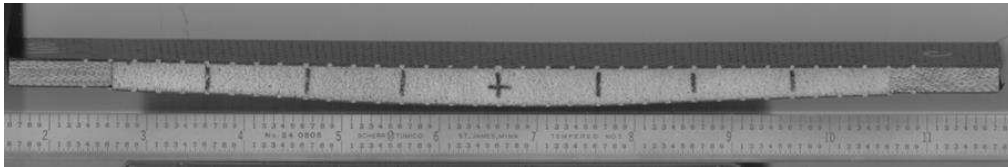


Figure 4-52: Contoured foam beam before bending.



Figure 4-53: Contoured foam beam, bent.

4.17 Validity of shear constraint

The purpose of adding phenolic end blocks to some beams was to simulate the effect of local heating. By comparing the bent geometry of the locally heated beams without end constraints in Figure 4-54 and Figure 4-55 to shear-constrained beams that were globally heated, confidence was established that the phenolic blocks produced an acceptable simulation.



Figure 4-54: 2-M-b at 0.5" – Locally heated.



Figure 4-55: 2.5-M-a at 0.6" – Locally heated.

4.18 Shape stability

To investigate the shape stability of beams cooled after bending with liquid nitrogen vapor, as discussed in Section 4.8, an undamaged beam from Set 4 was deflected 1.0" at 80°C, super cooled to below room temperature with liquid nitrogen vapor, then immediately removed from the test chamber and photographed. The beam and camera setup were left undisturbed in ambient lab conditions. Three days later the sample was photographed again to compare the two curvatures. Examination of the start and end photos in Figure 4-56 and Figure 4-57, respectively, does not reveal any noticeable creep. This indicates that although beams were super cooled before removal from the bend fixture during incremental deflection tests, it is unlikely that any change in geometry occurred after equilibrating to room temperature.



Figure 4-56: Beam profile at start of room temperature stability test.



Figure 4-57: Beam profile at end of room temperature stability test.

5 FUTURE WORK

- Investigate the potential advantages of local reinforcement under the center of bending and locally thickening the foam for the prevention of compression failure in end constrained beams. Failure at higher bending temperatures was related to smaller upper facesheet bending radii. By maintaining greater mid-span thickness, and separating the global facesheet buckling peak into two smaller peaks away from the beam center, more deflection capability may be generated.
- Increase the beam length to produce a greater aspect ratio. Typical geometry for composite sandwich structures is large, but fairly thin panels. Distribution of bending strain over a longer distance between supports should be studied.
- Perform deflection tests with 4-point bend fixture to induce only moment, not shear into the mid-span of the beam. Removing the normal component of loading provides a better study of hybrid facesheets used to delay compression-induced EMC failure.
- Use unidirectional conventional plies instead of woven plies to eliminate the weave-induced fiber buckling initiation sites. The compression stiffness of the conventional plies in bending is due to axial fibers only. Additionally, to reduce out-of-plane fiber buckling in the conventional unidirectional ply, a transverse unidirectional ply could be used on the innermost bending surface. Determine if this configuration would allow additional deflection at similar weight.
- Generate a more accurate definition and inspection practice for failure, in line with degradation of beam performance. Within the definition used in this work, “failed” beams may still be functional.
- Test on a fixture that provides additional deflection capability in order to achieve failure in all specimens. Hybrid beams should be tested to failure, and beyond, to provide proper comparison of deflection capability and behavior after failure.

6 CONCLUSION

The addition of conventional plies to the compression surface of the shape memory composite sandwich panels more than doubled the deflection achievable prior to compression-side facesheet failure, with the beam geometry tested. Compressibility of the foam, and the shear end-constraints, also had significant influence on facesheet failure by altering the deformation away from simple beam bending mechanics.

This work investigated the behavior of a temperature-sensitive, viscoelastic shape memory sandwich structure under typical variables of forming, and how this behavior changed when conventional matrix plies were substituted into the compression facesheet. The variables chosen were bending temperature, bending rate, local heating vs. global heating, and hold time at maximum deflection. In the configurations tested, the use of shear end-constraints had a greater effect on the bending force than including conventional plies in the upper facesheet.

6.1 Significant findings

- Inclusion of shear constraints changes the profile of the deflected beam. It reduces the radius of curvature at the center of the beam which induces higher stress at equivalent deflection values, versus open-ended beams. The inability of end-constrained beams to shear for compression stress relief causes the upper facesheet to globally buckle into the foam. The stiffer the facesheet, the thinner the foam becomes, because the force required to compress the foam is in balance with the force required to bend the beam.
- Initiation of facesheet buckling failure, defined as unrecoverable alteration to the matrix or fibers, is not typically detectable on a force vs. deflection curve at elevated forming temperatures, nor at room temperature in small deflection bending.
- Deflection of SM-only beams resulted in distributed compression microbuckling, which may have been recoverable if the transverse weave of the carbon cloth did not provide initiation sites for fiber disbond at tow overlap locations.

- After heat cycling to restore SM materials, crack lines and roughness on the compression surface of the beams containing conventional epoxy plies makes it easier to detect damage locations, as opposed to SM-only facesheets, which can restore to a smoother surface.
- Visual indication of first ply damage did not coincide with a reduction in stiffness, rather additional deflection sufficient to cause failure through all compression plies would be reflected in load capability.
- Of the temperatures tested, 56°C is most conducive to bending to maximum deflection because the stiffness of the foam prevents excessive mid-span compression, hence increasing mid-span bend radius of end-constrained beams. However, lower temperature results in higher bending loads, with more viscous response to bending rates.
- Stress relaxation affects beam failure by causing additional strain in the foam during slow deflection rates or extended hold periods. In end-constrained beams, the mid-span compression drives the minimum bend radius of the compression facesheet, and in open-ended beams, high end shear can cause foam tearing. Given sufficient time at constant deflection, equivalent load and deformation results will develop, regardless of deflection rate.
- Little to no elastic strain was observed after cooling bent beams to room temperature. The highest values observed ~10% were on SM-only beams that had significant failure due to deflection at 56°C. Likewise, room temperature creep was unnoticeable. Concerns that strain energy in conventional plies could be strong enough to overcome the glassy SM materials proved incorrect.
- The tighter bend radius and foam compression mode imposed by shear end constraints increases required bending force.
- The stress relaxation percentage of maximum force above T_g is lower than at 56°C; but happens rapidly, taking about half as much time to reach steady state.

- Bending stiffness is far more sensitive to test chamber temperature fluctuation below T_g . Temperature fluctuation of $\pm 1-2^\circ\text{C}$ around 56°C results in load curve differences comparable to the entire distinction between bending at 71°C and at 80°C .
- The addition of a conventional ply on top of a SM-only beam gained very little deflection advantage over an unmodified SM-only beam, and was inferior in bending to a similar hybrid beam with one conventional ply substituted at the extreme fiber for an SM ply.

Besides increasing deflection capability, conventional plies have relatively little effect when compared to variables like shear end-constraints, and bending temperature. Like SM-only beams, hybrid beams are also shape stable at room temperature. Creating a hybrid beam with the same number of plies above and below the core is preferred to adding a conventional ply onto an otherwise symmetric EMC. This is also a benefit at room temperature, where warping could otherwise occur. End constraints significantly change the beam bending mechanics, making stiffness prediction and stress calculation difficult.

Fiber kinking and tow delamination occurs locally at initiation sites before maximum loading of the compression facesheet occurs. This requires that a better definition of failure be defined; one which conveys the reduction of structural capability. Very small deflection at room temperature does not provide an adequate damage inspection method.

Bending below T_g , and with higher fractions of conventional plies is best for accomplishing maximum facesheet deflection. This should be traded against preserving cross section thickness to maintain structural capability, as well as the desire to form at higher rates and with minimal required load. If bending at temperatures above T_g , hold time should be minimized to reduce foam thinning due to stress relaxation. If bending below T_g , reduction of deflection rate will reduce required bending force.

The tests performed in this work demonstrate that including conventional epoxy matrix plies in the compression surface of shape memory composite sandwich panels does produce superior deformability over SM-only panels by delaying or preventing facesheet failure due to compression buckling.

7 REFERENCES

- [1]Arzberger, S. C., Tupper, M. L., Lake, M. S., Barrett, R. Mallick, K., Hazelton, C., Francis, W., Keller, P. N., Campbell, D., Feucht, S., et al. "Elastic Memory Composites (EMC) for Deployable Industrial and Commercial Applications." *Proc., SPIE 5762, Smart Structures and Materials 2005: Industrial and Commercial Applications of Smart Structures Technologies*, 35 (2005).
- [2]Liang, C., Rogers, A. and Malafew, E. "Investigation of Shape Memory Polymers and Their Hybrid Composites." *Journal of Intelligent Material Systems and Structures* 8.4 (1997): 380-386.
- [3]Campbell, D., Lake, M. S., Scherbarth, M. R., Nelson, E. and Six, R. W. "Elastic Memory Composite Material: An Enabling Technology for Future Furlable Space Structures." *Proc., 46th AIAA/ASME/ASCE/AHS/ASC Structures, Structural Dynamics, and Materials Conference*, Austin, Texas (2005). Paper No. 2005-2362.
- [4]Barrett, R., Taylor, R., Keller, P., Codell, D. and Adams, L. "Deployable Reflectors for Small Satellites." *21st Annual AIAA Conference on Small Satellites* (2007). pp. 109.
- [5]Wang, X., Zhang, W., Lan, X., Liu, Y. and Leng, J. "Basic Properties and Application of Shape Memory Polymer Composite to Deployable Hinge for Solar Arrays." *Proc. SPIE 6423, International Conference on Smart Materials and Nanotechnology in Engineering* 642356 (November 01, 2007).
- [6]Sokolowski, W. M. and Hayashi, S. "Applications of Cold Hibernated Elastic Memory (CHEM) Structures." *Proc., SPIE 5056, Smart Structures and Materials 2003: Smart Structures and Integrated Systems* 534 (August 5, 2003).
- [7]Atli, B., Gandhi, F. and Karst, G. "Thermomechanical Characterization of Shape Memory Polymers." *Journal of Intelligent Material Systems and Structures* 20.1 (2009): 87-95.
- [8]Liu, Y., Gall K., Dunn, D. L. and McCluskey, P. "Thermomechanical Recovery Couplings of Shape Memory Polymers in Flexure." *Smart Materials and Structures* 12.6 (2003): 947-954.
- [9]Dietsch, B. and Tong, T. "A Review: Features and Benefits of Shape Memory Polymers (SMPS)." *Journal of Advanced Materials* 39.2 (2007): 3-12.
- [10]Hayashi, S. "Properties and Applications of Polyurethane Series Shape Memory Polymer." *International Progress in Urethanes* 6 (1993): 90-115.
- [11]Gall, K., Tupper, M. L., Munshi, N. A. and Mikulas, M. "Micro-Mechanisms of Deformation in Fiber Reinforced Polymer Matrix Elastic Memory Composites." *Proc., 42nd AIAA/ASME/ASCE/AHS/ASC Structures, Structural Dynamics, and Materials Conference and Exhibit, Seattle, Washington* (2001). Paper No. 2001-1419.
- [12]Lan, X., Liu, Y., Leng, J. and Du, S. "Thermomechanical Behavior of Fiber Reinforced Shape Memory Polymer Composite." *Proc., SPIE 6423, International Conference on Smart Materials and Nanotechnology in Engineering* 64235R (November 01, 2007).
- [13]Gall, K., Mikulas, M., Munshi, N. A., Beavers, F. and Tupper, M. "Carbon Fiber Reinforced Shape Memory Polymer Composites." *Journal of Intelligent Material Systems and Structures* 11.11 (2000): 877-886.

- [14]Hexcel Composites, "HexWeb™ Honeycomb Sandwich Design Technology" Publication No. AGU075b, December 2000. <http://www.hexcel.com/> Visited 3/12/2016
- [15]Di Prima, M. A., Lesniewski, M., Gall, K., McDowell, D. L., Sanderson, T. and Campbell, D. "Thermo-Mechanical Behavior of Epoxy Shape Memory Polymer Foams." *Smart Materials and Structures* 16.6 (2007): 2330-2340.
- [16]Francis, W. H., Lake, M. S. and Mayes, J. S. "A review of classical fiber microbuckling analytical solutions for use with elastic memory composites." *American Institute of Aeronautics and Astronautics* (2006): 006-1.
- [17]Lips, J. A., Maji, A. K. and Ng, T-T. "Deployment Rate Prediction of Elastic Memory Composites." *Proc., 46th AIAA/ASME/ASCE/AHS/ASC Structures, Structural Dynamics and Materials Conference. Austin, Texas. 7* (2005):4961-4988.
- [18]Murphey, T. W., Meink, T., and Mikulas, M. M. "Some Micromechanics Considerations of the Folding of Rigidizable Composite Structures." *Proc., 42nd AIAA/ASME/ASCE/AHS/ASC Structures, Structural Dynamics, and Materials Conference and Exhibit, Seattle, Washington* (2001). Paper No. 2001-1418.
- [19]Campbell, D. and Maji, A. "Failure Mechanisms and Deployment Accuracy of Elastic-Memory Composites." *Journal of Aerospace Engineering*, 19.3 (2006): 184-193.
- [20]Monaghan, M. R., "Effect of Diaphragm Stiffness on the Quality of Diaphragm Formed Thermoplastic Composite Components." *Proc., International SAMPE Symposium and Exhibition* 35.1 (1990): 810-824.
- [21]Schmachtenberg, E. and Strohacker, J. "Durable Thermoplastic Sandwich Panels for Various Composite Applications." *SAMPE Journal* 42.1 (2006): 24-27.
- [22]Mills, A., Barker, J. Gamble, N. and Ferman, S. "Conformable Racing Seat." *Colorado State University, Dept. of Mechanical Engineering, Senior Practicum Projects Program* (2007).
- [23]Radford, D. W. and Antonio, A.. (2009) "Shape memory sandwich panels." *ICCM-17*, IOM Communications Ltd, Edinburgh, Scotland, B6.6.
- [24]Radford, D. W. and Antonio, A. (2011), "Enhancing the Deformation of Shape Memory Sandwich Panels." *Strain*, 47: 534–543. doi:10.1111/j.1475-1305.2009.00722.x
- [25]Abrahamson, E. R., Lake, M. S., Munshi, N. A. and Gall, K. "Shape Memory Mechanics of an Elastic Memory Composite Resin." *Journal of Intelligent Material Systems and Structures* 14.10 (2003): 623-632.
- [26]Tobushi, H., Hashimoto, T., Hayashi, S. and Yamada, E. "Thermomechanical Constitutive Modeling in Shape Memory Polymer of Polyurethane Series." *Journal of Intelligent Material Systems and Structures* 8.8 (1997): 711-718.
- [27]Diani, J., Liu, Y. and Gall, K. "Finite Strain 3D Thermoviscoelastic Constitutive Model for Shape Memory Polymers." *Polymer Engineering & Science* 46.4 (2006): 486-492.

- [28]Xiong, Z. Y., Wang, Z. D., Li, Z. F. and Chang, R. N. "Micromechanism of Deformation in EMC Laminates." *Materials Science and Engineering: A* 496.1 (2008): 323-328.
- [29]Campbell, D. and Maji, A. "Deployment Precision and Mechanics of Elastic Memory Composites." *Proc., 44th AIAA/ASME/ASCE/AHS/ASC Structures, Structural Dynamics, and Materials Conference*. 2003.Campbell, D., Lake, M. S. and Mallick, K. "A Study of the Bending Mechanics of Elastic Memory Composites." 45th AIAA/ASME/ASCE/AHS/ASC Structures, Structural Dynamics, and Materials Conference, Palm Springs, California (2004).
- [31]Schultz, M. R., Francis, W. H., Campbell, D. and Lake, M. S. "Analysis techniques for shape-memory composite structures." *Proc., 48th AIAA/ASME/ASCE/AHS/ASC Structures, Structural Dynamics, and Materials Conference, Honolulu, Hawaii* (2007). Paper No. 2007-2401.
- [32]Lake, M. and Beavers, F. "The Fundamentals of Designing Deployable Structures with Elastic Memory Composites." *Proc., 43rd AIAA/ASME/ASCE/AHS/ASC Structures, Structural Dynamics, and Materials Conference* (2002).
- [33]Volk, B. L., Lagoudas, D. C. and Chen Y.-C. "Thermomechanical Characterization of the Nonlinear Rate-Dependent Response of Shape Memory Polymers." *Proc., SPIE 6929, Behavior and Mechanics of Multifunctional and Composite Materials* 69291B (April 03, 2008).
- [34]Tobushi, H., Hayashi, S., Hoshio, K. and Ejiri, Y. "Shape Recovery and Irrecoverable Strain Control in Polyurethane Shape-Memory Polymer." *Science and Technology of Advanced Materials* 9.1 (2008) 015009 (7pp).
- [35]Brinson, H. F. and Brinson, L. C. *Polymer Engineering Science and Viscoelasticity: An Introduction* New York: Springer, 2008.
- [36]Hexion, Technical Data Sheet for EPIKURE™ Curing Agent 3140, Re-issued August 2007. <http://www.hexion.com/> Visited 3/31/2016
- [37]Gdoutos, E. E. "Failure Modes of Sandwich Structures." *Applied Mechanics and Materials* 7-8 (2007): 23-28.
- [38]Fiedler, T. and Öchsner, A. "Experimental Analysis of the Flexural Properties of Sandwich Panels with Cellular Core Materials." *Materialwissenschaft und Werkstofftechnik* 39.2 (2008): 121-124.

APPENDIX A

A.1. Sources of error

The potential sources of error in this work fall in to the categories of manufacturing errors and measurement errors.

A.2. Manufacturing error

Variation in sample geometry induced by the manufacturing process affects the bending stiffness of samples within each set. The width difference, which was caused by tolerance in the sample parting procedure, was normalized to one inch wide it test data based on the beam center measurement. Thickness difference, specifically in the center of the specimen, appeared to be induced by heat produced by the curing shape memory epoxy. Foam core was cut to the same nominal thickness, but after upper face sheet curing, a localized thinning was observed. Wet layup onto the open cell foam with SM epoxy resulted in uncontrolled filling of the foam, although full thickness filling was not observed. Thickness measurements for each beam are shown below.

	Width (in)			Thickness (in)		
	End - B	Center	End - T	End - B	Center	End - T
1-L-a	0.999	1.006	1.000			
1-M-a	1.001	1.002	1.003			
1-H-a	0.997	0.998	0.994			
1-L-b	1.004	1.008	1.010			
1-M-b	1.005	1.006	1.003	0.285	0.275	0.268
1-H-b	1.010	1.008	1.006	0.288	0.276	0.271
2-L-a	1.003	1.006	1.008	0.292	0.283	0.276
2-M-a	1.007	1.009	1.010	0.292	0.282	0.279
2-H-a	1.008	1.005	1.003	0.292	0.282	0.275
2-L-b	0.996	1.001	1.000	0.293	0.283	0.279
2-M-b	0.999	0.998	0.999	0.291	0.282	0.276
2-H-b	0.994	0.994	0.994	0.290	0.279	0.269
2.5-L-a	0.995	0.996	0.995	0.293	0.293	0.285
2.5-M-a	0.999	1.000	0.999	0.292	0.293	0.285
2.5-H-a	1.006	1.005	1.008	0.295	0.293	0.285
3-L-a	0.996	0.997	1.001			
3-M-a	1.011	1.005	1.002	0.297	0.256	0.283
3-H-a	1.006	1.004	1.003			
3-L-b	0.994	0.998	0.999	0.292	0.249	0.295
3-M-b	0.996	0.997	0.997	0.299	0.268	0.287
3-H-b	0.995	1.001	0.999	0.296	0.248	0.285
4-L-a	1.009	1.002	1.010	0.295	0.238	0.300
4-M-a	1.006	1.006	1.005	0.292	0.252	0.292
4-H-a	1.010	1.012	1.012	0.297	0.259	0.286
4-L-b	1.008	1.003	0.999	0.295	0.251	0.293
4-M-b	1.005	1.005	1.006	0.295	0.257	0.290
4-H-b	1.003	1.004	1.002	0.295	0.255	0.291
5-L-a	1.002	1.004	1.002	0.299	0.259	0.292
5-M-a	1.004	1.002	1.003	0.290	0.251	0.285
5-H-a	1.004	1.005	1.004	0.294	0.257	0.292
5-L-b	1.009	1.008	1.006	0.295	0.235	0.290
5-M-b	1.013	1.014	1.013	0.290	0.260	0.285
5-H-b	1.004	1.005	1.010	0.295	0.245	0.298
6-M-a	0.975	0.966	0.971	0.309	0.259	0.296
6-H-a	1.006	1.006	1.004	0.309	0.262	0.303
6-L-b	0.975	0.975	0.966	0.304	0.264	0.300
6-M-b	1.006	1.008	1.009	0.311	0.256	0.301
6-H-b	1.012	1.017	1.013	0.309	0.274	0.298

A.3. Load cell temperature sensitivity

The load cell was more “jumpy” above room temperature, making low load range measurement more difficult. At the same time, the shape memory materials were softer, resulting in lower overall test loads. The load cell reading was zeroed prior to each test. The offsets required during incremental deflection tests are shown as an example.

	Total Test Deflection	0.3"	0.4"	0.5"	0.55"	0.6"	0.7"	0.8"	0.9"	1.0"	1.1"	1.2"	1.3"	1.4"	1.5"	1.6"
Test Temp	Sample	Load Cell Offset at Test Temperature (lb)														
56°C	U-1HA	no test	no test	0.066	no test	0.066	0.081	0.079	0.089	0.088	0.110	0.101	0.104	0.102	0.104	0.096
	2MB	no test	no test	0.060	no test	0.065	0.073	?	0.089	0.089	0.108	0.090	0.088	0.080	0.092	0.097
	2.5MA	no test	no test	0.064	no test	0.064	0.077	0.089	0.091	0.101	0.112	0.098	0.097	0.091	0.100	0.097
	3HB	no test	no test	0.067	no test	0.073	0.092	0.099	0.102	?	0.105	0.103	0.103	0.105	0.093	0.110
	4LB	no test	no test	0.069	no test	0.082	0.094	0.104	0.106	0.111	0.117	0.110	0.102	0.100	0.099	0.097
	5LB	no test	no test	0.069	no test	0.086	0.096	0.116	0.106	0.110	0.105	0.087	0.102	0.101	0.101	0.098
80°C	1HB	no test	no test	0.117	no test	0.117	0.117	0.117	0.117	0.249	0.221	0.154	0.203	0.179	0.182	no test
	2LB	no test	no test	0.114	no test	0.219	0.114	0.225	0.114	0.222	0.132	0.171	0.114	0.114	0.114	0.178
	2.5LA	no test	no test	0.112	no test	0.213	0.112	0.112	0.212	0.112	0.179	0.112	0.183	0.188	0.188	0.174
	U-3MA	no test	no test	0.110	0.110	0.110	0.236	no test	no test	no test	no test	no test	no test	no test	no test	no test
	4MB	no test	no test	0.108	no test	0.205	0.111	0.108	0.219	0.209	0.172	0.172	0.171	0.165	0.156	0.163
	5MB	no test	no test	0.111	no test	0.212	0.111	0.111	0.237	0.111	0.182	0.150	0.150	0.167	0.181	0.171
	6MB	0.111	0.211	0.111	no test	0.111	0.111	0.111	0.156	0.139	0.164	0.111	0.168	no test	no test	no test

A.4. Load frame and test fixture compliance

The 3-point bending test set up is considered to be a spring in series with the stiffness of the load-applying machine, which includes the load frame, test fixtures, and load cell. For the current purpose, the machine, in its entirety, is treated as a single flexural entity.

$$\frac{1}{k_{total}} = \frac{1}{k_{sample}} + \frac{1}{k_M} \quad (A.1)$$

Compliance assessment of the machine was performed with a 7.5" (L) x 1" (W) x .376" (T) 6061-T6 aluminum bar and a 7.5" (L) x .988" (W) x .189" (T) mild rolled steel bar, which are roughly the same size as the sample beams. The elastic modulus of 6061-T6 is $10.0 \times 10^3 ksi$, and the steel bar has an elastic modulus of $29.5 \times 10^3 ksi$.

The Deflection vs. Force data is used to calculate the deflection of the machine (δ_M) as the difference between the mid-span deflection measured by the linear potentiometer and the ideal deflections calculated for elastic bending of the metal beams.

$$\delta_{meas} = \delta_{ideal} + \delta_M \quad (A.2)$$

Since equal force is applied to springs in series such that,

$$P_{meas} = P_{ideal} = P_M, \quad (A.3)$$

and the ideal deflection of a beam due to 3-point loading is calculated at mid-span by,

$$\delta_{ideal} = \frac{PL^3}{48EI}, \quad (A.4)$$

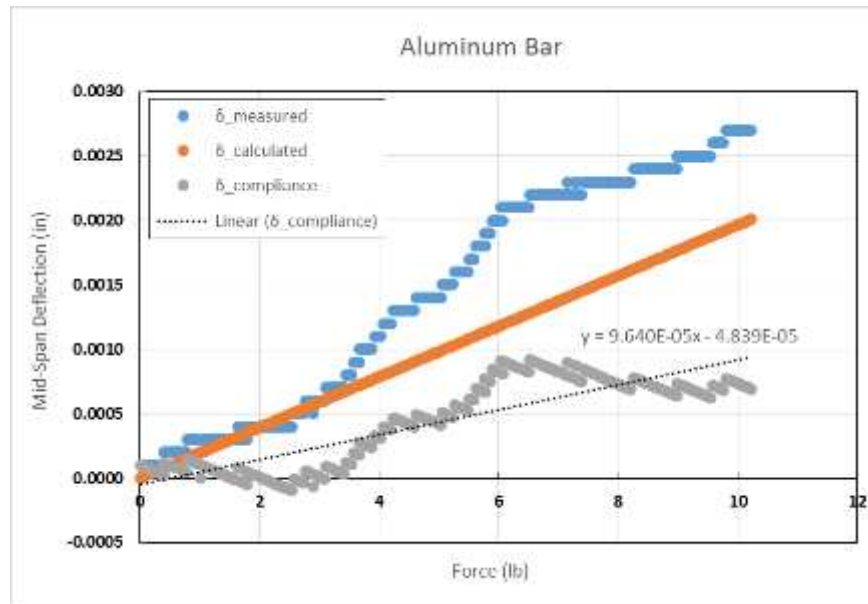
then the total compliance equation can be rewritten as,

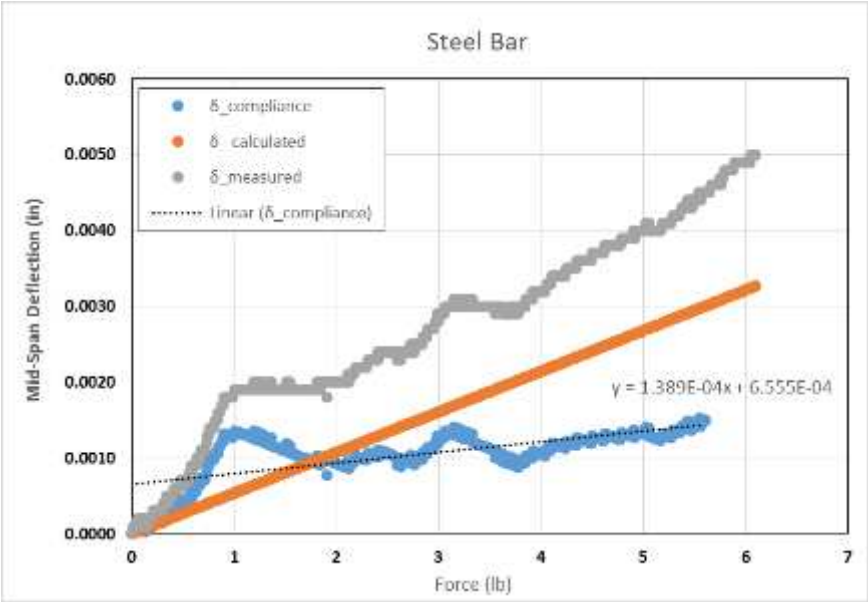
$$\frac{\delta_{meas}}{P_{meas}} = \frac{\delta_{ideal}}{P_{meas}} + \frac{\delta_M}{P_{meas}}. \quad (A.5)$$

Therefore the compliance of the machine is,

$$C_M = \frac{\delta_{meas} - \delta_{ideal}}{P_{meas}}. \quad (A.6)$$

A straight line approximation of the compliance data points plotted versus applied load has a slope of around 0.0001 inches per pound, as calculated from both the aluminum and steel bar bending. The force values recorded for all elevated temperature tests are less than 10 pounds. Since the compliance of the load application machine corresponds to a deflection error of only 0.001 inches at 10 pounds force, and deflection values of test data are reported to the nearest 0.01 inches, it is assumed that the error induced by compliance can be ignored.





APPENDIX B

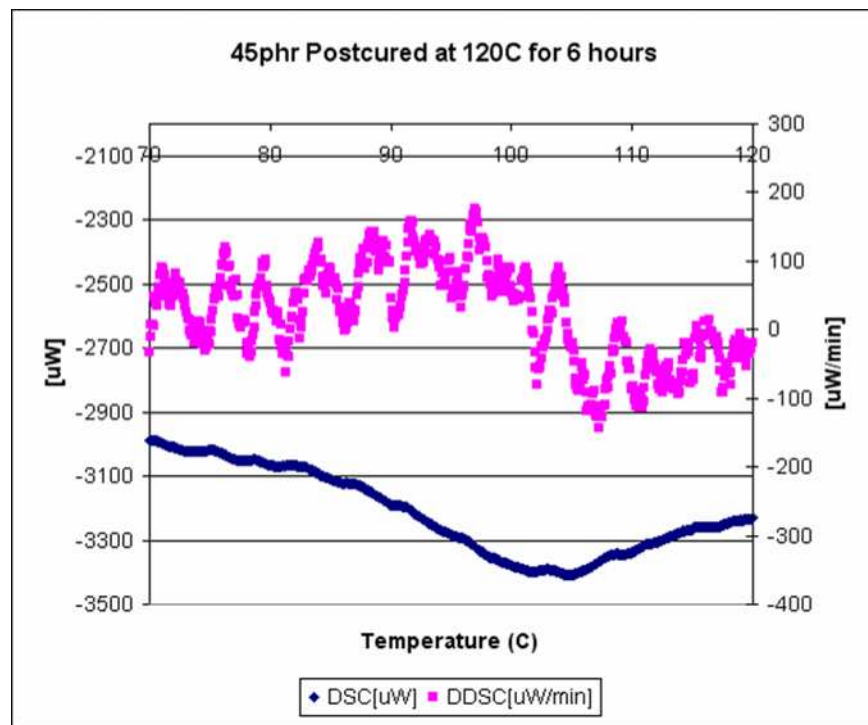
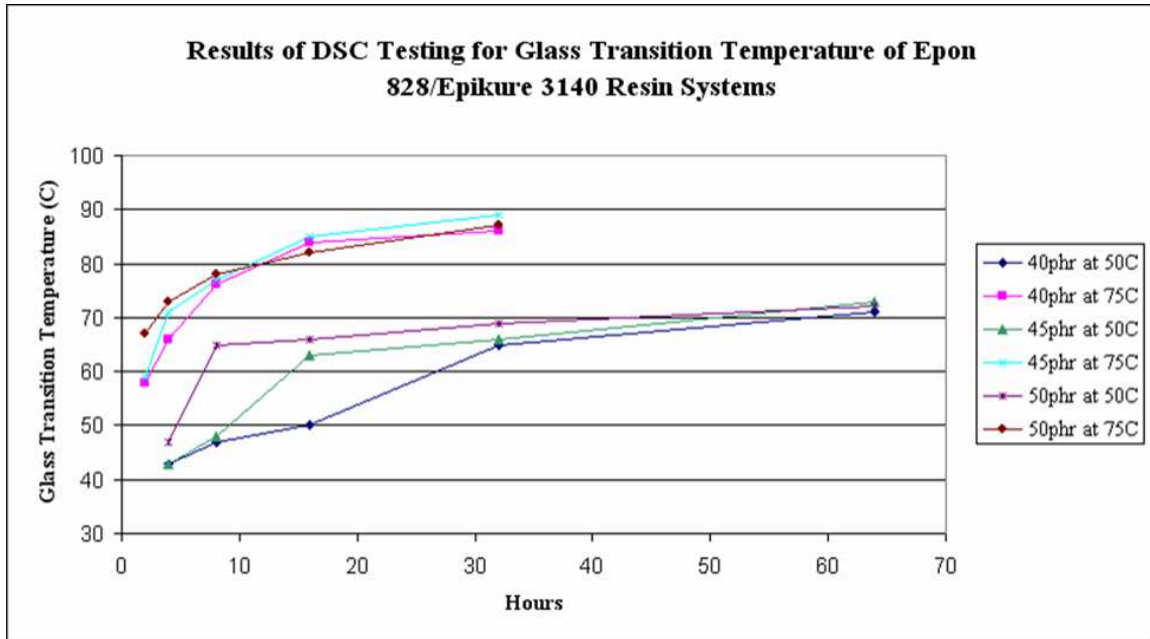
B.1. Room temperature stiffness

The variation in room temperature stiffness within sample batches is shown in the following table.

	Center Width (in)	Raw Stiffness (lb)	Normalized Stiffness (lb)	Set Average, Normalized	Deviation^2	Variance	Population Standard Deviation	Set Min, Normalized	Set Max, Normalized
1-L-a	1.006	158.7	157.8	164.5	45.7	54.8	7.4	155.7	174.4
1-M-a	1.002	170.5	170.1		31.5				
1-H-a	0.998	174.1	174.4		98.6				
1-L-b	1.008	159.7	158.5		36.8				
1-M-b	1.006	171.7	170.7		37.9				
1-H-b	1.008	156.9	155.7		78.6				
2-L-a	1.006	176.0	174.9	179.8	23.3	26.7	5.2	172.6	186.6
2-M-a	1.009	183.3	181.6		3.6				
2-H-a	1.005	187.6	186.6		47.4				
2-L-b	1.001	177.6	177.4		5.3				
2-M-b	0.998	184.9	185.2		30.1				
2-H-b	0.994	171.6	172.6		50.8				
2.5-L-a	0.996	170.7	171.4	175.3	14.8	30.2	5.5	171.4	183.0
2.5-M-a	1.000	171.4	171.4		15.3				
2.5-H-a	1.005	184.0	183.0		60.3				
3-L-a	0.997	140.5	141.0	154.9	194.4	134.1	11.6	141.0	170.4
3-M-a	1.005	155.4	154.6		0.1				
3-H-a	1.004	171.1	170.4		240.1				
3-L-b	0.998	151.5	151.8		9.3				
3-M-b	0.997	168.7	169.2		204.0				
3-H-b	1.001	142.5	142.4		156.7				
4-L-a	1.002	129.2	128.9	146.4	307.4	381.3	19.5	115.0	167.8
4-M-a	1.006	142.7	141.8		21.0				
4-H-a	1.012	169.8	167.8		455.9				
4-L-b	1.003	115.4	115.0		986.0				
4-M-b	1.005	163.7	162.9		271.0				
4-H-b	1.004	162.8	162.1		246.7				
5-L-a	1.004	118.2	117.7	134.7	288.0	254.4	16.0	117.7	157.2
5-M-a	1.002	122.3	122.1		159.1				
5-H-a	1.005	157.1	156.3		468.2				
5-L-b	1.008	128.7	127.7		48.9				
5-M-b	1.014	159.4	157.2		505.4				
5-H-b	1.005	127.8	127.1		56.9				
6-L-a (1)	0.999								
6-L-a (2)	0.860	129.4	150.4	138.4	145.9	354.9	18.8	110.9	166.5
6-M-a	0.966	114.3	118.3		402.1				
6-H-a	1.006	140.7	139.9		2.3				
6-L-b	0.975	108.1	110.9		755.3				
6-M-b	1.008	145.3	144.2		33.9				
6-H-b	1.017	169.3	166.5		790.0				

APPENDIX C

C.1. DSC results of EPON™ Resin 828 mixed with EPIKURE™ Curing Agent 3140 at 45 parts-per-hundred, after post cure



APPENDIX D

D.1. EPON™ Resin 828 Technical Data Sheet



Technical Data Sheet

Re-issued September 2005

EPON™ Resin 828

Product Description

EPON™ Resin 828 is an undiluted clear difunctional bisphenol A/epichlorohydrin derived liquid epoxy resin. When cross-linked or hardened with appropriate curing agents, very good mechanical, adhesive, dielectric and chemical resistance properties are obtained. Because of this versatility, EPON Resin 828 has become a standard epoxy resin used in formulation, fabrication and fusion technology.

Benefits

- Fiber reinforced pipes, tanks and composites
- Tooling, casting and molding compounds
- Construction, electrical and aerospace adhesives
- High solids/low VOC maintenance and marine coatings
- Electrical encapsulations and laminates
- Chemical resistant tank linings, flooring and grouts
- Base resin for epoxy fusion technology

Sales Specification

Property	Units	Value	Test Method/Standard
Weight per Epoxide	g/eq	185 – 192	ASTM D1652
Viscosity at 25°C	P	110 – 150	ASTM D445
Color	Gardner	1 max.	ASTM D1544

Typical Properties

Property	Units	Value	Test Method/Standard
Density at 25°C	lb/gal	9.7	ASTM D1475
Density at 25°C	g/ml	1.16	
Vapor pressure @ 25°C (77°F)	mm Hg	0.03	
Refractive index @ 25°C (77°F)		1.573	
Specific heat	BTU/lb*F	0.5	

Processing/How to use

General Information

The low viscosity and cure properties of EPON Resin 828 allow its use under various application and fabrication techniques including:

• Spraying and brushing	• Pultrusion
• Filament winding	• Casting
• Pressure laminating	• Molding
• Vacuum bag laminating	• Troweling

Curing Agents

EPON Resin 828 can be cured or cross-linked with a variety of curing agents depending on properties desired in the finished product and the processing conditions employed. Some commonly used curing agents, recommended concentrations, typical cure schedules employed in major end-use applications, plus sources for these curing agents are displayed in Table 1.

Performance Properties

Performance Characteristics of Cured EPON Resin 828

Mechanical Properties

High performance, high strength materials are obtained when this resin is cured with a variety of curing agents. Unfilled systems in common use have tensile values greater than 10,000 psi (69 MPa) with modulus values greater than 400,000 psi (2750 MPa). Such systems are normally very rigid. If greater flexibility is needed systems can be formulated to provide up to 300% elongation.

Adhesive Properties

One of the most widely recognized properties of cured EPON Resin 828 is strong adhesion to a broad range of substrates. Such systems exhibit shear strength of up to 6,000 psi (41 Mpa). One factor which contributes to this property is the low shrinkage shown by these systems during cure. Compared to other polymers, epoxy resins have low internal stresses resulting in strong and durable finished products.

Electrical Properties

EPON Resin 828 cured systems have very good electrical insulating characteristics and dielectric properties. For example, systems can be obtained with anhydride and amine curing agents having volume resistivities up to 1×10^{16} ohm-cm, dielectric constants of 3-5 and dissipation factors of 0.002 to 0.020 at ambient conditions. Electrical encapsulations, laminates and molding compounds are frequently based on EPON Resin 828.

Chemical Resistance

Cured EPON Resin 828 is highly resistant to a broad range of chemicals, including caustic, acids, fuels and solvents. Chemically resistant reinforced structures and linings or coatings over metal can be formulated with EPON Resin 828.

Formulating Techniques

The primary components of a thermosetting resin formula are the epoxy resin and the hardener or curing

agent. However, in practice other materials are normally incorporated to achieve special properties. For example, inert fillers such as silicas, talcs, calcium silicates, micas, clays and calcium carbonate can be added to further reduce shrinkage and improve dimensional stability. Also, reactive diluents can be added to EPON Resin 828 to reduce viscosity. The effect on viscosity by adding such materials is shown in Figure 1.

Table 1 / Curing Agents for EPON™ 828

Curing Agent ¹	Physical State	Recommended Concentration Range, phr ²	Typical Cure Schedule Time °C (°F)	Deflection Temperature °C (°F)	Applications ⁴	Suppliers ⁵
Aliphatic Amines						
EPIKURE™ 3223 (DETA)	Liquid	12	7d, 25 (77)	120(250)	ABCDEFHI	5
EPIKURE 3234 (TETA)	Liquid	13	7d, 25 (77)	120(250)	ABCDEFHI	5
EPIKURE 3200 (AEP)	Liquid	22	24h, 25 (77) & 1h, 150 (300)	120(250)	BCEFGH	5
EPIKURE 3270	Liquid	75	14d, 25 (77)	56(133)	ABCDEFHI	5
EPIKURE 3271	Liquid	18	14d, 25 (77)	66(151)	ABCDEFHI	5
EPIKURE 3274	Liquid	40	14d, 25 (77)	—	ABCDEFHI	5
EPIKURE 3230	Liquid	35	7d, 25 (77)	68(155)	ABCDEFHI	1
D-400 Type PEA	Liquid	55	30 min, 115(240)	31(88)	ABCEFH	1
Cycloaliphatic Amines						
EPIKURE 3370	Liquid	38	7d, 25 (77)	56(133)	ABCDEFHI	5
EPIKURE 3382	Liquid	63	7d, 25 (77)	63(145)	ABCDEFHI	5
EPIKURE 3383	Liquid	60	24h, 25 (77) & 2h, 100 (212)	54(129)	ABCDEFHI	5

EPON Resin 828

Polyamides

EPIKURE 3115	Liquid	120	1h, 100 (212)	85(185)	AB	5
EPIKURE 3125	Liquid	90	7d, 25 (77)	90(195)	ABCEFH	5
EPIKURE 3140	Liquid	75	7d, 25 (77)	115(240)	ABCEFH	5

Amidoamines

EPIKURE 3015	Liquid	50	16h, 25 (77) & 2h, 93 (200)	—	ABCDEFHI	5
EPIKURE 3055	Liquid	50	16h, 25 (77) & 2h, 93 (200)	67(153)	ABCDEFHI	5
EPIKURE 3072	Liquid	35	14d, 25 (77)	59(138)	ABCDEFHI	5

Aromatic Amines

EPIKURE W	Liquid					5
Metaphenylenediamine (MPDA)	Solid	14	2h, 80 (175) & 2h, 150 (300)	150(300)	BCDGH I	3
Methylene dianiline (MDA)	Solid	27	2h, 80 (175) & 2h, 150 (300)	160(320)	BCDEGH I	13
Diaminodiphenyl Sulfone (DADS)	Solid	25	5h, 125 (257) & 1h, 200 (392)	170(350)	BCDGH I	2, 13

Table 1 / Curing Agents for EPON™ 828, cont.

<u>Curing Agent:</u>	<u>Physical State</u>	<u>Recommended Concentration Range, phr²</u>	<u>Typical Cure Schedule Time</u>	<u>Deflection Temperature °C (°F)</u>	<u>Applications¹</u>	<u>Suppliers²</u>
----------------------	-----------------------	---	---	---	---------------------------------	------------------------------

EPON Resin 828

			°C (°F)				
Anhydrides							
Methyl tetrahydrophthalic Anhydride (MTHPA)	Liquid	80	2h, 120 (250) & 2h, 150 (300)	130(266)	BCDGH	9, 11, 14	
NADIC Methyl Anhydride (NMA)	Liquid	90	1h, 120 (250) & 2-24h, 260(500)	180(356)	BCDGH	9, 14	
Hexahydrophthalic Anhydride (HHPA)	Solid	80	1h, 80 (175) & 2h, 150 (300)	130(266)	BCDGH	8, 12, 14	
Catalysts and Miscellaneous							
2-Ethyl- 4-Methyl Imidazole (EMI-24)	Metastable Liquid	3	4h, 50 (122) & 2h, 170 (340)	170(340)	BCDGH	15, 16	
BF3-Monoethylamine (BF3-MEA)	Liquid	3	1h, 120 (250) & 2h, 170 (340)	170(340)	BCDGH	17	
Diethylaminopropylamine *	Solid	6	30 min, 115(240)	100(212)	ABC	6	
Dicyandiamide	Solid	4	1h, 177 (350)	150(300)	BCDGH	18, 19	

* Cures can be effected with these curing agents over a wide range of temperatures. Higher temperatures yield shorter cure times and highest Tg.

* Parts of curing agent per 100 parts of resin.

* Systems cured at room temperature were post cured at elevated temperature to achieve deflection values.

* Application codes: A - Coatings; B - Adhesives; C - Castings; D - Moldings; E - Flooring; F - Paving; G - Electrical Laminates; H - Structural Laminates; I-Filament Winding.

* Supplier Code:

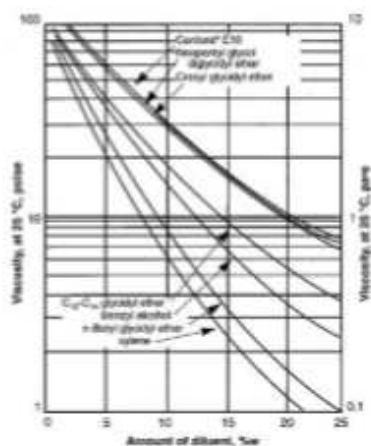
1. Huntsman Chemical
2. RSA Corporation
3. E.I. DuPont de Nemours & Co., Chemicals & Pigments Dept.
4. Harshaw Chemical Company
5. Hexion Specialty Chemical
6. BASF Corporation
7. American Cyanamid - Industrial Chemical Div.
8. Milliken & Company

EPON Resin 828

9. Lindau Chemicals, Inc.
10. Anhydrides and Chemicals, Inc.
11. Dixie Chemical Co., Inc.
12. Buffalo Color Corp.
13. Air Products and Chemicals, Inc.
14. Lonza
15. Interchem
16. Polyorganix
17. Atotech
18. SKW Trotsberg
19. Ashland Chemical

* Dimethylamino propylamine may be substituted at expense of slightly reduced pot life. Sources are 2 and 16.

Figure 1 / Viscosity at 25 °C of EPON™ Resin 828 blends with various diluents



Fusion Technology

EPON Resin 828 is the product of choice for a resin chemist using a specific fusion catalyst when processing proprietary solid epoxy resins or epoxy esters. Upon request, Hexion can provide EPON Resin 828 exhibiting extremely low hydrolyzable and total chlorine, two end groups that may be deleterious to resin curing and long term performance in electrical uses.

FDA Status

Provisions are made in the FDA regulations for the use of EPON Resin 828, when properly formulated, applied and cured, for food contact applications under Title 21 Code of Federal Regulations 175.300. The regulations should be consulted for complete details. In particular, we direct your attention to subparagraph (b) of 21 CFR 174.5 and the general provisions applicable to indirect food additives listed there.

Identification and Classification

EPON Resin 828

Chemical Abstract Service Registry Number: 25068-38-8 (EPA/TSCA inventory designation)

Generic name: Liquid Bisphenol A Epichlorohydrin based epoxy resin.

Chemical designation: Phenol, 4,4O - (1-methylethylidene) bis-polymer with (chloromethyl) oxirane.

Figure 2 / Viscosity - temperature profile for EPON™ Resin 828

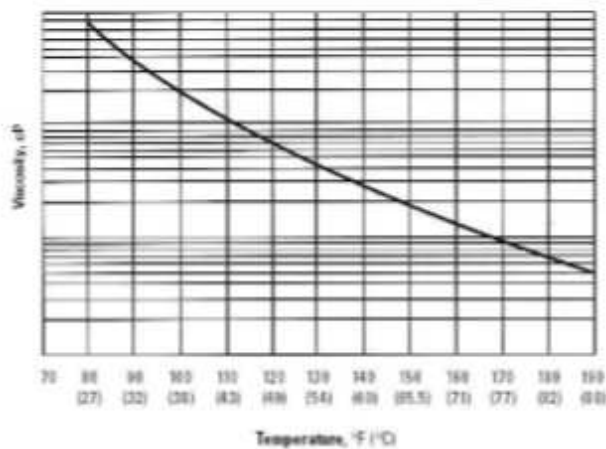
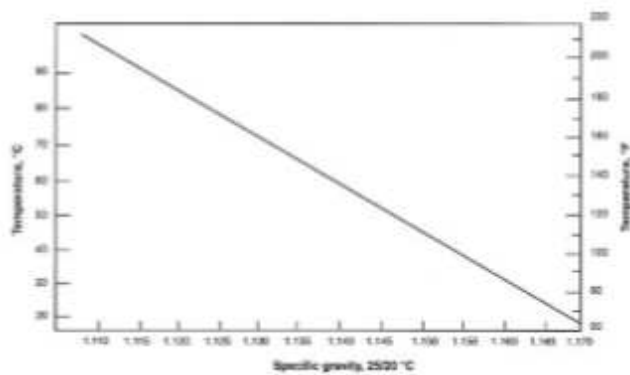


Figure 3 / Specific gravity - temperature profile for EPON™ Resin 828

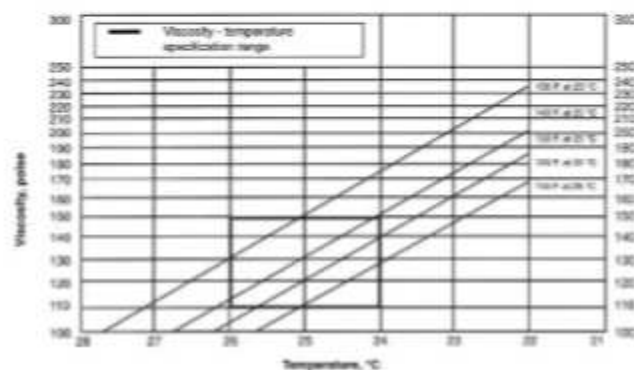


EPON Resin 828

Formulation and Application Information

For additional performance characteristics information covering adhesives, laminating, casting and molding applications, consult bulletin SC:87, entitled "EPON Resin Structural Reference Manual." For epoxy resin amine-cured coatings, consult bulletin SC:193, entitled "Formulating Amine-Cured Coatings with EPON Resin."

Figure 4 / Viscosity - temperature profile (for 5 samples of EPON™ Resin 828 ranging in viscosity from 110-150 poise)



Safety, Storage & Handling

Please refer to the MSDS for the most current Safety and Handling information.

Please refer to the Hexion web site for Shelf Life and recommended Storage information.

EPON Resin 828 is an undiluted liquid epoxy resin that is available in tank cars, tank trucks and 500 pound net closed head drums. EPON Resin 828 is normally shipped in bulk from 150 °F (66 °C) to 180 °F (82 °C) and can be stored at 120-140 °F (49-60 °C) for ease of handling. The viscosity/temperature profile and the specific gravity/temperature profile for EPON Resin 828 are displayed in Figures 2 and 3 respectively for your guidance.

NOTE OF CAUTION: When checking viscosity of EPON Resin 828 incoming samples, we caution you to make certain that the product is maintained at 25 \pm 0.01 °C before testing. You will note in Figure 4 that EPON Resin 828 can vary in viscosity by 10-15 poise for each degree in temperature the product varies from 25 °C.

Exposure to these materials should be minimized and avoided, if feasible, through the observance of proper precautions, use of appropriate engineering controls and proper personal protective clothing and equipment, and adherence to proper handling procedures. None of these materials should be used, stored, or transported until the handling precautions and recommendations as stated in the Material Safety Data Sheet (MSDS) for these and all other products being used are understood by all persons who will work with them. Questions and requests for information on Hexion Inc. ("Hexion")

EPON Resin 828.

products should be directed to your Hexion sales representative, or the nearest Hexion sales office.
Information and MSDSs on non-Hexion products should be obtained from the respective manufacturer.

Packaging

Available in bulk and drum quantities.

Contact Information

For product prices, availability, or order placement, please contact customer service:
www.hexion.com/Contacts/

For literature and technical assistance, visit our website at: www.hexion.com

® and ™ Licensed trademarks of Hexion Inc.

DISCLAIMER

The information provided herein was believed by Hexion Inc. ("Hexion") to be accurate at the time of preparation or prepared from sources believed to be reliable, but it is the responsibility of the user to investigate and understand other pertinent sources of information, to comply with all laws and procedures applicable to the safe handling and use of the product and to determine the suitability of the product for the intended use. All products supplied by Hexion are subject to Hexion's terms and conditions of sale. HEXION MAKES NO WARRANTY, EXPRESS OR IMPLIED, CONCERNING THE PRODUCT OR THE MERCHANTABILITY OR FITNESS THEREOF FOR ANY PURPOSE OR CONCERNING THE ACCURACY OF ANY INFORMATION PROVIDED BY HEXION, except that the product shall conform to Hexion's specifications. Nothing contained herein constitutes an offer for the sale of any product.

PDS-3942- (Rev. 3/31/2016 4:25:31 PM)